Pilot Testing, Simulation, and Scaling of an Oxyfuel Burner for Cement Kilns

Von der Fakultät Energie-, Verfahrens- und Biotechnik
Der Universität zur Erlangung der Würde eines Doktors der
Ingenieurwissenschaften (Dr.-Ing.) genehmigte Abhandlung

vorgelegt von

Francisco Carrasco Maldonado

aus Mexiko

Hauptberichter: Univ.-Prof. Dr. techn. Günter Scheffknecht
Mitberichter: Prof. Dr.-Ing. Roman Weber

Tag der mündlichen Prüfung: 02.06.2021

Institut für Feuerungs- und Kraftwerkstechnik (IFK)
der Universität Stuttgart

2021

Acknowledgments

I would first like to express my appreciation for the valuable guidance of Prof. Scheffknecht, who supervised my dissertation work. Additionally, I want to thank Prof. Weber, Prof. Kronenburg and Prof. Schnell whose insightful feedback pushed me to sharpen my thinking and helped me increase the quality of this work. The Mexican National Council of Science and Technology (CONACYT) is also acknowledged for granting a scholarship to conduct the doctoral studies.

Besides, I would like to thank my colleagues at IFK, and especially my colleagues of the department Firing Systems. J. Maier, S. Grathwohl, M. Escoto, R. Youssefi, M. Paneru, T. Matthies, T. Wagner and many others who supported the conduction of my experimental campaigns and were at all moments a great example of team spirit. Not only in technical matters they showed support, but also gave wise counsel and sympathetic ear in personal matters. Further, I want to acknowledge the great help of the students, whose bachelor and master thesis I supervised. They did an amazing work and helped me move my dissertation forwards.

Finally, I want to express a deep gratitude for the support of my family. I want to sincerely acknowledge the support of my wife Lucy, who believed in me when I had nothing and followed me to this adventure in Germany. Lastly, I deeply acknowledge the love and caring support of my parents, they departed way too soon. I think they would be proud of this achievement.

This thesis is part of a project supported by the H2020 research and innovation programme grant agreement No 641185.

Abstract

In the context of the present work the combustion concept oxyfuel, which entails the combustion to take place in an O_2/CO_2 atmosphere instead of air is investigated with reference to its application in cement kilns. Pilot testing at a 500 kW_{th} once-through furnace and numerical simulations were employed to investigate the influence of high CO_2 atmosphere and burner configuration on the combustion behavior of selected fuels. To investigate oxyfuel combustion in relevant cement production conditions, a modern kiln burner was scaled down and used as a prototype in the test rig. Conducted investigations in pilot-scale show that oxygen concentration in oxyfuel mode plays an important role in achieving an air-firing-like temperature profile. Flame length is also influenced under oxyfuel operation. As the oxygen concentration increases in combustion gas, the flame length shortens and the concentration of CO rises in the near burner region due to the influence of heterogeneous and homogenous reactions with CO_2. Further, the operation in oxyfuel mode opens the possibility to redistribute the oxygen mass flow in the primary and secondary gas stream to optimize combustion behavior. According to the tests conducted, when the oxygen concentration is increased in primary gas (with a corresponding decrease in secondary gas) the generation of CO in the near burner field decreases significantly. Finally, full-scale CFD simulations of a cement kiln show that the results in pilot scale can be applied to replicate similar temperature profile as in air-blown combustion with a slight increase in radiative heat fluxes to wall. According to these results, the prototype burner can be used to retrofit a cement kiln for operation in oxyfuel mode.

Kurzfassung

In Rahmen der vorliegenden Arbeit wird das Verbrennungskonzept Oxyfuel, bei dem die Verbrennung in einer O_2/CO_2-Atmosphäre anstelle von Luft stattfindet, im Hinblick auf seine Anwendung in Zementöfen untersucht. Pilotversuche an einer 500 kW_{th}-Verbrennungsanlage und numerische Simulationen wurden eingesetzt, um den Einfluss des hohen CO_2-Anteils in der Gasatmosphäre und der Brennerkonfiguration auf das Verbrennungsverhalten ausgewählter Brennstoffe zu untersuchen. Um die Oxyfuel-Verbrennung unter relevanten Zementherstellungsbedingungen zu untersuchen, wurde ein moderner Ofenbrenner verkleinert und als Prototyp in der Versuchsanlage eingesetzt. Durchgeführte Untersuchungen im Pilotmaßstab zeigen, dass die Sauerstoffkonzentration im Oxyfuel-Betrieb eine wichtige Rolle bei der Erreichung eines luftbefeuerten Temperaturprofils spielt. Die Flammenlänge wird auch im Oxyfuel-Betrieb beeinflusst. Mit zunehmender Sauerstoffkonzentration im Verbrennungsgas verkürzt sich die Flammenlänge und die CO-Konzentration steigt im brennernahen Bereich durch den Einfluss von heterogenen und homogenen Reaktionen mit CO_2. Darüber hinaus eröffnet der Betrieb im Oxyfuel die Möglichkeit, den Sauerstoffmassenstrom im Primär- und Sekundärgasstrom zur Optimierung des Verbrennungsverhaltens neu zu verteilen. Nach den durchgeführten Tests nimmt bei Erhöhung der Sauerstoffkonzentration im Primärgas (mit entsprechendem Rückgang des Sekundärgases) die CO-Erzeugung im Brennernahbereich deutlich ab. Schließlich zeigen CFD-Simulationen eines industriellen Zementofens, dass die Ergebnisse im Pilotmaßstab angewendet werden können, um ein ähnliches Temperaturprofil wie bei der Verbrennung mit Luftströmung zu erreichen, wobei es einen leichten Anstieg der Strahlungswärmeflüsse zur Wand gibt. Gemäß diesen Ergebnissen kann der Prototypbrenner für eine Nachrüstung eines Zementofens eingesetzt werden.

Table of Contents

Nomenclature

Latin symbols

Symbols	Unit	Meaning
a	-	parameter
D	m	Diameter
h	W/m^{2}K	Convective heat transfer
i	-	Number
G	N/MW	Specific flame momentum
I	N	Momentum
k	-	Jet flame factor
K	-	Proportionality constant
l	m	Disc thickness
m	-	Craya-Curtet parameter
$\dot{M}$	kg/s	Mass flow
n	-	Stoichiometric ratio
n	-	Number
Q	MW	Thermal Input
$\dot{Q}$"	W/m^2	Heat flux
r	-	Repeatability
r	m	Radius
R	m	Exit radius of nozzle
s	-	Standard deviation
S	-	Swirl number
T	K	Temperature
u	m/s	Axial velocity component
U	m/s	Velocity

Symbols	Unit	Meaning
w	m/s	Tangential velocity component
x	-	Measurement data
$\bar{x}$	-	Average of measurement data

Greek symbols

Symbols	Unit	Meaning
δ	m	Boundary layer thickness
Δ	-	Difference
ε	-	Emissivity
η	-	Burnout
γ	kg/kg	Mass fraction
λ	W/(mK)	Thermal conductivity
ρ	kg/m^3	Density
σ	W/(m^{2}K^4)	Stefan-Boltzmann constant
φ	-	Unburned carbon
θ	degrees	Nozzle inclination angle

Subscripts

Symbols	Description
A	Ash
$base$	Base
C	Carbon
$clinker$	Clinker
$coal$	Coal
$const$	Constant

Symbols	Description
el	Electric
f	Fuel
g	Gas Phase
$heat$	Heat of reaction
i	Imaginary number
o	Constant temperature
s	Solid phase
$sample$	Sample
$scaled$	Scaled
t	Tangential
tc	Thermocouple
th	Thermal
w	Wall
x	Axial
0	primary gas
1	secondary gas

List of Abbreviations

Abbreviation	Description
AF	Air firing
ASU	Air Separation Unit
BAT	Best Available Technology
CAPEX	Capital Expenditure
CCS	Carbon Capture and Storage
CCUS	Carbon Capture, Utilization and Storage
CFD	Computational Fluid Dynamics
CPU	CO_2 Processing Unit
DIN	Deutsches Institut für Normung
ECRA	European Cement Research Academy
ESP	Electrostatic Precipitator
FD	Forced Draft Fan
FGR	Flue Gas Recirculation
GDP	Gross Domestic Product
IEA	International Energy Agency
IEAGHG	IEA Greenhouse Gas R&D Programm
IFRF	International Flame Research Foundation
IPCC	Intergovernmental Panel on Climate Change
IRZ	Internal Recirculation Zone
KSVA	Kohlenstaubverbrennungsanlage
M.A.S.	Mono Airduct Systems
MEA	Monoethanolamine
NDIR	Nondispersive Infrared
OEM	Original Equipment Manufacturer
OF	Oxyfuel

Abbreviation	Description
OPEX	Operational Expenditure
PG	Primary Gas
PSA	Pressure Swing Adsorption
R&D	Research and Development
RTE	Radiative Heat Transfer Equation
RTS	Reference Technology Scenario
SCR	Selective Catalytic Reduction
SDS	Sustainable Development Scenario
SIMPLE	Semi-Implicit Method for Pressure-Linked Equations
SNCR	Selective Non-Catalytic Reduction
SRF	Solid Recovered Fuel
STP	Standard Temperature and Pressure
TOC	Total Organic Carbon
UV	Ultraviolet

1 Introduction

1.1 Baseline situation Carbon Capture

Global warming and its related goals to avoid climate change are topics that dominate the socio-political and economic agenda. According to the multinational consulting firm PricewaterhouseCoopers, the world economy is projected to nearly triple by 2050 [1], while greenhouse gas emissions should be in parallel reduced by more than half and become net-zero by the same year [2], [3]. This ambitious goal requires substantial stronger investments in advanced low-carbon technologies. A recent report published by the IPCC states that in order to limit global warming to 1.5°C the investment in energy systems should be in the range of 2.5% of the world GDP [4].

There is a consensus among the majority of the world´s climate scientists about the role of fossil fuels as responsible for current climate change. However, as the world economy moves forward, emerging economies will continue to rely on fossil fuels to provide energy and sustain their growth and development. Though the exploitation of renewable forms of energy is increasing worldwide, their intermittency will need to be hampered with the flexibility of fossil fuel electricity generation. As observed in Table 1.1, the overall share of fossil fuels in primary energy demand will continue to occupy an important place in fuel consumption in the years to come.

Carbon capture, and storage (CCUS), a portfolio of technologies that prevents carbon dioxide emissions from entering the atmosphere and safely stores them deep underground in dedicated geological sites, is a critical tool in climate change toolbox. These set of technologies could allow a continuous usage of fossil-based fuels while substantially reducing greenhouse gas emissions to the atmosphere.

CCUS is not restricted to fossil fuel power generation. These technologies can significantly shrink the CO_2 footprint of any kind of industrial processes such as steel, cement and chemicals manufacturing. For some of these industrial processes, CCUS represents the only technical option to comply with CO_2 reduction goals.

Table 1.1: World primary energy demand by fuel and scenario. Values in million metric tons of oil equivalent. Adapted from [5].

			Current Policies		Sustainable Development	
	2000	**2017**	**2025**	**2040**	**2025**	**2040**
Coal	2308	3750	3998	4769	3045	1597
Oil	3665	4435	4902	5570	4334	3156
Gas	2071	3107	3616	4804	3454	3433
Nuclear	675	688	803	951	861	1293
Renewables	662	1334	1798	2642	2056	4159
Solid biomass	646	658	666	591	396	77
Total	**10027**	**13972**	**15782**	**19328**	**14146**	**13715**
Fossil fuel share	*80%*	*81%*	*79%*	*78%*	*77%*	*60%*
CO_2 emissions (Gt)	23.1	32.6	35.5	42.5	29.5	17.6

In summary, CCUS allows a smooth transition towards low-carbon technologies without compromising energy supply and reliability for economic growth. Furthermore, CCUS is one of the few carbon abatement technologies that can be exploited to achieve “carbon negative” emissions if biomass-based fuels are combusted.

1.2 Decarbonizing the cement sector

Cement production is one of the world´s most energy and CO_2 intensive industrial production processes. In a recent report, emissions from this process were estimated to account for nearly 7% of the global anthropogenic CO_2 emissions [5]. Unlike in power generation where the main source of CO_2 emissions is the combustion of fossil fuels, in cement production, the main source of these emissions is the thermal decomposition of carbonates to produce clinker, the main component of cement. This calcination reaction represents, with near 63%, the largest share of CO_2 emissions of this process. The combustion of fossil fuels (e.g. coal, petroleum coke) represents approx. 37% of the total CO_2 emissions while other minor indirect sources of CO_2 are electricity and transportation [6]. This means, even if 100% of fossil fuels used in the cement industry are replaced with biomass-based alternative fuels, the largest portion of CO_2 emissions (process-related) would still be emitted.

The production of one kg of clinker releases approximately 0.84 kg of CO_2 [6], [7]. Over the years, the cement industry has established several measures to reduce its CO_2 emissions; those include fossil fuel substitution, an increase of process energy efficiency and clinker substitution. Even though these efforts have reduced the global CO_2 emissions significantly, further reductions by such conventional measures are limited. In a technology road map to decarbonize this industry prepared by IEA [8], the need of innovative technologies, including carbon capture and storage (CCS) was highlighted as the most important lever to realize the sustainable transition of the 2 degree Celsius Scenario (2DS) in this industry by 2050.

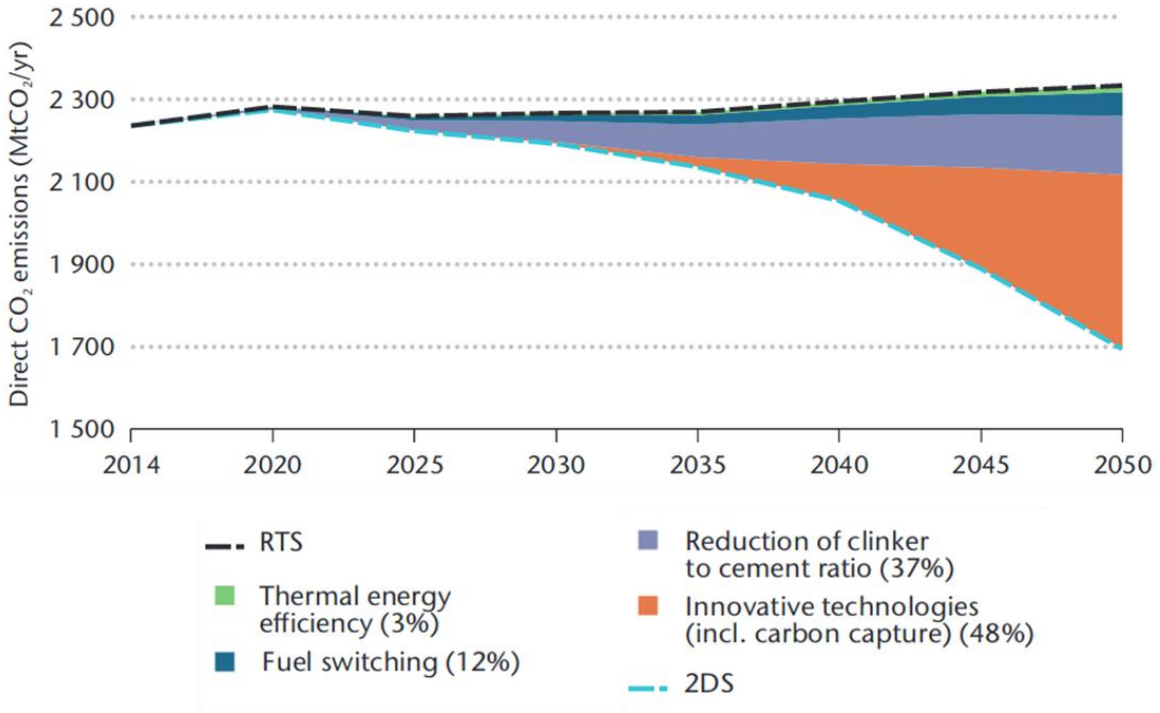

Figure 1.1: Key levers to reduce CO_2 emissions from cement plants. RTS: Reference Technology Scenario. 2DS: Sustainable transition of the 2 degree Celsius Scenario [8].

Oxyfuel combustion has been highlighted as one of the most promising CCS technologies in recent techno-economic analyses [9], [10]. This technology demands combustion to be carried out in the presence of nearly pure oxygen and recirculated flue gases rich in CO_2. The implications of a combustion atmosphere rich in CO_2 on the pyroprocessing of cement clinker need to be evaluated in order to ensure its technical feasibility without compromising the stability of the rotary kiln operation and product quality. The CEMCAP Project, a European H2020 Project focused on investigating the implementation of CCS technologies in the cement industry, devoted a significant amount of work to investigate three key components of a cement plant that are directly affected

when imposing oxyfuel combustion in the cement kiln. One of these components is the focus of the present work: the main burner of the cement kiln.

1.3 Objectives of the present work

The goal of the present study is the investigation of the combustion behavior of relevant fuel qualities in an O_2/CO_2 atmosphere under cement production conditions. For a correct assessment, the experimental setup should reflect relevant process conditions similar to a rotary kiln including a suitable burner. For this purpose, in the frame of this study, a modern cement burner was downscaled and installed in a semi-technical combustion facility with a capacity of 500 $kW_{th,}$ where combustion tests are conducted. Furthermore, numerical simulations and demonstrations at pilot scale are undertaken with the following specific objectives:

- Determination of the combustion and emission behavior of reference fuels in a O_2/CO_2 combustion atmosphere.
- Determination of optimized oxygen concentration to obtain similar temperature and radiation heat flux profile as in air-blown combustion.
- Determination of optimized burner configuration.

With the above objectives in perspective, this dissertation is organized as follows:

Chapter 2 summarises the current situation and general aspects of carbon capture technology, oxyfuel combustion and burner technology applied to cement production. This introductory chapter is a more extended description of a literature review paper published by the author [11] describing the state-of-the-art research and technology development on oxyfuel combustion for cement production. Chapter 3 presents the work plan and methodology followed to conduct the experimental tests. Chapter 4 is dedicated to the scaling of the burner. Chapter 5 presents the results of the experimental work, which was based on oxyfuel demonstrations in air and oxyfuel modes using the scaled burner. Chapter 6 describes the results of the numerical investigations conducted to investigate a full-scale cement kiln in air and oxyfuel conditions with optimized burner configuration and design. Finally, Chapter 7 presents the final conclusions and recommendations for further research.

For further reference to the reader, the author has published the results of the pre-sent investigations in open access reports and in scientific journals [12]–[14]. The reference [12] describes the main findings of the experimental work conducted with the prototype burner in air and oxyfuel atmospheres focusing on the variables that can be adjusted to obtain similar flame behavior in both combustion modes. The reference [13]

presents the validation of numerical simulation using CFD against the results of the combustion tests in oxyfuel mode. Finally the reference [14] is an open access report that summarizes all the experimental work done with the prototype burner.

2 Present State of Knowledge

2.1 Portland Cement manufacturing process

Cement is a finely ground, non-metallic, inorganic powder, and when mixed with water forms a paste that sets and hardens due to hydration reactions [15]. There are different types of cement according to the application. Portland cement is the most widely used cement in concrete construction. The manufacturing of Portland cement is mainly divided into three steps: raw material preparation, clinker burning process, and cement preparation.

The preparation of raw materials comprises the grinding and mixture of materials to prepare a “raw meal” or “raw mix”. This mixture is mainly composed of limestone with smaller portions of sand and clay typically. These materials supply the required chemistry compounds to the process: $CaCO_3$, SiO_2, Al_2O_3, and Fe_2O_3. In the first stage, limestone is crushed separately while other materials like clay and sand are dried. In the second stage, the crushed and dried materials are milled together with small amounts of additives in predefined quantities in order to obtain a desired raw meal composition. Cement has specific quality requirements; therefore, a precise raw meal composition must be attained to comply with the performance standards (e.g. compressive strength).

After final grinding, the material mix is ready to enter the clinker burning process, which is considered the heart of the cement plant. Figure 2.1 shows a sketch of this process.

The raw meal is fed to the highest section of the pre-heater tower, consisting of a series of vertical cyclones from where the material enters in contact with hot gases from a rotary kiln in countercurrent mode. For the correct operation of the cyclones, a correct relation between material mass flow and gas velocity is crucial. Pre-heating of raw meal in this way helps optimize the energy demand of the process. After passing through a series of cyclones, the temperature of materials increases to near 850 °C and the calcination starts. Calcination is the thermal decomposition of Calcium Carbonate to Calcium Oxide with the liberation of CO_2 (see Eq. 1). This strong endothermic reaction is mainly carried out as the material enters the calciner, a pyroprocessing unit operated at near 1000°C.

$$\mathrm{CaCO_{3\,(s)}} \xrightarrow{heat} \mathrm{CaO_{(s)}} + \mathrm{CO_{2(g)}} \qquad \text{(Eq. 1)}$$

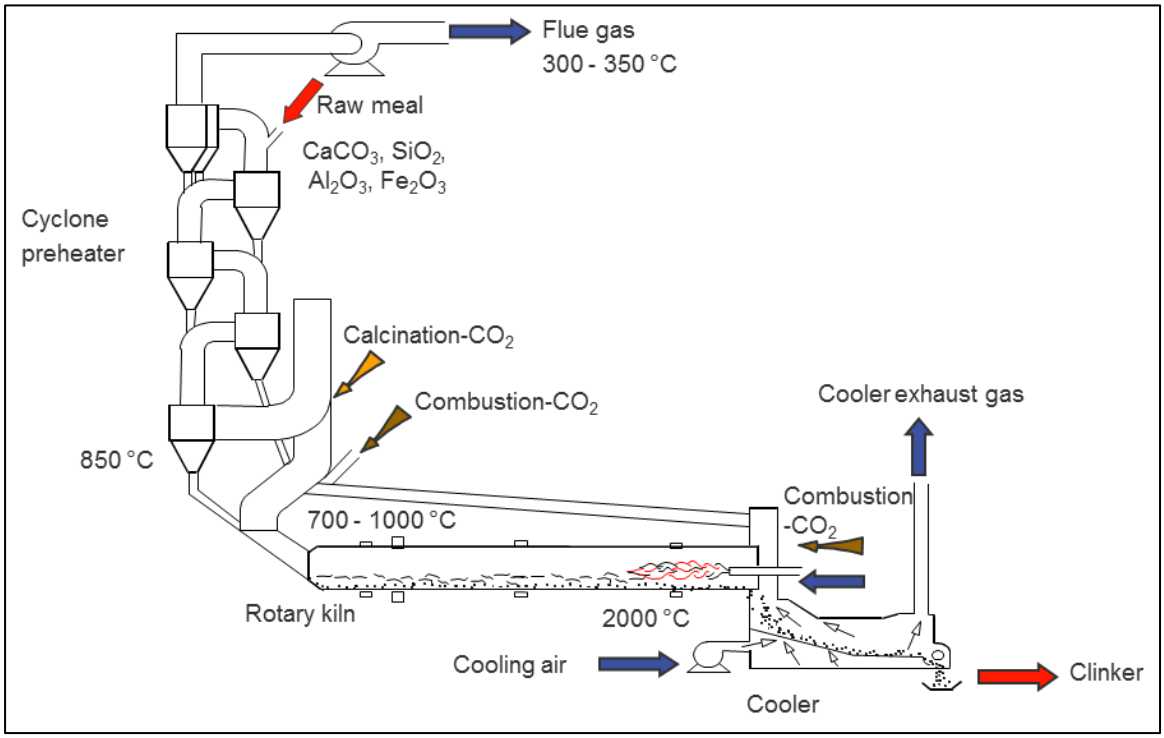

Figure 2.1: Simplified diagram of the conventional cement production process. Adapted from [16].

To obtain a required degree of calcination (conversion to CaO), substantial energy input is supplied to the calciner. Here, either fossil fuels, e.g. coal or petcoke, as well as alternative fuels are employed. The thermal input to the calciner can reach 60% of the total energy demand of the clinker burning process (see Table 2.1), the rest is introduced in the rotary kiln. Air necessary for combustion is provided by the kiln or through a tertiary gas duct, which transports hot gas from the clinker cooler.

The calcined materials are received at the upper end of the rotary kiln end and are heated as they slowly approach the kiln burner. In the kiln burner, fossil or alternative fuels are used to increase gas temperature near 2000 °C. Fuel energy is transferred to the material both by radiation from the flame and indirectly via the kiln walls. The materials reach a sintering temperature near 1450°C and partially melt forming new chemical compounds or clinker phases, which give cement its properties. Table 2.1 presents the chemical reactions that take place in the clinker burning process including respective enthalpies of reaction.

Table 2.1: Main chemical reactions in the clinker burning process. Adapted from [17]

Reaction	Equation	Standard enthalpy of reaction (kJ/kg)
Dissociation reactions		
	$CaCO_3 \rightarrow CaO + CO_2$	+1780
	$MgCO_3 \rightarrow MgO + CO_2$	+1395
Formation of clinker phases		
	$CaO + Al_2O_3 \rightarrow CA$	-110
	$2\ CaO + Fe_2O_3 \rightarrow C_2F$	-114
	$2\ CaO + SiO_2 \rightarrow C_2S$	-732
Sintering reactions		
	$CA + C_2F + CaO \rightarrow C_4AF$	+25
	$CA + 2\ CaO \rightarrow C_3A$	+25
	$C_2S + CaO \rightarrow C_3S$	+59

The most important constituent of Portland cement is Alite and Belite. Alite or tricalcium silicate (Ca_3SiO_5 abbreviated C_3S) represents 50-70% of clinker mass and it is one of the most crucial constituent phases for early strength development (ages up to 28 days). Belite or dicalcium silicate (Ca_2SiO_4 abbreviated C_2S) constitutes 15-30% of Portland clinker. It reacts slower than Alite and is substantially responsible for strength at later ages. Other minor clinker constituents are C_4AF and C_3A. Tetra calcium alumina ferrite (C_4AF), has a chemical composition of $4CaOAl_2O_3Fe_2O_3$. This compound has little contribution to strength and it is responsible for the colour in cement. Finally, C_3A, also called Aluminate or tricalcium aluminate, has a chemical composition of $3CaOAl_2O_3$. This compound contributes little to long term strength. Besides, it provides early heat generation in hydration (rapid hydration) thus responsible for the setting time of cement. More information on clinker phases can be found elsewhere [17].

In the last section of the kiln, the material temperature is reduced to preserve the relation between Alite and Belite. Here, reaction conditions, as well as the cooling velocity, are crucial to preserve clinker quality [18]. The temperature in this zone is controlled by the burner position inside the kiln and the secondary gas temperature.

The hot granulate clinker exits the kiln and is cooled usually by air flow in a grate, called clinker cooler. In order to improve heat recovery, the energy content of this air stream

is used for combustion in the kiln burner (secondary gas) and/or injected in the calcination chamber (tertiary gas).

The last step in cement manufacturing consists of grinding the clinker to required fineness and adding additives e.g. gypsum, which control the setting of concrete during hydration.

2.2 Carbon capture technologies in cement production

Carbon capture technologies, in general, are classified into three types: pre-combustion, post-combustion and oxy-combustion (oxyfuel).

Pre-combustion technologies refer to the reaction of fuel and oxygen in a gasifier to yield a synthesis gas (or syngas), which consists mainly of carbon monoxide and hydrogen. Additional hydrogen is recovered in a shift reactor by the reaction of carbon monoxide (in the syngas) with water vapor.

Post-combustion methods are also known as end-of-pipe CCS technologies. The advantage of these methods lies in the ability to be installed in any operating plant without altering its operation. Either physical or chemical methods are employed to capture carbon dioxide from the exhaust gas stream. Some of the more common methods are:

- Absorption with solvents
- Adsorption with sorbents
- Cryogenic separation
- Membrane separation

By far, the most common capture method is the absorption with regenerable solvents. Typically, amine-based solvents, e.g. MEA, are injected in countercurrent mode in an absorber reactor to separate CO_2 from other gases. In a second step, the weak bond between CO_2 and solvent is broken using heat at a low-pressure in a stripping column.

The third method is oxyfuel combustion. This capture technology uses pure oxygen from an air separation unit as an oxidant for combustion. By removing nitrogen from the air, the composition of the combustion products results in a high share of CO_2 followed by water vapor and minor amounts of pollutants.

The specific application of carbon capture technologies for cement production can be classified in post-combustion and oxyfuel combustion methods. Pre-combustion methods in the frame of cement production are of less importance since they can only capture fuel-derived CO_2 emissions, not the large proportion emitted by the raw meal calcination.

2.2.1 Post-combustion carbon capture

Post-combustion methods applied to the gaseous effluent of a cement plant have been extensively investigated during the last years and even test trials have been carried out at semi-industrial scale. Table 2.2 shows post-combustion methods tested for cement production in recent years as well as some advantages and disadvantages related to them.

Table 2.2: Post-combustion CCS technologies tested for cement production.

Method	Advantages	Disadvantages	Demonstrations
Chemical solvent scrubbing	Maturity of technology. High capture efficiency (80 – 95%). Regeneration of solvent possible.	High thermal energy demand for solvent regeneration. Cost of solvent. Equipment corrosion. Emissions related to solvent degradation.	• NORCEM CCS project – Aker Solutions ACC™, Brevik, Norway [19] • Capitol – SkyMine™ project, Texas, USA [20]
Physical adsorption	Reversible process. Adsorbent recycling possible. High adsorption efficiency (> 85% - mainly with PSA). Resistant for long-term use.	Cooling and drying of the flue gas. High energy demand for CO_2 desorption. High adsorbent temperature. Influence of SO_x and NO_x on sorbent performance.	• NORCEM CCS– RTI project, Brevik, Norway [21] • CEMEX – RTI project, Houston, USA [22]
Calcium looping	Low energy efficiency loss (4 –7%). A highly promising technology for the cement industry due to heat recovery.	Attrition depending on raw meal/limestone hardness.	• NORCEM – Alstom Power RCC project, Brevik, Norway [23] • ITRI – Taiwan Cement Corp. project [24] • CEMEX-Imperial College of London [25] • CLEANKER project, Piacenza, Italy [26]
Membrane separation	The process has been adopted for separation of other gases. High separation efficiency is achievable.	Influence of minor components (i.e. water, SO_2) on gas permeation performance. High cost and high energy demand for compression equipment.	• NORCEM - DNV GL, NTNU & Yodfat Engineers CCS project, Brevik, Norway [27]

Method	Advantages	Disadvantages	Demonstrations
		Limited CO_2 purity. Large membrane area demand for large facilities.	
Biological capture with algae	Oil produced can be used as bio-diesel or coal replacement. Economically competitive compared to other capture technologies.	The need for process up-scaling to an industrial level. Creation of algae´s products and markets.	• Pond Biofuels bioreactor capture project, St. Marys, Ontario, Canada. [28] • Algae pond in HeidelbergCement's Morocco cement plant. [29]

As shown in Table 2.2, important investigations on post-combustion capture methods for cement production were conducted in the frame of the Brevik Project. In the frame of this project four post-combustion technologies were tested in real cement conditions [27], [30]:

- Chemical absorption with amines
- Solid sorbent technology
- Membrane technology
- Calcium looping

Results from these pilot tests were summarized in a Benchmarking study [31], [32], which included information regarding capture rate, feasibility, CAPEX and OPEX costs, and maturity. The conclusion of the Benchmarking highlights that in a 2020 perspective amine technology is the only one ready for a full-scale project [32].

2.2.2 Oxyfuel carbon capture

Since the early 2000s, the oxyfuel technology has been identified as a CCS technology that could achieve a high capture efficiency at a lower cost than alternative post-combustion processes [33]. Oxyfuel firing uses O_2 instead of air for combustion. The exclusion of N_2 from the process leads to a flue gas composition that consists mainly of CO_2 and H_2O. This stream can be cleaned from impurities, dried, compressed and liquefied for further transport and storage or utilization. In oxyfuel combustion, flue gas recirculation is required to control the temperature in the kiln and to provide suitable gas velocities to the cement process. Many articles and several reviews discussed the application of the oxyfuel concept to power plants [34]–[39]. However, only part of the knowledge from the power sector is transferable to the cement process due to

differences in the process layout and boundary conditions (e.g.: additional CO_2 generation by raw meal calcination, higher temperature of recirculated flue gases, simultaneous material processing, etc.). In the last years, the implementation of the oxyfuel technology in the cement clinker burning process has been discussed and investigated by several research groups, especially in Europe, where the European Cement Research Academy (ECRA) is encouraging the decarbonisation of this industry through oxyfuel technology.

2.3 Oxyfuel technology in cement production

2.3.1 Process configurations

Considering the process stage where combustion takes place two main configurations have been proposed: a partial application with oxy-combustion conditions only maintained in the calciner and a full application when these conditions are applied both in the calciner and the rotary kiln.

A simplified flowchart for the cement manufacturing process is presented in Figure 2.2. The process can be seen as heat exchange flow in countercurrent mode between solid materials and hot gases. This process will be useful to explain the differences between both oxyfuel configurations.

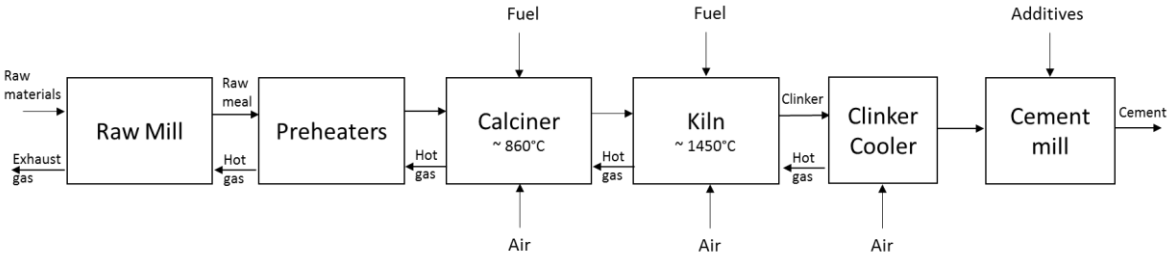

Figure 2.2: Simplified diagram of the conventional cement production process.

Partial oxyfuel

The partial oxyfuel configuration is based on the fact that most of the CO_2 emissions in a cement plant are generated in the calciner. This concept requires two preheater lines for operation. As shown in Figure 2.3, just one of the preheating lines (PH2) is operated under oxyfuel conditions. The calciner employs a mixture of flue gases from PH2 and oxygen from an air separation unit (ASU) as oxidizing gas for combustion. The other preheater line (PH1) operates conventionally with the hot gases coming from the air-fired kiln. The preheated material from both preheater lines passes through the oxyfuel fired calciner before entering the kiln.

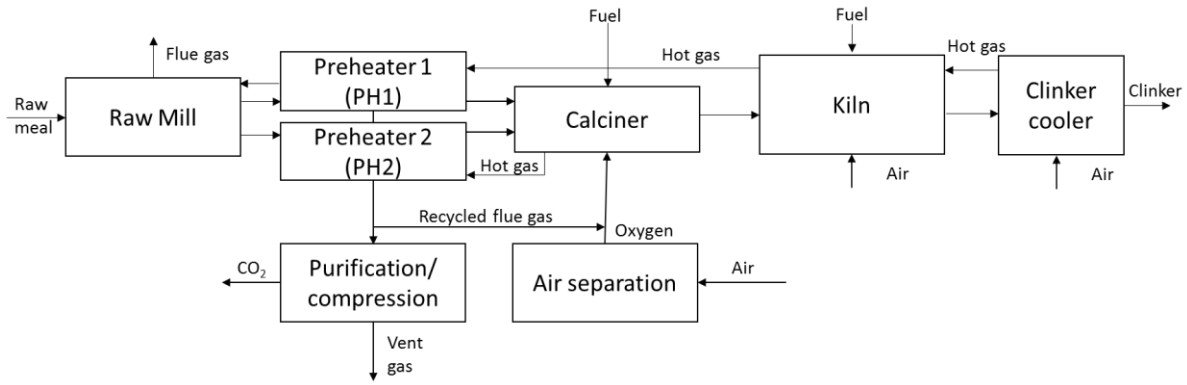

Figure 2.3: Layout of partial oxyfuel configuration.

With this partial oxyfuel configuration between 60% and 75% of the total CO_2 emissions can be captured [16]. The partial oxyfuel process has the advantage that other installations (kiln, cooler, raw mill) are operated conventionally, which makes it a very promising CCS option for retrofitting to existing cement plants. However, modifications and efforts to avoid air leakage in the preheating tower are required. In addition, different operating conditions in the calciner need to be considered in order to avoid changes in clinker quality. The first pilot plant tests of this configuration have been successfully performed in the FLSmidth R&D pilot plant in Dania, Denmark [40].

Full oxyfuel

In a full oxyfuel configuration, both the calciner and the cement kiln are operated under CO_2/O_2 conditions (see Figure 2.4). The full oxyfuel configuration requires no complete redesign of the preheating tower as the partial oxyfuel process. However, the kiln burner needs to be adapted or redesign for oxyfuel operation. Some authors [41], [42] have highlighted the necessity of incorporating a two-stage clinker cooler into the flue gas recirculation loop to increase energy efficiency.

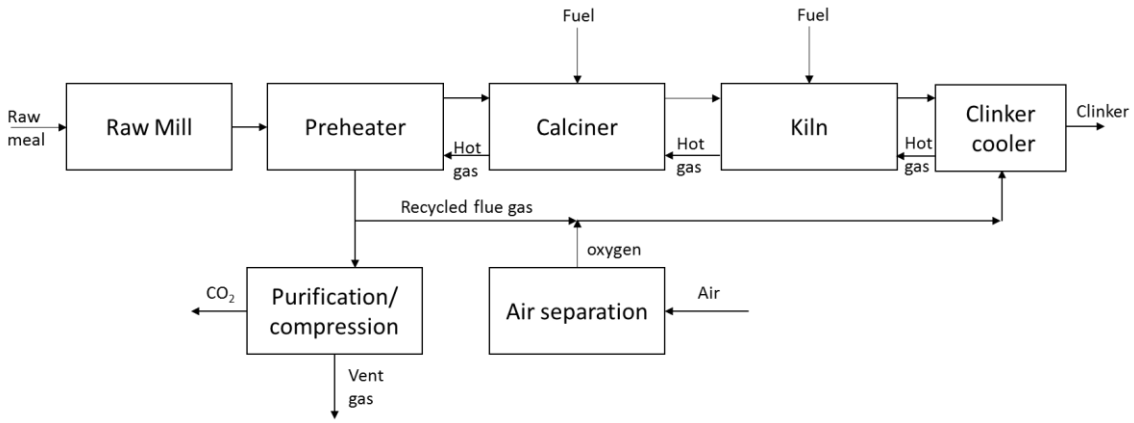

Figure 2.4: Layout of full oxyfuel configuration.

With a full oxyfuel implementation higher CO_2 capture rates are possible (>90%), but also a higher overall electrical energy consumption is expected (higher quantity of O_2 from ASU required). A comparison between the partial and full oxyfuel configuration is given in Table 2.3.

Table 2.3: Evaluation of different aspects concerning the full and partial oxyfuel technology. Adapted from [43].

Topic	Partial Oxyfuel	Full Oxyfuel
Spec. unabated CO_2 emissions [$kg_{CO2}/kg_{clinker}$]	0.25-0.35	0.08-0.1
CO_2 capture efficiency	60-75%	90-99% (depending on CPU)
Retrofitting	feasible with constraints	complex, but feasible
Electric energy demand (compared to conventional process, per $t_{clinker}$)	+82%	+104%
Thermal energy demand (compared to the conventional process, per $t_{clinker}$)	+8%	+/-0%
CO_2 avoidance costs (direct emissions-retrofit) [43]	53.8 €/t_{CO2}	41.2 €/t_{CO2}
Plant modification	Calciner and preheater	Clinker cooler and burner
Sealings	High effort necessary	Higher effort necessary

Topic	Partial Oxyfuel	Full Oxyfuel
Maintenance	Higher effort due to more piping and aggregates	Effort mainly resulting from sealings
Influence on material	High influence on calcination	High influence on calcination, less influence on clinker formation

2.3.2 Modifications/additions for an oxyfuel cement plant

In contrast to post-combustion CO_2 capture technologies, the oxyfuel process requires the addition and modification of several aggregates involved in the production of cement clinker. Highlights regarding these aggregates are mentioned in the following sections.

ASU (Air separation unit)

A reliable supply of oxygen for combustion is required. For a medium-sized cement plant the oxygen demand is estimated to be around 0.25-0.35 $t_{O2}/t_{clinker}$. For logistical reasons, such an amount of oxygen can only be provided by an on-site supply system. From all oxygen production methods, cryogenic distillation is currently the most mature and reliable technology for the production of large quantities of oxygen [44], [45].

The O_2 purity produced in the ASU has a direct influence on the composition of the flue gases. For oxyfuel implementation in power plants, an oxygen purity from the ASU of 95-97 vol% was claimed to be an economic optimum [46], [47]. Due to the high power consumption of the ASU aggregate, the design of more energy-efficient methods is still a research necessity.

Flue Gas Recirculation

The flue gas recirculation (FGR) ratio, defined here as the ratio of gas flow that returns to the furnace (in this case the cement kiln) over the volume of gases that exit the burning process, provides an additional degree of freedom to control the temperature profile in the kiln by adjusting the O_2 content in the oxidant. In power plant applications typical values of FGR ratio range from 60 to 80 [34], [36].

In a CFD study, Granados [48] investigated the influence of eight different FGR ratios in oxyfuel operation on several operational parameters in a 2.5 m diameter and 40 m

length cement kiln. The value of the FGR ratio was calculated as the proportion of the flue gas volume from the kiln that is recirculated (calciner and preheater cyclones were not considered). They employed a non-premixed combustion model based on mixture fraction, as well as a Lagrangian approach for particle tracking. Additionally, a discrete ordinates model was used for heat transfer modeling by radiation. He found that a recirculation ratio of around 72% (35% O_2 in the combustion gas) could reproduce similar flame lengths as in air-fired operation.

In a cement plant, the FGR ratio should additionally be adjusted to maintain suitable flow velocities for material transport in the calciner and for correct cyclone operation in the preheating tower. Considering this restriction an IEAGHG report [43] suggested that the FGR ratio (calculated as the total gas volume recirculated to the clinker cooler over the flue gas exiting the preheating tower) should be in the range of 52-56% for retrofitting a full oxyfuel configuration to existing cement plants, while a range between 35-40% was suggested for partial oxyfuel implementations.

In the full oxyfuel configuration, another concern is whether the recirculated flue gas needs to be dried or can be injected to the kiln without moisture removal. The main drawback of wet recirculation is the risk of corrosion since the condensation of moisture and subsequent absorption of acidic gas components such as SO_2 may lead to the formation of acid condensates. Due to that risk, the installation of a flue gas condenser is recommended.

Clinker cooler

With the purpose of energy recovery, the clinker cooler is added to the flue gas recirculation circuit. Considering the cooling demand of a clinker cooler in a full oxyfuel configuration a new concept has been proposed, which requires the cooler to be split into two stages [41], [42]. The first stage is to be operated with recirculated flue gas that is subsequently used for combustion in the kiln, while the second stage is operated with supplemental air that completes the clinker cooling and is then used for raw material drying or fuel preparation.

Recently, a prototype clinker cooler in oxyfuel conditions has been tested in a plant located in Hannover, Germany. The aim of that experimental work was the investigation of the cooling performance as well as the influence of cooling gas (CO_2 from tanks) on clinker quality. The results showed no negative impact on cement strength due to cooling with CO_2 rich gas. Sealing for false air ingress, as well as moisture and dust content in recirculated gases, were highlighted as aspects that demand attention [49], [50].

CPU (CO_2 purification unit)

This aggregate is essential to obtain the conditions for CO_2 transport and storage. For oxyfuel demonstrations in the power sector, several configurations have been proposed and tested. The knowledge that has been developed for the power industry can be used for cement applications. However, there are differences in the flue gas composition of a conventional cement plant after dedusting compared to power plants. For example, the concentration of CO_2 is approximately doubled in the cement case, while differences in the concentration of minor components also exist.

With recent progress on cryogenic technology, it is possible to achieve a CO_2 purity >99%. However, the operating costs increase with target purity. A recent study mentioned an increase of 1.82 €/ton_{CO2} when increasing target purity from 95 to 99.9% in an oxy-cement plant [51].

2.4 Kiln Burner Technology

2.4.1 Air-fired burner technology for cement production

Over the last 50 years, kiln burner technology has undergone substantial improvements. From single-channel burners to two-channel and more recently multiple-channels, burner design has evolved into more complex geometries in order to adapt to new fuels and emission limits. Nowadays cement burners provide flexibility in adjusting flame shape and intensity by controlling primary airflow in axial and swirl channels as well as by adjusting burner position in the kiln [52].

Air for combustion mainly comes from the clinker cooler at a temperature between 600 °C – 1000 °C before it is transported to the kiln hood. This gas stream is named *secondary air* and supplies the bulk of oxygen for combustion. Secondary air temperature should be as high as possible in order to maximize heat recovery.

Only a small portion of air, typically in the range of 6% - 13% flows through the burner [53]. This stream, called *primary air* is divided into axial, radial, swirl, central or fuel carrying streams according to the burner design. Primary air is injected at high velocity by firing fans and gives the fuel momentum. As a result, there is an acceleration of the coal dust flow and the hot secondary air is drawn into the coal flow as sketched in Figure 2.5, which assures the ignition of the fuel.

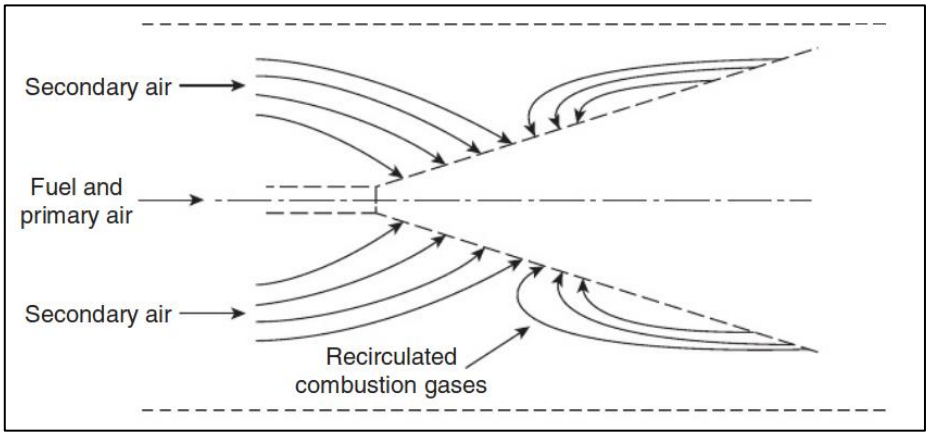

Figure 2.5: Secondary gas entrainment in rotary kilns [54].

Recirculation of combustion gases to the flame root supports flame stabilization. As observed in Figure 2.5, the recirculation of the combustion gases takes place as soon as secondary gas entrainment declines. This onset of external recirculation (i.e. longitudinal start point of recirculation) is governed by the excess of primary air momentum and can be estimated by the Craya-Curtet similarity parameter m [54] which is given by:

$$m = -1.5\,a^2 + a + k\frac{a^2}{\frac{D_0}{D_1}} \qquad \text{(Eq. 2)}$$

where:

$$a = \frac{(U_0 - U_1)\rho_0\left(\frac{D_0}{2}\right)^2}{U_1\rho_1\left(\frac{D_1}{2} - \delta\right)^2 + (U_0 - U_1)\rho_0\left(\frac{D_0}{2}\right)^2} \qquad \text{(Eq. 3)}$$

This parameter m is essentially a ratio between the primary and secondary jets momentum and a measure of the aerodynamic mixing of the two streams [55]. The value of m varies between unity and infinity. However, practical experience has shown that m = 1.5 ensures that the burner jet will have momentum in excess of that required to entrain all the secondary gas present in the burner vicinity and to cause vortex shedding that returns combustion products to the flame front [54]. For flames with $m \leq 1.0$, the entrainment is such that the flame tends to be long and lazy [55]. For cement kilns, a parameter value between 2 and 2.5 has been seen to produce short and intense flames [56].

The parameter k is the jet shape factor (1 for round jets), D_0 and D_1 are the primary and secondary air equivalent diameters, respectively; U stands for velocity, ρ for density and δ is the boundary layer thickness.

A common parameter in burner design is specific flame momentum. Specific flame momentum G_0 is defined as the sum of all primary air mass flows multiplied by their respective absolute ejection velocities (at the burner tip) divided by the burner thermal power input [57]:

$$G_0 = \frac{\dot{M}_0 U_0}{Q_{th}} \quad \text{(Eq. 4)}$$

The rate of entrainment of secondary air into the primary air and fuel jet depends on the ratio of the momentum of the combined jet of primary air and fuel, to the momentum of secondary air. Therefore, the higher the flow rate and velocity of primary air, the more rapid the fuel/air mixing [54].

In the '80s, kiln burner design was driven by the goal of lowering NO_x emissions. Later, in the mid '90s the IFRF CEMFLAM projects were launched to try to advance the understanding of NOx formation in rotary kilns and derive burner design principles. The main conclusions were that the design criteria for a low NOx kiln burner for solid fuel should include [58]:

- Specific flame momentum lower than 7 N/MW
- Flame ignition as close to the burner as possible
- The minimum of air mixed with the coal volatiles prior to ignition, achieved by creating an internal recirculation zone

Further, low NOx strategies were tested based on the following concepts:

- Reducing (optimizing) primary air mass flow
- Recirculating flue gas
- Oxygen enrichment [59]
- Staged combustion
- Water injection

Some of the above-mentioned concepts were only tested briefly due to low efficiency in significantly damper NO_x formation [60]–[62]. One of the concepts that prevailed is the optimization of primary gas mass flow. It was observed that due to the high flame temperature and the availability of oxygen and nitrogen at the base of the flame, the levels of NO_x were increased significantly. To moderate these emissions, the mass flow of primary air was reduced and the pressure increased. A parallel advantage is

the increase in energy efficiency since the percentage of cold primary air is replaced with hot secondary air and less electrical energy is demanded by primary air fan/blowers. However, a lowering of the primary gas in excess would weaken flame momentum and further secondary gas entrainment. The current consensus among most OEMs for a kiln burner is that total primary air (not counting conveying air) should be from 6-10% of stoichiometric air [57]. Besides, low-NOx burners are also designed to produce very early ignition, especially of the volatile compounds in the fuel, in an oxygen-deficient atmosphere.

The demand for low NO_x burners has declined in the last decades as secondary methods for NO_x reductions e.g. SCR and SNCR spread in the cement industry. Currently burner design is focused on increasing the use of non-fossil fuels to lower the emission of non-biogenic CO_2, especially through the design of multichannel burners.

Multichannel burners offer significant benefits, among others the possibility to include a permanent-installed oil-gun burner, which minimizes additional efforts of inserting additional piping during kiln startup. Furthermore, it allows tailoring of residence time for specific solid fuels, which results in advantageous to increase the burnout of difficult fuels like petcoke or alternative fuels [54]. The sketch of a typical kiln burner with these characteristics is presented in Figure 2.6.

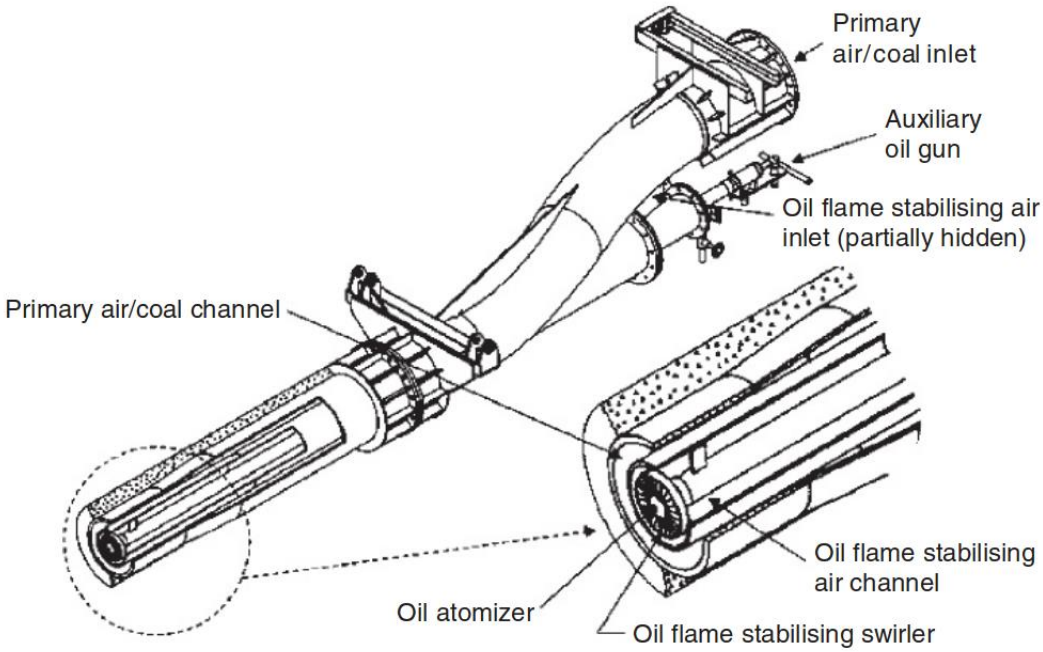

Figure 2.6: Typical pulverized coal burner with auxiliary oil firing for rotary kilns [54].

One important difference between OEMS is how primary air is injected and distributed in the burner tip. Classic multi-channel burners have two to four independent channels for primary air. This stream is then divided into the axial, radial, swirl, etc. compartments and the amount of gas flowing through each respective channel is controlled by valves, dampers or multiple fans/blowers which are used. The position of the coal channel with respect to the primary gas channel (in between, outside or inside) varies from OEM to OEM. In some cases, the primary air channels are located outside the coal channel to delay the mixing of fuel with secondary gas and thus lower flame temperature and NO_x formation.

A recent innovation is the use of adjustable primary air jets instead of channels (see Figure 2.7). The angle of injection of primary gas is adjustable, which allows a more efficient shaping of the flame without energy loss in the mixing of two air streams (axial and radial). Additional advantages include avoidance of high-pressure blowers and a reduction of the burner diameter.

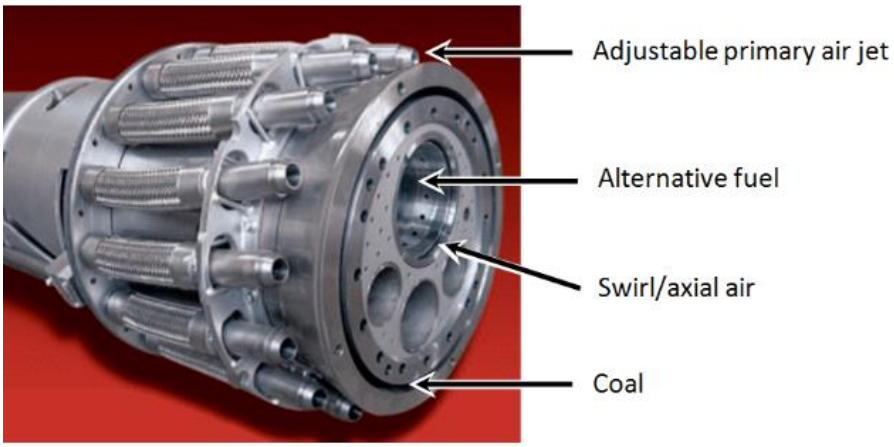

Figure 2.7: Use of adjustable primary air jets in cement kiln burners [63].

2.4.2 Operational implications in oxyfuel burners

The implementation of a rich-CO_2 combustion atmosphere in the rotary kiln demands dedicated investigations to determine its impact on kiln operation and to preserve the clinker quality. Following aspects related to oxyfuel combustion need to be considered in burner design:

- Possible increase of ignition delay under CO_2/O_2 atmospheres

- Altered heat transfer to walls (CO_2 and H_2O emit and absorb radiation at certain wavelengths compared to N_2)
- Volume reduction of flue gases (when maintaining similar adiabatic flame temperature)
- Aerodynamic influence of the char gasification reaction.

Kiln burner concepts for cement production need to be reviewed in order to determine if improvements in the design are needed. The next sections present state-of-the-art technology in cement kiln burners and recent developments in oxyfuel burner concepts.

2.4.2.1 Aerodynamics

ECRA reported results from a CFD simulation of a rotary kiln including a generic burner and kiln hood where flame behavior under air and oxyfuel conditions was assessed comparatively at different recirculation ratios [42]. Standard sub-models for turbulence and heat transfer, including conduction and radiation to the kiln walls were employed. The Lagrangian multiphase model was used to account for fuel solids' kinematics and additional reaction submodels were included to account for the homogeneous and heterogeneous fuel reactions as well as the mineral phase reactions.

The simulation of a generic burner in oxyfuel operation shows a doubling of the CO production in the sintering zone (see Figure 2.8) with corresponding temperature drop compared to the reference case. This behavior is attributed, to a large degree, to the endothermic nature of the CO_2 gasification reaction of char, also known as Boudouard reaction:

$$C_f + CO_2 \rightarrow 2CO \qquad \text{(Eq. 5)}$$

Further, flame aerodynamics is disturbed by a high concentration of CO in the near burner area. The result is a long flame caused by volume expansion and oxidation of the produced CO to CO_2, which shifts the energy towards the kiln inlet away from the burner.

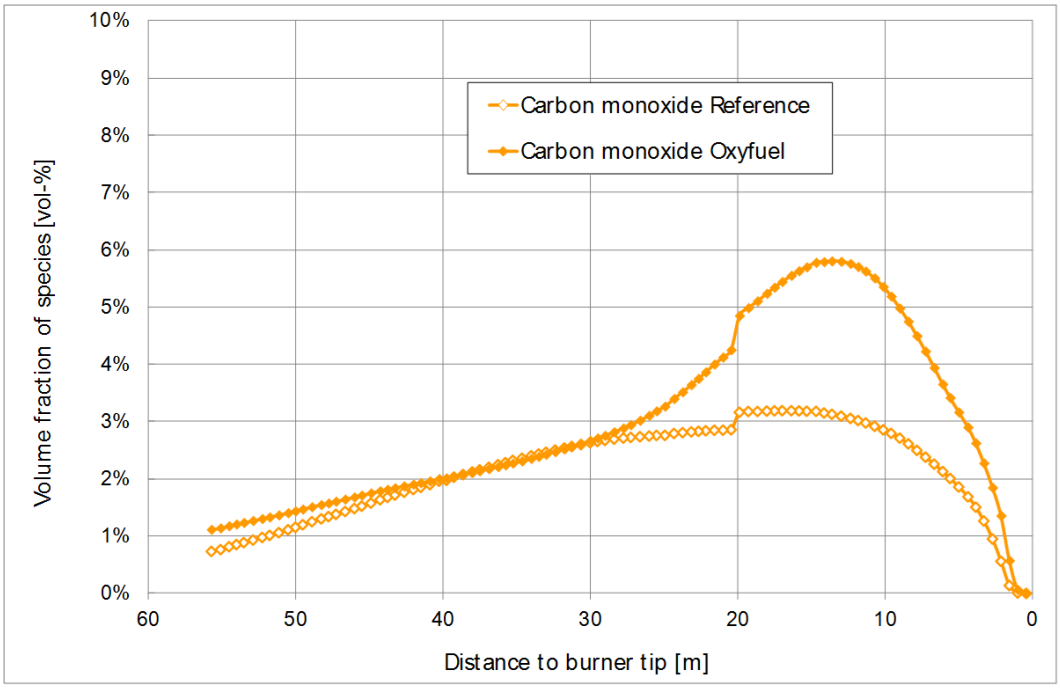

Figure 2.8: Simulation results of carbon monoxide profiles in reference (air) and oxyfuel firing mode [42].

To counteract these phenomena the following design characteristics were suggested for an optimized oxyfuel kiln burner design:

- Higher oxygen concentration in the primary gas to enhance the re-oxidation of CO.
- Increase of swirl angle to obtain a more compact and stable flame.

These findings are similar to the results of experiments in the power industry sector. Scheffknecht et al. [36] discussed the effect of elevated levels of CO_2 on the ignition of coal particles in oxyfuel burners for power plants. It was reported that high CO_2 levels can impact coal ignition negatively when the aerodynamics of the burner and the proportion of O_2 in the oxidant are not optimized. In pilot-scale tests, it was found that a key aspect in the design of oxyfuel systems is the introduction of sufficient O_2 into the pulverized coal flame to ensure a satisfactory ignition and flame stability.

2.4.2.2 Heat transfer

In cement kilns, heat transfer is mainly dominated by radiation. Moreover, radiation heat transfer is determined by particle and gas radiation. In oxyfuel combustion, higher concentrations of CO_2 and H_2O in combustion gases are expected. In comparison to N_2, these gases are not transparent to radiation. This difference has a high impact on

radiation behavior inside the kiln. Andersson et al. [64] employed a 100 kW lignite-fired reactor to compare the radiation intensities when changing from air to oxyfuel combustion. They found that gas radiation intensity is increased considerably due to a high concentration of CO_2 under oxyfuel conditions even when the temperatures are slightly lower. In the numerical simulation of Granados, et al. [48] the effect of FGR on convective and radiative heat transfer during oxy-coal firing in a cement kiln was also investigated. The discrete ordinates model was implemented for the calculation of radiative heat flux, which included radiation interaction between gas and particles. The model predicted an increase in radiative heat flux of 2-4.5 times higher under oxyfuel conditions compared to the reference air-fired kiln for all FGR ratios investigated.

Additional investigations, however, highlight that the impact of gas radiation is reduced by the overlapping of particle-gas radiation. Andersson et al. [64] reported similar radiation intensity profiles between air and oxyfuel mode explained by the influence of particle radiation dominating flame radiation as shown in Figure 2.9. Johansson et al. [65] used the same Chalmers 100 kW reactor to investigate the influence of particle and gas radiation under oxyfuel conditions. They calculated the radiative properties of particles using the Mie theory, while gas radiation was modeled using the statistical-narrow-band model. Their results show that the presence of particles suppresses the influence of gas composition. Variations in temperature and dust load were also identified as parameters that influence radiation heat transfer. In an investigation made by Bäckström et al. [66] in a down-scaled pilot of an iron ore kiln furnace, the influence of particle radiation was also addressed. They combined radiation measurements and modeling while firing two different coals and mixtures with biomass. In their results, particle radiation was observed to dominate the heat transfer in the furnace with only a small contribution of gas radiation.

The operation of a cement kiln produces a very significant concentration of dust even in the burner area. Under oxyfuel conditions, the effects of increased gas radiation could be suppressed by the influence of particle radiation in the near burner region. If dust concentrations are altered due to gas volume reduction, as in oxy-conditions, the relevance of particle radiation becomes even higher. The challenge of new investigations is to determine to which extent radiation to the material is altered and which oxyfuel configuration (FGR ratio) could produce a similar heat transfer profile in the kiln to avoid detrimental effects in clinker quality.

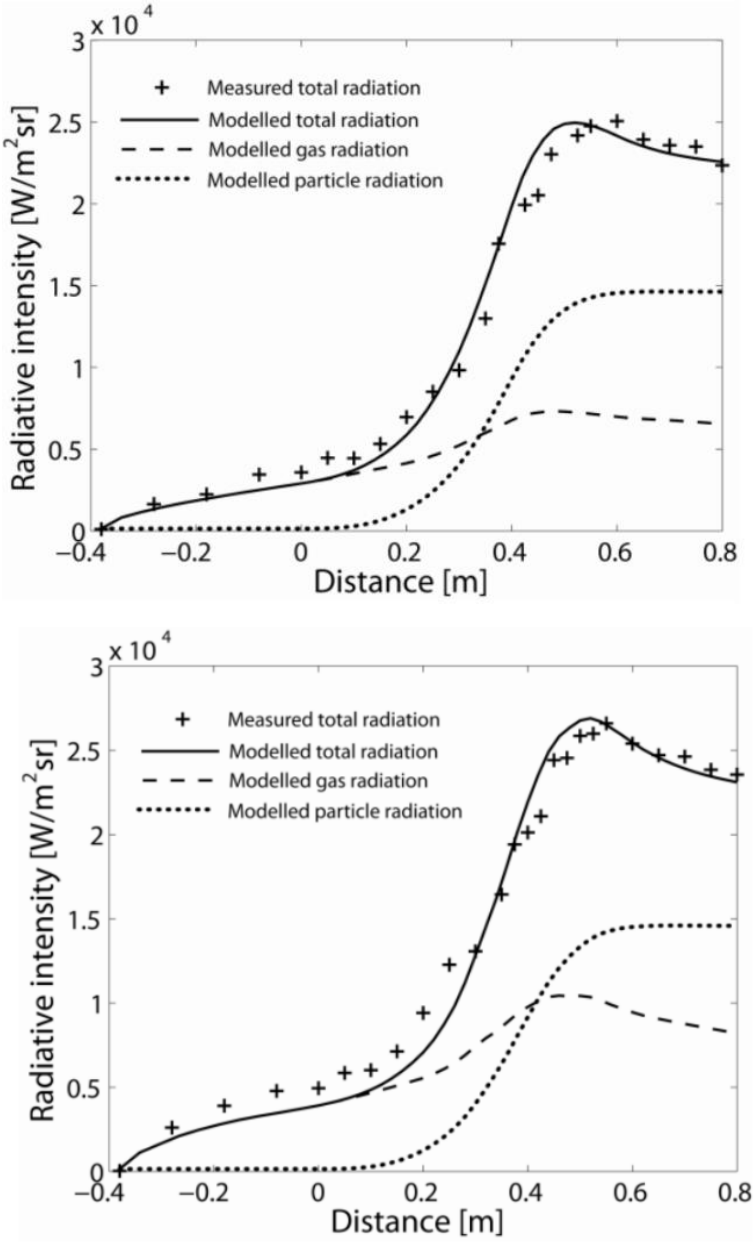

Figure 2.9: Radiation intensity measured and modeled over the radial axis at 384 mm from burner in air (top) and oxyfuel OF27 (bottom) firing conditions [64].

2.4.2.3 Clinker quality conservation

The issue of product quality is a major concern when discussing the possible effects of implementing oxyfuel conditions in both the calciner and kiln. In a calciner, the calcium carbonate contained in the raw meal is converted to calcium oxide and carbon dioxide. Calcium carbonate exists in equilibrium with calcium oxide and carbon dioxide

at a wide range of temperatures according to Figure 2.10. By increasing the partial pressure of CO_2 in the calciner, as observed in oxyfuel conditions, higher reaction temperature is required to shift the reaction to the CaO and finally to obtain a comparable degree of decarbonation/calcination.

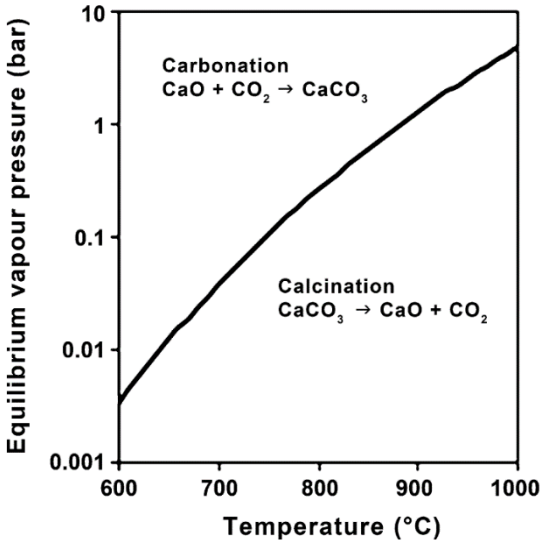

Figure 2.10: Equilibrium vapor pressure of CO_2 over CaO as a function of temperature. [67]

Koring [68] performed laboratory tests to investigate the degree of decarbonation (i.e. the proportion of $CaCO_3$ that is converted to CaO) of three different raw meals at different temperatures and CO_2 partial pressures and fixed residence time. The target of the experiment was to assess the influence of oxyfuel combustion conditions on raw material calcination with regard to the other constituents and simultaneous reactions. Pure calcium carbonate was also analyzed and results used as a reference. The samples were placed in glass containers and were electrically heated for 5 minutes in a tube reactor while exposed to a defined gas atmosphere. Since the calcination reaction is fast, equilibrium was assumed. As the last step, the degree of decarbonation of each sample was determined through mass loss quantification. The results show a shift of the equilibrium reaction at higher CO_2 partial pressures (>0.9 bar) to higher temperatures (by up to 80°C). Paneru [69] obtained similar results in an electrically heated drop-tube furnace used to investigate the shift in temperature when changing the calcination atmosphere from air firing (AF) to oxyfuel conditions (OF), see Figure 2.11. The experiments were conducted with and without fuel combustion in a temperature range from 760 – 960 °C and samples were taken to analyze the degree of calcination. A 60 °C temperature shift was registered in order to achieve a calcination degree of 90%.

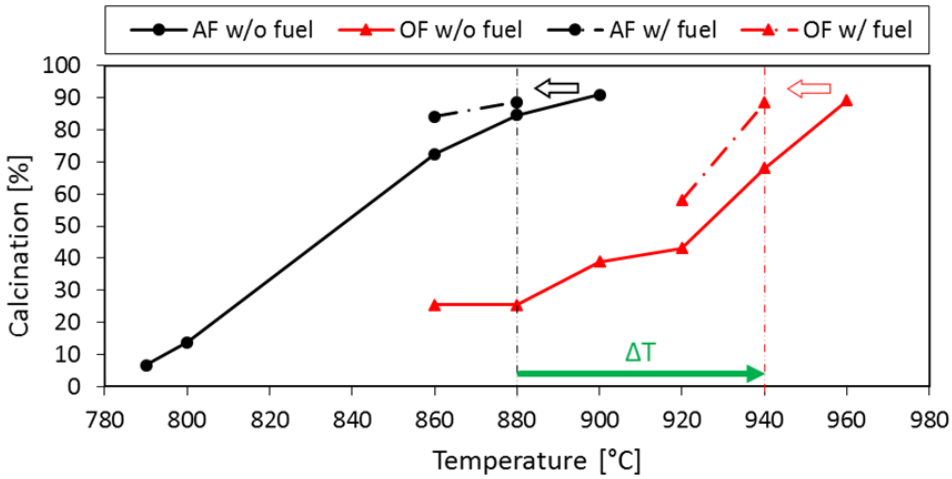

Figure 2.11: Temperature shift during calcination in oxyfuel conditions. Legend: AF:Air firing; OF:Oxyfuel; w/o fuel: without fuel addition; w/ fuel: with fuel addition [69].

In line with these results, investigations were performed on the FLSmidth R&D Dania oxyfuel pilot plant's calciner. Their results showed high raw meal calcination levels (>92%) when the calciner temperature was increased by 60-70 °C compared to the conventional air-fired temperature. Changes of temperature in the cyclones and pre-calciner are commonly associated with the formation of deposit build-ups. However, during these investigations, no increase in the formation of build-ups was observed under oxyfuel conditions [40].

ECRA [42] performed additional experiments to investigate the effect of high CO_2 partial pressures on clinker phase formation and cooling to assess possible impacts on clinker quality. An electrically heated laboratory kiln was used for the production of clinker samples under CO_2-rich conditions. Subsequent to the burning, the lab clinker was cooled under CO_2 rich atmospheres to assess the re-carbonation. The laboratory analysis showed only slight variances (below 3%) in key properties such as compressive strength, compared to standard cement. It was concluded that impacts of oxyfuel combustion on the clinker quality seem to be negligible.

2.4.2.4 Energy demand

The electrical demand of an oxyfuel cement plant is greatly influenced by the integration of the ASU and CPU. As shown in Figure 2.12, together the CPU and ASU and additional auxiliary components account for an increase in the electrical energy demand of 86% and 128% compared to the base scenario in the partial and full oxyfuel configurations, respectively [16].

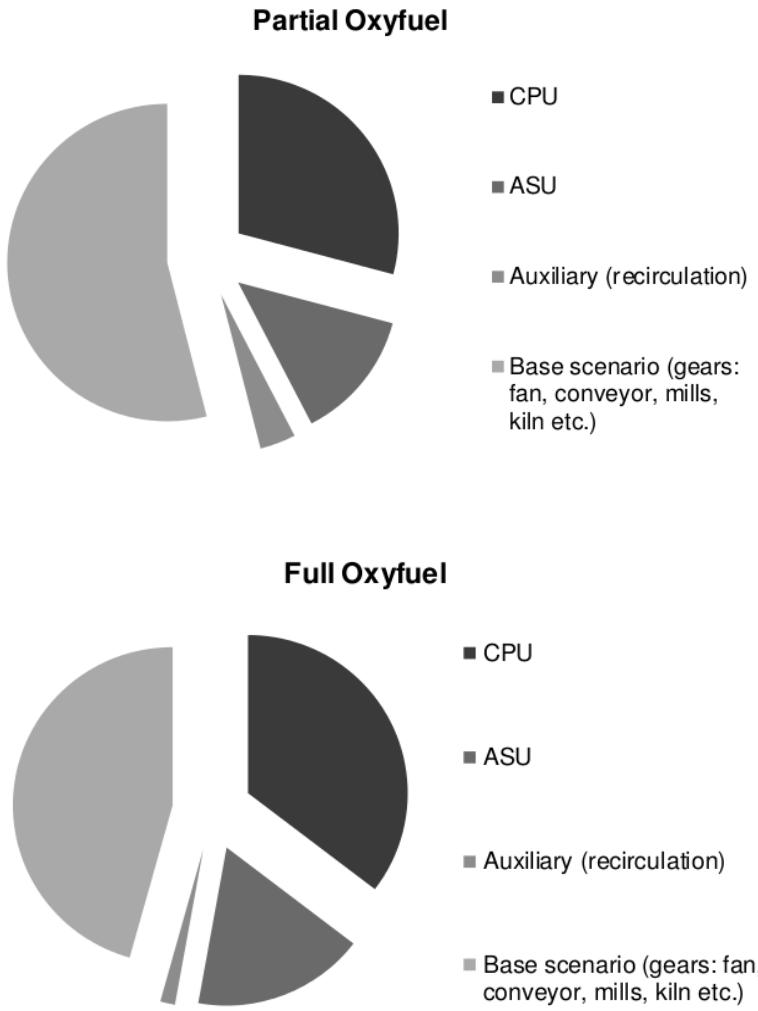

Figure 2.12: Electrical energy demand in partial (top) and full (bottom) oxyfuel configurations. [16]

On the other hand, the thermal energy demand is influenced by the recirculation ratio in the full oxyfuel configuration. The thermal demand of a reference BAT cement plant is 3026 kJ/$kg_{clinker}$. Figure 2.13 shows the parabolic behavior of the fuel demand with respect to the recirculation ratio obtained from process simulations. When decreasing the amount of recirculated gas, the concentration of oxygen is increased and less thermal (fuel) energy is needed in the process to reach the required temperatures. However, for recirculation ratios lower than 0.44 the thermal energy demand starts to increase again. The reason for this is that the total volumetric flow is not high enough to sufficiently preheat the material to the calcination temperature for which then additional thermal energy is required.

The thermal energy balance in the case of the partial oxyfuel configuration is different. In a conventional operation, tertiary air with a temperature of up to 1000°C is fed to the calciner. In contrast, in oxyfuel mode, the recirculated flue gases with a temperature of about 380°C are used instead. In order to achieve comparable temperature levels, a solution could be the addition of gas-to-gas heat exchangers. In any case, the thermal demand for a partial oxyfuel configuration is increased by approx. 8-9% [16].

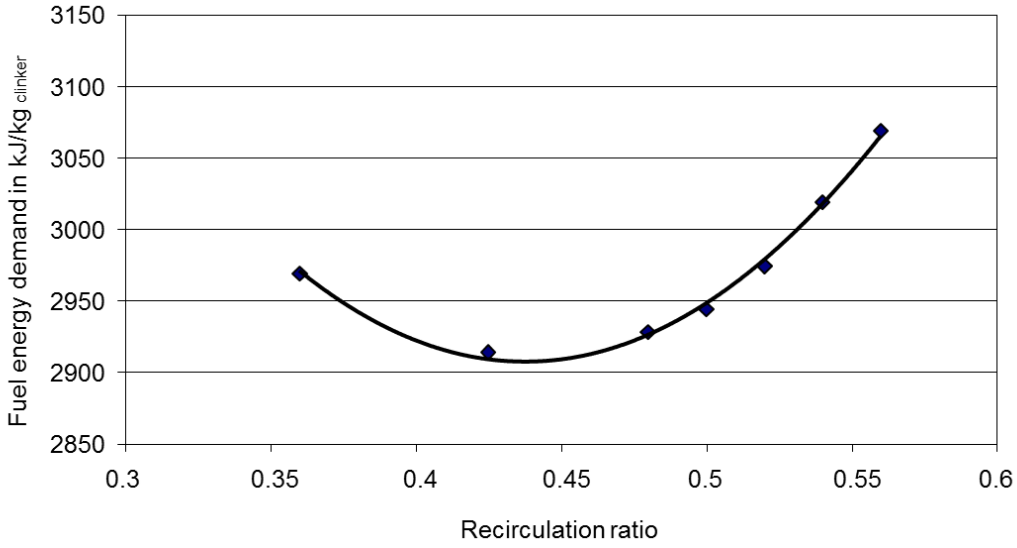

Figure 2.13: Simulation results on the fuel energy demand of a full oxyfuel plant related to the recirculation ratio [68]. Thermal demand of a reference BAT cement plant is 3026 kJ/$kg_{clinker}$.

Some preliminary studies have investigated ways to decrease energy demand. Process simulations and thermodynamic modeling have been used to asses different integration concepts in both full and partial oxyfuel configurations [70], as well as for the optimization of ASU and CPU aggregates [71].

2.4.2.5 Air ingress

Impurities in the oxygen stream produced in the ASU and the level of air ingress in the process have a significant detrimental effect on final CO_2 purity. Figure 2.14 shows the effect of air ingress on the CO_2 concentration at the inlet of the CPU. Ordinary cement plants have an air ingress of 6-10%, while old facilities can have more than 10% air ingress [72]. The higher the proportion of non-condensable gases (N_2, Ar, O_2, NO_x) in the CO_2-rich stream to liquefy, the higher the pressure and lower the temperature that is required in the CPU to separate these impurities, which increases the power consumption of this process. According to the results of a study made by PRAXAIR [51],

an increase in air ingress from 2% to 6% increases the relative power for condensation in the CPU by 3%. Other studies highlight an increase of 2.7-3.5% in the specific power consumption of the CPU (kJ/kg$_{CO2}$) per 2% increase in false air [73].

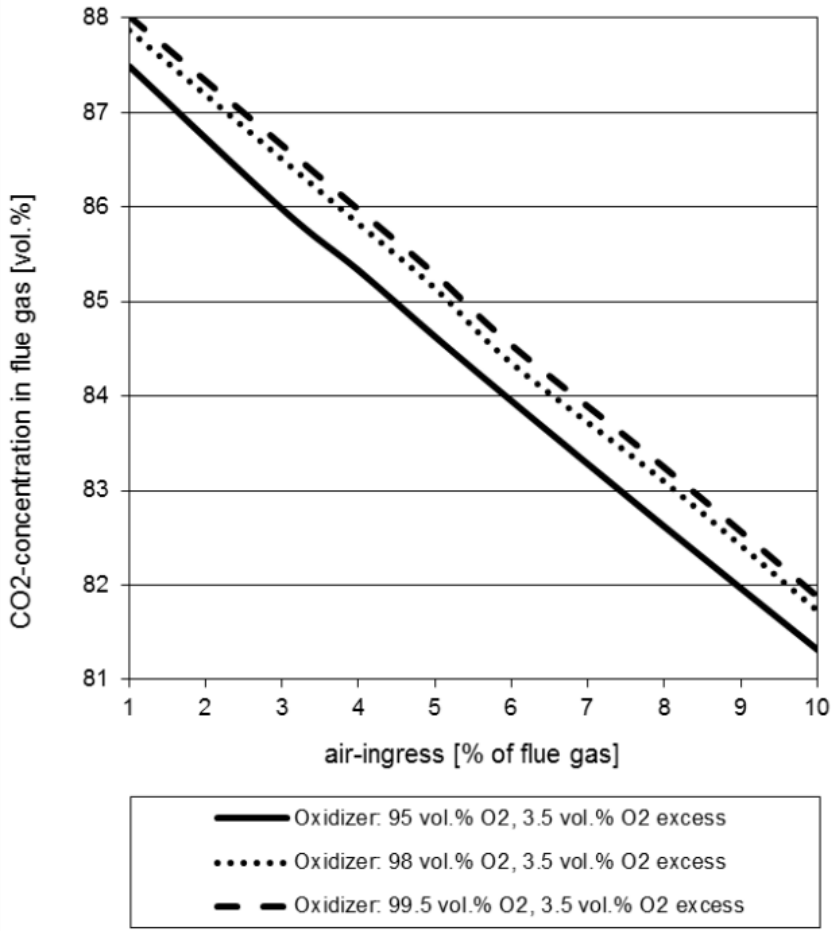

Figure 2.14: Effect of air ingress on CO_2 concentration at the inlet of the CPU. [68]

In cement plants, the kiln in- and outlets are the biggest sources for air ingress. Other major sources are poke holes, inspection doors, and pendulum flap boxes. Some ideas have been proposed to reduce air ingress: Zeman [41] proposed to encase the kiln in a non-structural sheath charged with CO_2. This and other possible solutions have been investigated as part of the ECRA CCS project. They found that a combination of increased efforts of maintenance in inspection doors, poke holes and pendulum flap box covers, together with gas-flushed sealings in feed ports and sluices are the best techno-commercial solutions [42].

2.4.2.6 Refractory lining

Depending on the kiln zone and the thermal and chemical stresses, basic or non-basic refractory lining is used in the cement kiln and calciner. A non-basic refractory material

is normally used in sections where lower thermal stresses are expected (e.g. preheater, calciner, kiln inlet/outlet, cooler). ECRA [42] performed laboratory tests to investigate the durability of basic and non-basic refractory material under oxyfuel conditions using an electrically heated furnace. Their results showed that brickwork consisting of basic material withstands the modified firing atmospheres, while the non-basic material is affected by a higher degree of thermo-chemical attack. According to these results, the refractory lining should be adjusted in the zones where non-basic material cannot withstand oxyfuel operation.

2.4.3 Impact on pollutant formations

NO_x

In contrast to coal power plants, where only approx. 20% of total NO emissions origin from the Zeldovich mechanism (i.e.: thermal NO_x produced from airborne N_2), in cement kilns due to higher operational temperatures, thermal NO_x is the dominant mechanism for NO_x formation in the main firing [74], [75]. Cement plants that implement a firing system in the calciner offer the possibility to reduce NO_x emissions. The calciner firing system works on a lower temperature level, compared to the kiln burner, therefore the fuel-NO_x generation is the main source of these emissions.

An advantage of oxyfuel technology is the exclusion of air-borne N_2 from combustion, which directly affects the generation of thermal NO_x. Furthermore, some NO_x reduction occurs as the recirculated flue gas passes through the reducing zones near the flame where recirculated NO_x can be reburned efficiently. This reduction has been reported to depend on the residence time and burner stoichiometry [36], [76].

Despite an anticipated lower specific NO_x emission (i.e.: in mg NO_x/MJ_{th}), considerably higher NO_x concentrations are possible in the oxyfuel fired process compared to the air-fired one, depending on flame temperature and burner design.

SO_2

Sulfur compounds are introduced in the cement clinker process from two sources: raw meal and fuel. Raw material-borne sulfur is existent as sulfate and sulfide. Sulfide from raw material as well as fuel sulfur is oxidized in the kiln system, mainly to SO_2. However, due to the alkaline nature in the sintering zone and calciner, most of the SO_2 forms sulfates after reacting with the calcined raw meal. Just a small portion of produced SO_2 exits the calciner with the flue gases while most of it is bound to the clinker in the form of sulfates and therefore, captured by the process [77], [78].

Due to the capture behavior that eliminates sulfur oxides from the cement process flue gas, knowledge generated for the power sector regarding oxyfuel SO_2 emissions is not directly applicable to the cement sector. However, due to reduced volumetric flow rates at recirculation ratios above 21% in oxyfuel operation, increased SO_2 concentrations are locally possible. Moreover, enrichment of SO_2 levels can be expected if SO_2 is recirculated with the flue gas. In the full oxyfuel configuration, an additional sulfur sink of the process is present in the form of the flue gas condenser within the recycle loop that can eliminate practically all sulfur oxides from the recirculated flue gas. It was shown in the power sector at the Callide oxyfuel pilot plant that with the addition of caustic solution to this direct contact cooler condenser SO_2 could be removed down to concentrations below 10 ppm [79]. With such a configuration in a full oxyfuel cement plant, no considerable changes in sulfur levels and loads are expected compared to an air-fired system. This remains to be demonstrated in an integrated full oxyfuel cement demo trial.

Mercury

Mercury and its related compounds are highly volatile and show a cyclic behavior in the clinker burning process. The sources of mercury are both the raw materials and fossil fuels. Fuel-mercury is volatized as elemental mercury (Hg°) in the kiln, while raw material mercury is volatized in the pre-heater. As flue gas temperature decreases some of the mercury reacts to form $HgCl_2$ and HgO. The formed HgO reacts further with chlorine to form $HgCl_2$ or $HgSO_4$ below 325°C [80]. These compounds and residual elemental mercury travel with the exhaust gases to the kiln filter. At lower temperatures (<200 °C) a portion of oxidized mercury condenses onto the kiln dust and returns to the preheater tower building an external cycle. The rest of mercury leaves through the stack. If the exhaust gases are linked to the raw mill operation some of the mercury returns with the raw meal. Besides, some cement plants are equipped with a so called “kiln bypass”, which consists of a partial removal of the gases at the kiln inlet to avoid enrichment in the system.

The fate of mercury during oxyfuel combustion for the specific application in the cement production is an open field of research. However, some studies on the impact of a rich O_2/CO_2 combustion atmosphere in mercury speciation are available. These studies have been done mainly for the power sector and have therefore, limited applicability to the cement industry. The studies reveal variable results. Axelbaum and Biswas [81] investigated mercury speciation during combustion of coal in mixtures of O_2/CO_2 and air. They found similar ratio of oxidized to elemental mercury (approximately 4:1) in the flue gas of both combustion conditions. Similar result was found by Fry et al. in the comparison of air and oxyfuel combustion of a bituminous coal in semi-industrial

facilities [82]. Spörl et al. reported a significant increase in the ratio of oxidized to elemental mercury during oxyfuel combustion compared to air firing of three Australian coals. Their investigations were conducted in a 20 kW_{th} once-through furnace with impurities injection [83]. Higher mercury removal via particle-bound mercury during oxyfuel combustion has also been reported by several authors [84], [85]. However, this result has been explained by a higher proportion of unburned carbon in fly ash compared to air firing.

Dust

Regarding dust control in the cement clinker process, mainly two types of dedusting devices are employed: electrostatic precipitators (ESP) and fabric filters [15]. Results from power plant pilot tests under oxyfuel conditions indicate a smoother operation and a higher level of voltage (~50%) compared to air firing [86]. On the other hand, no serious concerns have been reported regarding the performance of fabric filter units [87].

The rest of SO_2, NO_x, and Hg that are not captured in previous units (dedusting filters, deNO_x, deSO_x) and the flue gas condenser, can also be removed in the CPU. At high pressure, NO_x and SO_x can dissolve and therefore be efficiently removed from the flue gas with condensing water or with an additional scrubber during or after flue gas compression [88], [89]. As shown by Stanger et al. [90] also Hg can be dissolved in the formed nitric acid and thus be removed with the acid condensates. Another possibility is the capture by activated carbon, for example in a carbon bed after compression. Different configurations of the CPU have been proposed and tested in pilot oxyfuel power plants. A combined SO_x and NO_x removal system called sour gas compression, for example, was tested in Vattenfall's oxyfuel pilot plant. However, an important issue observed was the corrosion of parts of the compressor by the acidic condensates and the formation of deposits [91], [92]. To date, it is still not clear which is the best CPU configuration for flue gas conditioning. Moreover, it is yet to be determined, what levels of impurities are expected from an oxyfuel cement process and what would be the best CPU arrangement for such a system. In these respects, more research is required in the future.

2.5 The future of oxyfuel in cement production

The attention towards the implementation of CCS technologies increases steadily, especially in Europe, where the CO_2 allowances have experienced an important price increase in the last years. The European Cement Research Academy (ECRA) launched in 2007 a long-term CCS research project funded by ECRA members and

industrial project partners. The goal is to examine the technical and economic feasibility of CCS for application in the cement industry [93]. This project has studied the high-potential carbon capture technologies and has identified oxyfuel combustion as the most cost-effective solution [42]. This result is in alignment with a recent European project called CEMCAP, where both post-combustion and oxyfuel combustion CCS technologies were investigated and then benchmarked for its application in the cement industry. According to the published techno-economic analysis [9], [94], oxyfuel is the option that demands the lowest CO_2 avoidance cost (see Figure 2.15).

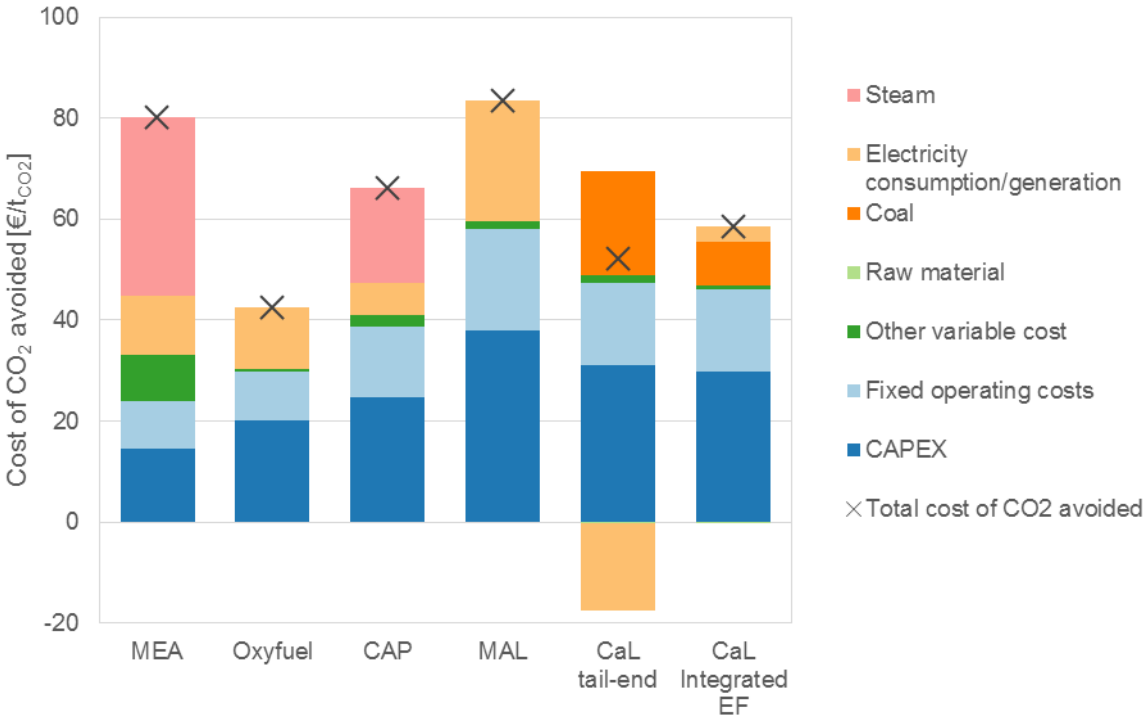

Figure 2.15: Cost of CO_2 avoided. Comparison and breakdown for the investigated capture technologies in the CEMCAP Project [9]. MEA: Monoethanolamine, CAP: Chilled Ammonia Process, MAL: Membrane-assisted CO_2 liquefaction, CaL: Calcium looping, EF: Entrained Flow.

The pre-engineering studies of an oxyfuel cement pilot plant have been completed and the next phase is the conduction of the first demonstration tests at an industrial scale [95]. Due to the high CAPEX and OPEX required for an oxyfuel plant, a full deployment of this technology is only economically feasible if the price of the CO_2 allowances meets the price of the CO_2 avoidance.

3 Experimental Method

This chapter contains a description of the work program and the methodology for the investigation of the oxyfuel burner and firing concept. This section also presents the test facility and the undertaken modifications in the furnace and experimental set-up to conduct the pilot tests under operation conditions relevant to cement production. A detailed description of fuel qualities used during the tests together with a description of instrumentation and measurement methods are presented in this chapter. Finally, relevant parameters to evaluate the quality of the measurements are presented.

3.1 Work Program

The experimental investigations presented in this work have the goal of testing and evaluating the combustion performance of reference fuels in an O_2/CO_2 atmosphere under cement production conditions. The work plan and methodology to achieve this goal are depicted in Figure 3.1. These investigations are based on the premise that retrofitting of current cement production facilities is preferred over new machinery design. Therefore, the compatibility of modern burner designs currently on the market to oxyfuel operation is investigated and preferred over a new burner design. The investigations were carried out with a downscaled version of a modern burner currently in the cement market.

The test facility was adapted in order to carry out burner tests in relevant operating conditions. A major adaptation was the design and incorporation of a flexible preheater system for secondary gas flow to account for temperature increase in a clinker cooler. In a first step, the experimental work was focused on investigating the combustion and emission behavior of selected fuels under O_2/CO_2 and O_2/N_2 in the aforementioned adapted facility and with the constructed burner. Later, experimental work was performed focusing on investigating burner settings including individual oxygen enrichment in both primary and overall gas, and the use of swirling flows, together to create similar air-firing combustion behavior. Finally, theoretical investigations supported by CFD simulations were conducted to investigate the upscaling of the burner prototype and optimized configuration in a full-scale cement kiln operated in oxyfuel combustion.

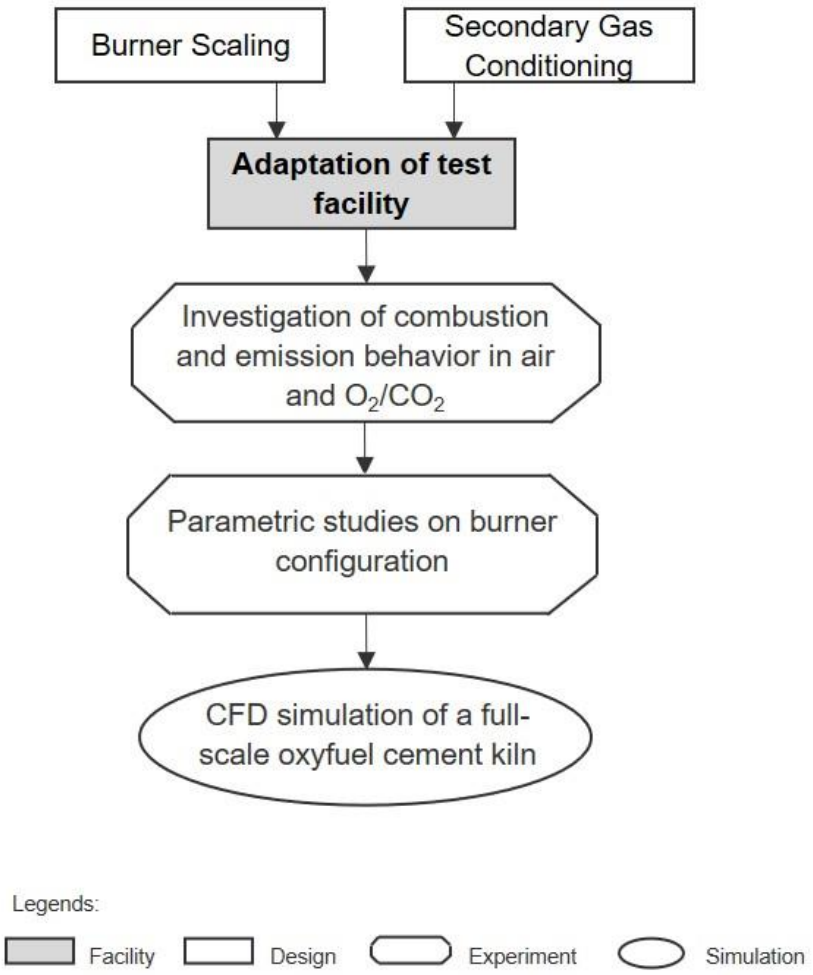

Figure 3.1: Work program to develop an oxyfuel concept for retrofitted cement kiln burners.

The measurement campaigns can be divided into three categories according to the fuels used. Table 3.1 presents a summary of the test cases and investigated parameters in each campaign.

Table 3.1: Overview of test cases according to fuels used.

Fuel	Test cases	Parameters tested
Petcoke	Air case	Temperature profile
	OF27	Gaseous species
	OF32	Total heat flux
		Radiative heat flux
		Fuel Burnout
Lignite	Air Case	Temperature profile
	OF29	Gaseous species
	OF32	Total heat flux
		Radiative heat flux
		Oxygen enrichment in primary gas
		Fuel Burnout
Lignite + SRF	Air Case	Temperature profile
	OF30	Gaseous species
		Oxygen enrichment in primary gas

In the experimental campaigns using petcoke as fuel, three combustion cases were compared: a reference air case and two oxyfuel cases with 27 and 32 vol.% O_2 in total gas for combustion. These oxyfuel cases were selected considering that in a retrofit scenario a temperature profile comparable to conventional air-fired kiln is preferred and in a CO_2/O_2 atmosphere, higher oxygen concentration as in air is needed for this purpose. The differences between tested cases were disclosed by comparing detailed measurements of gas temperature and composition at furnace centerline and 3 radial measurements at different distances from the burner tip. Heat fluxes and radiation heat flux to walls were also measured in the near-wall region.

In the measurement campaigns with pre-dried lignite two oxyfuel cases were demonstrated with 29 and 32 vol.% O_2, respectively. These cases also comply with the condition of similar air-like adiabatic flame temperature and were compared against a reference air case with similar stoichiometry. Besides axial and radial measurements of gas temperature and gas composition, the impact of oxygen enrichment on fuel ignition, heat fluxes to walls and fuel burnout was evaluated.

Finally, SRF, a common alternative fuel used in cement plants was used in co-combustion mode together with pre-dried lignite. Two oxyfuel cases with 30 vol.% O_2 were compared to a reference air case in similar stoichiometric conditions. The investigations were focused on the impact of oxygen enrichment on CO formation in the near burner region, in order to confirm the findings of the second test campaign. In addition, measurements of gaseous species (including SO_2 and NO_x) were also analyzed.

3.2 Description of the Pilot Facility

Burner tests were carried out in the solid-fuels combustion facility (KSVA by its initials in German), installed at the Institute of Combustion and Power Plant Technology of the University of Stuttgart. The facility has been used for decades to test innovative technologies to improve combustion efficiency and reduce pollutant emissions. Though most of the experimental work performed in this facility has served the power sector, its flexibility allows a large range of investigations even to other industry sectors, like cement production. A brief description of the combustion rig and measuring equipment will be given hereafter.

3.2.1 Combustion rig

Figure 3.2 shows a sketch of the 500 kW_{th}-combustion facility. The top-fired furnace has a total height of 7 m and an inner diameter of 0.8 m. The refractory lining covers the inner surface of the upper four meters of the combustion chamber. The furnace is equipped with multiple ports distributed along the height of the reactor where specialized probes are introduced to perform inflame measurements.

The flue gas path is equipped with a NO_x reduction system (SCR), an electrostatic precipitator (ESP), and a bag filter. The injection of secondary gas into the furnace is possible by means of a forced draft fan (FD). This stream is preheated using the furnace outlet gases before it is conducted to the burner. During oxyfuel operation mode storage tanks supply O_2 and CO_2 for secondary gas. Fuel carrier gas during oxyfuel mode is only carbon dioxide.

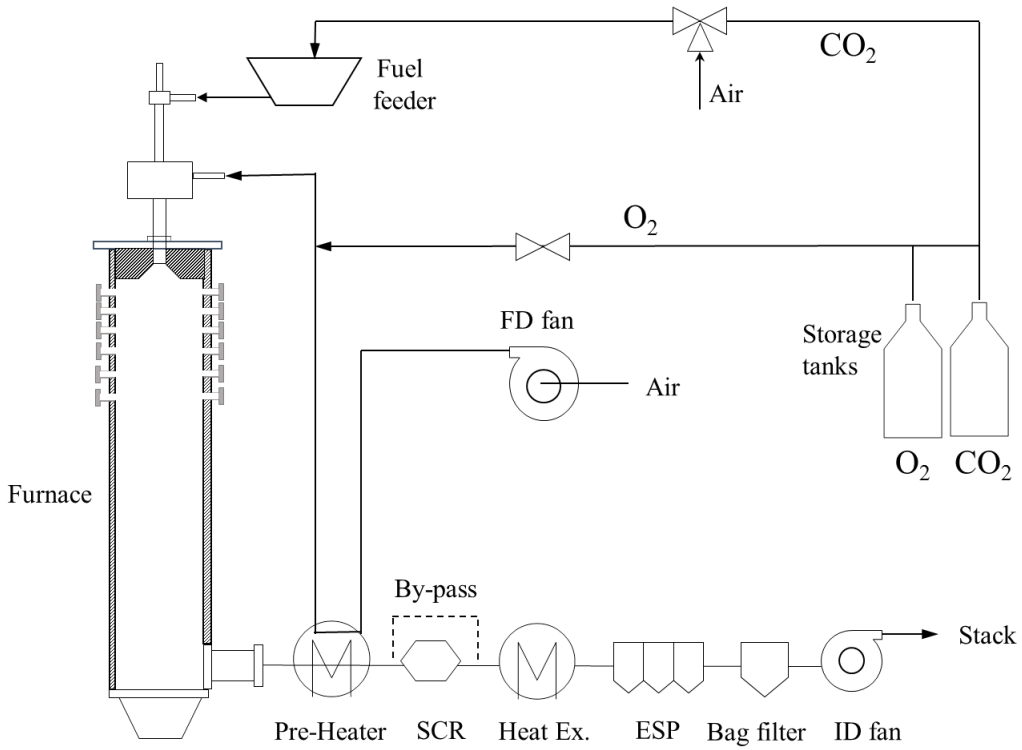

Figure 3.2: 500 kW_{th}-combustion rig at the University of Stuttgart.

3.2.2 Adaptation for cement production conditions

In a typical rotary kiln, three gas lines provide the necessary gas for combustion. Primary gas represents a high-velocity stream injected through the burner and contains only a small fraction of the air needed to burn the fuel (near 15 vol.%). The carrier gas is also injected through the burner, at lower velocity and its main function is the transportation of solid fuel. The secondary gas passes into the kiln outside the burner pipe and supplies the bulk of the oxygen needed for combustion. The secondary gas usually comes from the clinker cooler at high temperatures (> 800 °C).

The facility was modified to incorporate the before mentioned characteristics of cement rotary kilns. The burner is introduced into the furnace (similar to an industrial scale) at a distance of 90 mm. Two gas streams are injected through the burner (primary and fuel carrier gas). The secondary gas line passes directly to the furnace through an annular slot surrounding the burner pipe. Besides, the upper section of the furnace was adapted for these tests by installing an electrical preheater system. Figure 3.3 shows a sketch of the secondary gas preheater system installed in the furnace ceiling surrounding the burner. The secondary gas is distributed to the individual preheaters, each one with a capacity of 15 kW_{el}, by means of a circular manifold. The outlet of the

secondary gas was also modified to account for gas velocities typical in rotary kilns (5-6 m/s). Figure 3.4 shows the adaptations in the facility diagram.

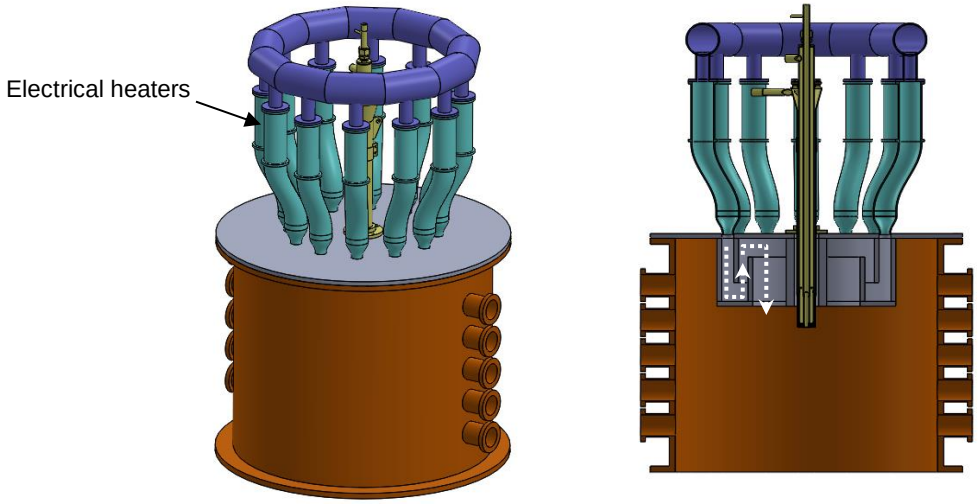

Figure 3.3: Sketch of preheater system for secondary gas.

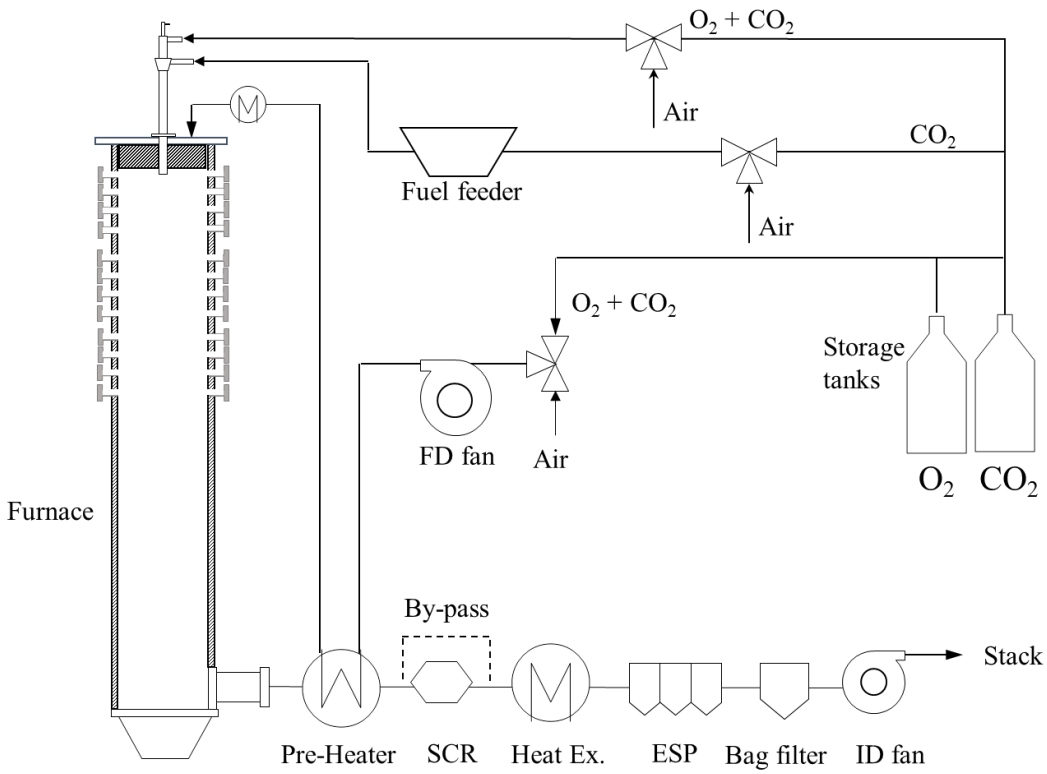

Figure 3.4: 500 kW_{th}-combustion rig at the University of Stuttgart adapted for oxyfuel burner tests.

3.3 Instrumentation and methods

In this section, the instrumentation and methodology to perform inflame measurements are described. Gas measurements and ash probes were used to characterize the combustion performance of the air and oxyfuel scenarios in the test facility. The evaluation of the emission behavior of investigated combustion cases was performed using both continuous and discrete measurements of the combustion gas at different locations in the furnace. Figure 3.5 presents the layout of the measurement locations.

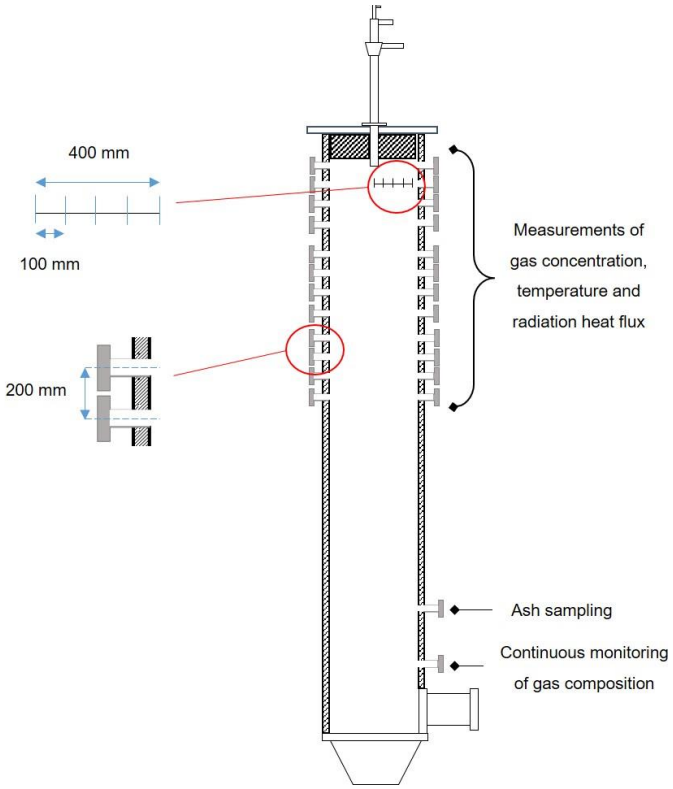

Figure 3.5. Location of measurements to characterize combustion.

3.3.1 Local Gas Species

A gas analyzer monitored on a continuous basis the main components of the gases exiting the furnace: carbon dioxide (CO_2), carbon monoxide (CO), oxygen (O_2), nitrogen monoxide (NO), nitrogen dioxide (NO_2) and sulfur dioxide (SO_2). A heated probe located near the furnace outlet sucks a small volume of the gases. The sample undergoes condensed water removal before being conducted to the gas analyzer.

A second gas analyzer fulfills the function of a movable suction probe used to perform inflame measurements in a radial direction from the centerline of the furnace towards

the furnace wall (400 mm from centerline). The probe can also be positioned in furnace ports at different distances from the burner in the first three segments (upper three meters) of the furnace to create axial profiles of gas temperature and concentration.

Similar to the continuous measurements, the combustion gas is sampled using a heated probe. After a filter to trap water, the gas is transported to the gas analyzer to determine the composition of carbon dioxide (CO_2), carbon monoxide (CO), oxygen (O_2), nitric oxides (NO_x) and sulfur dioxide (SO_2).

Table 3.2 gives an overview of this equipment and the respective principle of operation.

Table 3.2: Overview of equipment for both continuous and discrete measurements of gas concentration.

	Gas component	Range of measurement	Principle of operation
Continuous	CO	0-10000 ppmv	NDIR-Absorption
	CO_2	0-100 vol.%	NDIR-Absorption
	O_2	0-25 vol.%	Paramagnetic
	NO	0-5000 ppmv	UV-Absorption
	NO_2	0-150 ppmv	UV-Absorption
	N_2O	0-150 ppmv	NDIR-Absorption
	SO_2	0-0.6 vol.%	UV-Absorption
Discrete	CO	0-5000 ppmv 0-15 vol.%	NDIR-Absorption
	CO_2	0-100 vol.%	NDIR-Absorption
	O_2	0-50 vol.%	Paramagnetic
	NO, NO_x	0-10000 ppmv	Chemiluminescence
	SO_2	0-10000 ppmv	NDIR-Absorption

3.3.2 Gas temperature

Gas temperature was measured using a thermocouple type B installed at the tip of the previously discussed heated probe. The material used in this thermocouple is platinum and rhodium and the range of operation of the thermocouple is 0 -1700 °C. A disadvantage of this technique to measure gas temperature is that at high temperature the

radiative loss from the thermocouple becomes large and this heat loss influences the temperature of the thermocouple and the measurement accuracy.

During the oxyfuel combustion tests with petcoke, in addition to measurements with the thermocouple, a suction pyrometer probe was used for comparison purposes. This probe has the advantage that the thermo-element is shielded by ceramic tubes to avoid heat losses. The flue gas is sucked from inside the combustion chamber with high velocity through the ceramic tubes towards the thermo-element located at the gas inlet opening.

Figure 3.6 shows the comparison of temperature measurements at furnace centerline using both methods. It can be observed that only in furnace regions where the temperature is higher than 1300 °C the measurements with thermocouple register values 50-100 °C lower than the suction pyrometer. This small difference is attributed to radiant heat loss from the thermocouple to the slightly cooler furnace wall, as shown later in section 5.2.1. For practical reasons only thermocouple measurements were conducted in subsequent combustion tests with additional fuels.

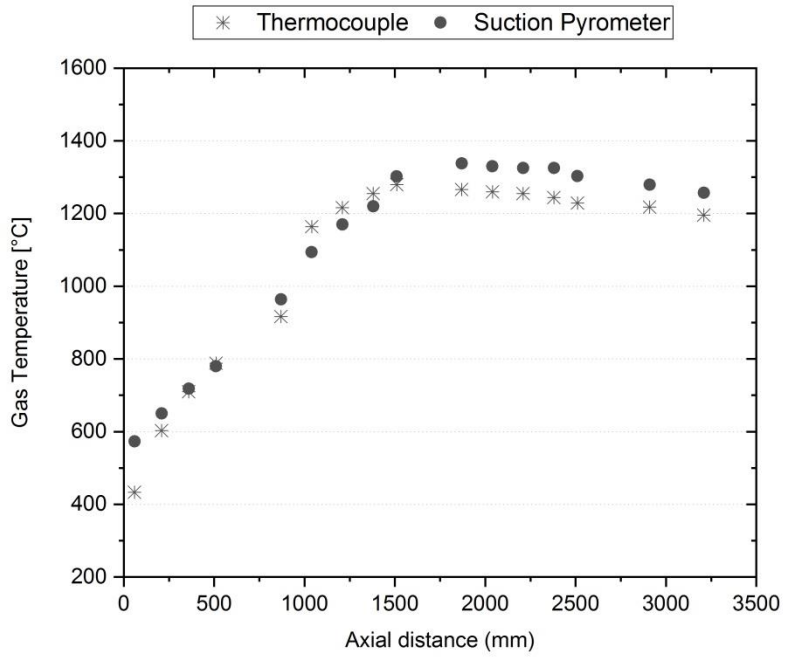

Figure 3.6: Comparison of temperature measurements with thermocouple and suction pyrometer. Centerline measurements during air combustion with petcoke in the 500 kW_{th} -combustion rig.

3.3.3 Total and Radiative Heat Flux

In many heat transfer applications, the simple knowledge of the temperature is not enough to describe the process. Further information can be obtained by heat flux measurements. Especially in combustion systems, detailed information about the heat flux is important for evaluating the efficiency of the heat transfer, the heat losses, the behavior of different materials exposed to flame, etc.

In the case of cement production kilns, the heat flux generated by the flame is essential in providing sufficient energy to the raw material for the chemical and physical changes to take place that finally turns it into cement clinker. An alteration of the radiation heat fluxes could cause a detriment of clinker quality by an alteration of the clinker phases [96]. Due to the absence of a clinker bed in the test facility, heat fluxes incident to the wall were measured instead.

Two different types of heat flux meters were used during the tests: a total heat flux meter and a hemispherical radiometer. A total heat flux meter is used to measure the sum of radiation and convection heat fluxes to its front surface. The principle of the total heat flux measurements is based on the measurement of the temperature gradient through a stainless steel plug of known thermal conductivity mounted at the tip of the probe. The plug is surrounded by two guard rings of the same material, cooled at the rear face only so that radial heat exchange is negligible. Two thermocouples inserted inside the plug that are separated by a known distance and are used to measure the temperature gradient in the axial direction [97]. A sketch of the probe set and tip indicating the main parts is shown in Figure 3.7.

The hemispherical radiometer was employed during the experiments to measure only radiative heat flux. The probe consists of a gardon gauge sensor of the company MEDTHERM mounted in a water-cooled jacket of own manufacture (see Figure 3.8a). This kind of sensor measures incident hemispherical radiation and has been successfully used in similar investigations [98]. On account of this, the probe was designed to integrate an optical filter and a gas purging (N_2) in order to avoid the inference of convective heat flux in the measurement and to avoid smoke particles in the absorber of the sensor, respectively.

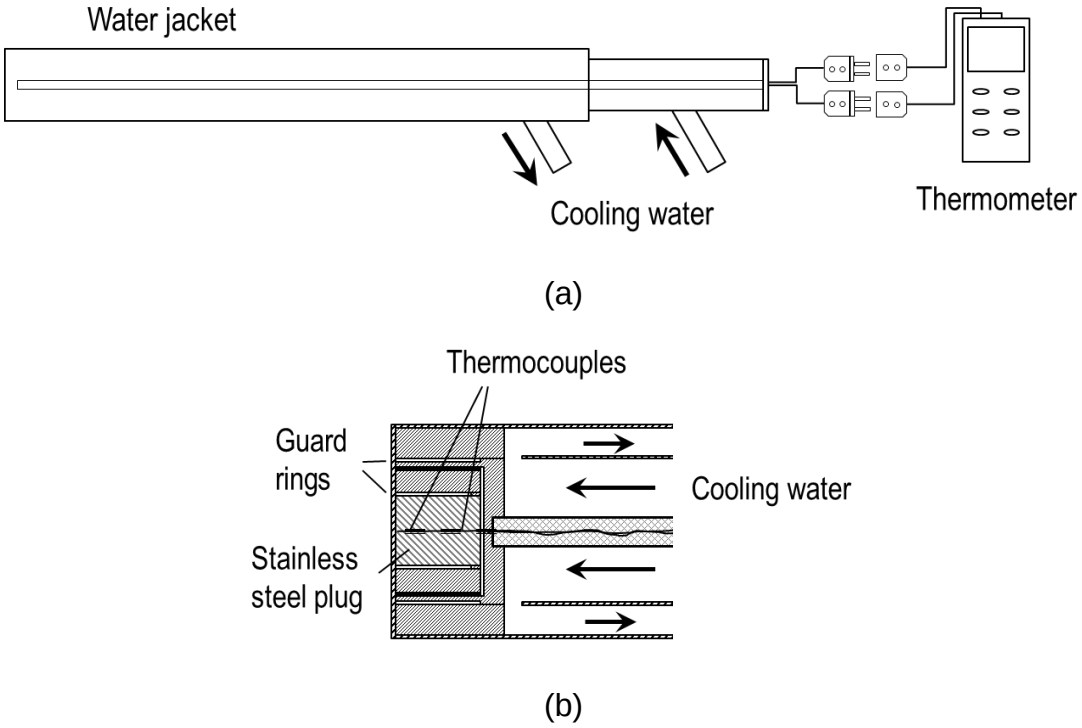

Figure 3.7. (a) Experimental setup for measurement of total heat flux and (b) overview of the probe tip.

The differential temperature heat flux sensor uses a thin constantan disc as a receiver, which is connected to a copper heat sink at its periphery (see Figure 3.8b). Considering the thermal conductivity λ of the foil disc as constant with temperature (λ_0) an expression for the heat flux can be derived [99]:

$$\dot{Q}'' = \frac{4 l \lambda_o \, \Delta T}{r^2} \qquad \text{(Eq. 6)}$$

where ΔT is the measured temperature difference between the center and the periphery of the disc, l is the thickness of the disc and r its radius (see Figure 3.8b).

Both heat flux probes were calibrated in a black body furnace prior to experimental tests.

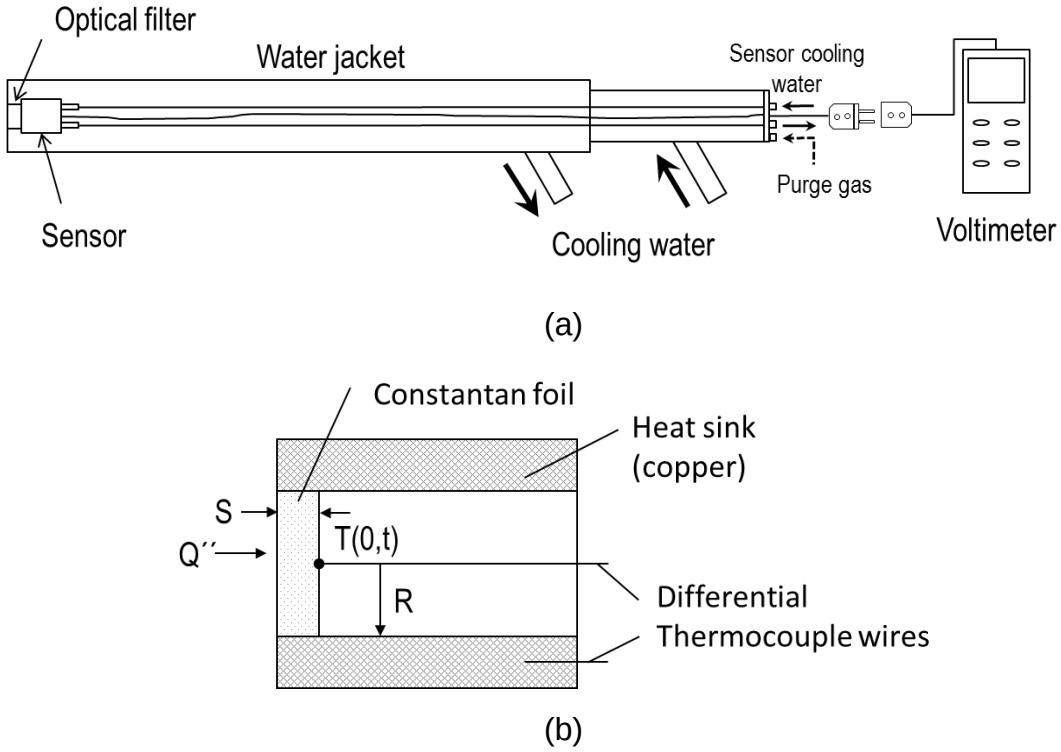

Figure 3.8: (a) Experimental setup for the measurement of total radiative heat flux and (b) operation principle of Gardon gauge sensor.

3.3.4 Combustion efficiency

The combustion efficiency can be characterized by several methods which are all based on the analysis of ash samples, either fly or bottom ash or both. In the present work, the calculation of burnout and unburned carbon are used to compare the efficiency of combustion between burner tests in air and oxyfuel mode and between the different oxyfuel settings.

The burnout (η) is determined by the ash tracer method which is described by [100]–[102]. Only the ash content of dry coal and the dry sample is required.

$$\eta = \frac{1 - \frac{\gamma_{A,coal}}{\gamma_{A,sample}}}{1 - \gamma_{A,coal}} \qquad \text{(Eq. 7)}$$

In Eq. 7 $\gamma_{A,coal}$ is the ash content of the dry coal and $\gamma_{A,sample}$ the ash content of the dry ash sample. This burnout definition gives information on the degree of combustibles burned related to its initial content.

The unburned carbon (φ) provides information regarding the unburned carbon fraction in the ash sample relating it to the initial content in the dry coal. To obtain the total

amount of unburned carbon mass flow only a multiplication of φ with the coal mass flow is requested. The unburned carbon is best calculated using the total organic carbon (TOC) and the ash content taken from the proximate analysis.

$$\varphi = \frac{\gamma_{A,coal}}{\gamma_{A,sample}} \cdot \gamma_{C,sample} = \frac{\dot{M}_{unburned\ carbon}}{\dot{M}_{coal}} \qquad \text{(Eq. 8)}$$

Where $\gamma_{C,sample}$ is the carbon content of the dry ash sample and the following assumption is made: $\dot{M}_{sample} \cdot \gamma_{A,sample} = \dot{M}_{coal} \cdot \gamma_{A,coal}$

3.3.5 Fuels characterization

The decision on using three different fuel qualities was based on the necessity to evaluate results in the spectrum of typical fuel qualities used in cement plants. The fuels used for the combustion tests are known as the most frequent fuels used in the European cement industry: brown coal (lignite), petcoke and SRF [103].

Table 3.3 presents the laboratory analysis of these fuels and Figure 3.9 shows the particle distribution of lignite and petcoke. The German lignite used during the experimental tests comes from the Rhineland region. This material was received ready for combustion, i.e. it was previously dried and crushed before arrival. As observed in Table 3.3, lignite is characterized by its high content of volatiles, which is beneficial for particle ignition.

Table 3.3: Proximate and ultimate analysis results of employed fuels.

		Lignite	Petcoke	SRF
Water	wt.% (ar)	10.7	4.6	4.9
Volatiles	wt.% (waf)	53.9	12.2	88.8
Ash	wt.% (wf)	3.3	2.2	16.4
Fixed C	wt.% (waf)	46.1	87.8	11.2
C	wt.% (waf)	67.6	82.5	56.7
H	wt.% (waf)	4.9	3.6	8.4
N	wt.% (waf)	0.84	1.57	1.34
S	wt.% (waf)	0.36	3.23	-
O	wt.% (waf)	26.3	9.1	33.6
LCV	MJ/kg (ar)	22.200	32.237	17.120

ar = as received; wf = water free; waf = water and ash free

Petroleum coke, also known as petcoke is a carbonaceous solid residue from oil refinery coker units or other cracking processes. This material is characterized for its higher carbon and low volatile content as well as high sulfur content, which limits its field of utilization. Distinct to the other fuels used in this work, petcoke is characterized as a difficult fuel in terms of ignition and flame stability [104]. Figure 3.9 exhibits the particle distribution of lignite and petcoke. Both fuels display a similar distribution curve with a mean particle size of 30 and 33 µm for lignite and petcoke, respectively.

Solid Recovered Fuel (SRF) is prepared typically from municipal solid waste's fractions. It´s deployment in cement kilns to substitute fossil-based fuels has increased in the last years due to its associated low cost and reduced carbon footprint. Different to the other fuels used in the tests, SRF is normally fired in cement kiln burners without pretreatment (grinding and drying). The typical range of particle size is 3-25 mm. For the present study, this material was milled in a hammer mill and sieved to a maximum particle size of 1 mm in order to be efficiently combusted in the facility. The particle size distribution is shown in Figure 3.10. Although this will certainly make the comparison against industrial burners difficult, the emphasis was placed on the resultant temperature and gas composition profiles.

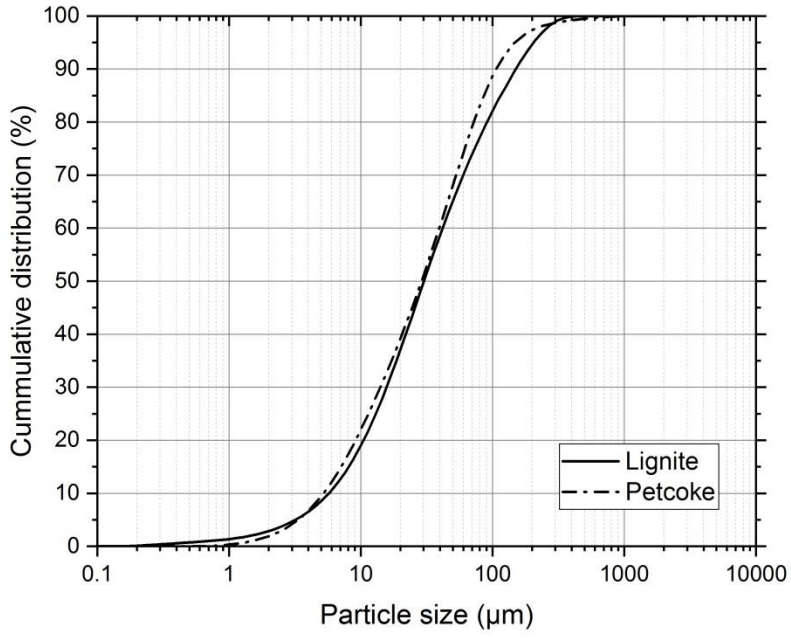

Figure 3.9: Particle size distribution of lignite and petcoke.

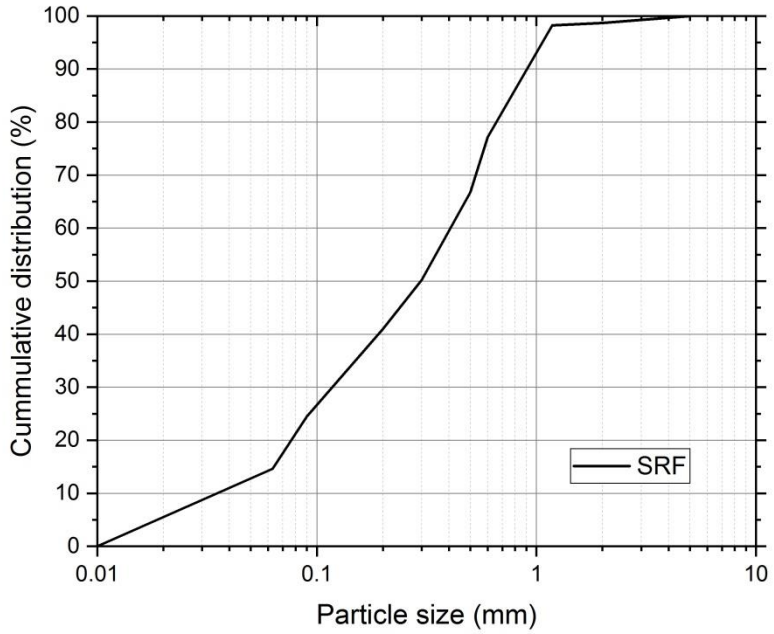

Figure 3.10: Particle size distribution of SRF.

3.4 Uncertainty of measurements

Every measurement is subject to some uncertainty. Measurement uncertainties can come from the measuring instrument, the item being measured, the measurement/sampling method, the environment, the person doing the measurement, and from other sources. According to the norm DIN 1319-1, there are two types of error: random or systematic, depending on how the measurement was obtained [105]–[107]. Random errors arise from unpredictable or stochastic temporal and spatial variations which give rise to variations in repeated observations of the measurands and can be reduced by increasing the number of observations. From a measurement procedure with a number of repetitions n, the arithmetic average of all measurement data x_i is equal to:

$$\overline{x} = \frac{1}{n}\sum_{i=1}^{n} x_i \qquad \text{(Eq. 9)}$$

The standard deviation (Eq. 10), a measure of the deviation from the averaged value, can be calculated as:

$$s = \sqrt{\frac{1}{n-1}\sum_{i=1}^{n}(x_i - \bar{x})^2} \qquad \text{(Eq. 10)}$$

Another important issue is repeatability. The difference between two values of independent measurements is expected to be smaller than r in 95% of the cases, or in other words 95% of the measurements should be within 1.96 standard deviations of the mean [107].

$$\mathrm{r} = 1.96 \cdot \sqrt{2} \cdot s \qquad \text{(Eq. 11)}$$

Systematic errors arise from a recognized effect of an influence quantity on a measurement result. The effect can be quantified and a correction factor can be applied to compensate the effect. The error cannot be reduced by repeating measurements. Other methods e.g. different measurements methods or calculations are needed to estimate uncertainties due to systematic effects.

Measurement of uncertainty in the determination of gas concentration was carried out both for random and systematic errors. Systematic errors were calculated using calibration gas tanks with known concentration and registering the value obtained from the gas analyzer. Two sets of calibration gases were used during the tests, one for combustion in air and one for oxyfuel combustion. The reason for this decision lays on the significant differences in gas concentration of certain gases like oxygen and carbon dioxide during oxyfuel combustion compared to air firing. Table 3.4 and Table 3.5 summarize the statistical values for the determination of gas concentration.

Table 3.4: Statistical values of uncertainty in gas analysis – air mode

Gas	Calibration point	*n*	$\bar{x}$	*s*	r
O_2	2.95 vol.%	6	3.10 vol.%	0.1 vol.%	0.2 vol.%
CO_2	15.95 vol.%	6	15.80 vol.%	0.1 vol.%	0.2 vol.%
CO	393 ppm	6	398 ppm	2 ppm	5 ppm
NO	894 ppm	6	880 ppm	10 ppm	27 ppm
SO_2	1847 ppm	6	1860 ppm	23 ppm	65 ppm

Table 3.5: Statistical values of uncertainty in gas analysis – oxyfuel mode

Gas	Calibration point	*n*	$\bar{x}$	*s*	r
O_2	8.0 vol.%	6	8.1 vol.%	0.1 vol.%	0.3 vol.%
CO_2	90.1 vol.%	6	89.8 vol.%	0.2 vol.%	0.7 vol.%
CO	393 ppm	6	389 ppm	4 ppm	12 ppm
NO	925 ppm	6	931 ppm	9 ppm	24 ppm
SO_2	1847 ppm	6	1852 ppm	16 ppm	45 ppm

4 Burner Scaling

4.1 Introduction

As explained in section 2.4.1, there is a wide variety of air-fired burner designs in the cement sector. Modern burners are the result of decades of research to improve flame development, energy efficiency, low pollutants formation, and flexibility. Flexibility in burner technology becomes a benefit especially if the process boundary conditions are not constant over time. For instance, regarding variation in fuel types, the price and availability of conventional fuels as well as evolving environmental legislation have pushed the cement industry to widen its spectrum of fuel usage. Burner manufacturers have understood the importance of fuel flexibility. Nowadays modern kiln burners integrate dedicated outlets/channels/nozzles to fire gaseous, liquid, pulverized and alternative fuels. Thanks to these advancements, two or more fuel types can be fired simultaneously without process interruption.

Oxyfuel operation represents a new boundary condition that demands burner flexibility or a redesign to avoid quality detriments. The possibility to switch from air firing to oxyfuel mode using standard modern cement burners currently installed in cement plants represents a significant advantage in the retrofitting plans towards oxyfuel implementation. Burner flexibility in this sense demands research including pilot testing, which is the aim of the present work.

4.2 Base burner design

The scope of the present thesis includes the performance of oxyfuel demonstration tests with a scaled cement burner. The full industrial-size burner taken as a base for scaling purposes is commercialized by the German burner manufacturer ThyssenKrupp Industrial Solutions [108]. The tip of this burner is depicted in Figure 4.1. The main outlets in the sketch correspond to outlets for primary gas and fuel ejection. The center of the burner groups additional channels, which are optional and can be tailored according to the client´s request. These optional channels are used to incorporate alternative fuels (liquid, gaseous fuels, or even solid recovered fuels).

Primary gas is injected into the combustion space through concentrically arranged nozzles. This gas stream represents just a small portion of total oxidizer gas (typically near 15%). However, the momentum of this stream should be high enough to ensure the entrainment of hot secondary gas into the combustion zone (see Figure 4.2) ensuring an adequate mixing between fuel particles and preheated oxidizer. The angle of injection of primary gas can be tuned to create a swirl flow pattern by adjusting the direction

of the nozzles in the radial and tangential planes. In this way, the flame shape, fuel ignition, and burnout are influenced. By increasing the swirl angle, the mixing of fuel and hot secondary gas is improved and the reaction zone shortens.

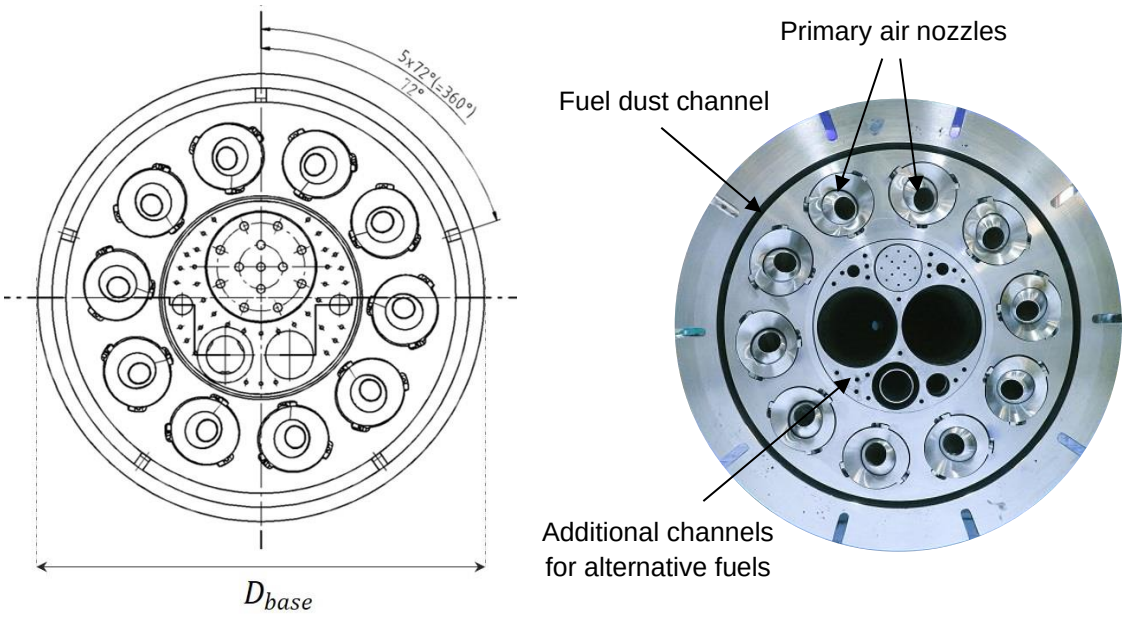

Figure 4.1: Detail of the burner tip from large-scale kiln burner. D_{base} represents a burner diameter which varies with scale (thermal input).

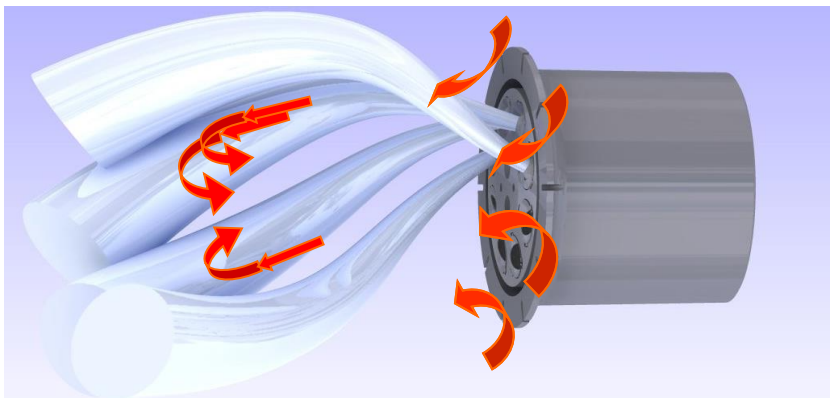

Figure 4.2: Entrainment of secondary gas into the combustion zone.

Pulverized fuels are injected into the combustion chamber via a channel located near the burner periphery. Fuel particles meet the hot secondary gas as this stream is drawn into the jet flame, boosting ignition and burnout.

4.3 Burner scaling criteria

Scaling of combustion systems has been a focus of research since the second half of the 20th century. It involves consideration of aerodynamics, combustion and heat transfer in the furnace. The works of Spalding [109] and Beér [110] set general theoretical considerations in the form of dimensionless groups derived using the fundamental differential equations for momentum, energy, and mass balance. A broader source of literature on this topic is regarded to the work of the IFRF (International Flame Research Foundation), which contributed substantially with numerous experimental and modeling tests on this field with thermal input ranging from 0.176 to 50 MW [111]–[116]. In general, authors agree on two practical criteria for the scaling down of pulverized coal burners: the constant velocity and the constant residence time criteria, respectively.

The basic mathematical expression for the burner thermal input (Q) can be written as follows:

$$Q = K\rho \mathrm{U} D^2 \qquad \text{(Eq. 12)}$$

where the variable ρ is a characteristic inlet fluid property, typically expressed as the combustion air density. U and D are the characteristic burner velocity (combustion air velocity) and characteristic burner diameter, respectively; K stands for a proportionality constant.

When employing the constant velocity criterion ($\mathrm{U} = const$) to scale a burner to a different thermal input the following relationships are established:

$$\frac{Q_{base}}{Q_{scaled}} \sim \left(\frac{D_{base}}{D_{scaled}}\right)^2 \qquad \text{(Eq.13)}$$

$$D \sim Q^{0.5} \qquad \text{(Eq.14)}$$

These expressions allow the calculation of a new burner diameter according to the scaled thermal input. As geometric similarity is maintained, all other burner dimensions can be calculated.

Under the constant residence time criterion, the purpose is to maintain the D/U ratio constant while reducing/increasing the burner thermal input. In swirl-stabilized coal

burners, fuel particles and air are initially segregated by a distance proportional to the characteristic burner diameter D. The turbulent mixing between the two reactants should overcome this segregation in order to attain stable combustion. The ratio D/U represents then the large macro mixing timescale of fuel particles and air [112], [117]. This ratio is also proportional to the normalized jet penetration distance into the IRZ [112]. Thus, as $D/U = const$, the following equations are valid:

$$Q = K\rho \mathrm{U} D^2 \sim D^3 \quad \text{(Eq.15)}$$

$$\frac{Q_{base}}{Q_{scaled}} \approx \left(\frac{D_{base}}{D_{scaled}}\right)^3 \quad \text{(Eq.16)}$$

$$D \sim Q^{0.33} \quad \text{(Eq.17)}$$

These two criteria for burner scaling have been tested under varying operation conditions. Smart and Morgan [112] used both scaling criteria to scale down a 50 MW burner to 2.5 MW firing a German coal. They concluded that constant residence time scaling is the most appropriate scaling criterion for pulverized coal flames. This conclusion was partly based on the observation that NO_x emissions in the furnace exhaust increased when employing the constant velocity scaling. Weber and Breussin [115] also evaluated both criteria in experiments of flame scaling in the range of 0.9- to 12 MW with special attention on NO_x emissions. They determined that for prototype experiments at thermal inputs larger than 4 MW the NO_x emissions are representative of full industrial-scale applications using either the constant velocity or the constant residence time principle. However, in experiments with thermal input lower than 2-3 MW, the NO_x emissions decrease with thermal input using the constant velocity criterion. Therefore, constant residence time scaling was recommended. Additional experiments using both criteria concluded that both methods have limitations, particularly when applied to two-phase combustion it is considerably difficult to scale the interaction between the gaseous and solid (liquid) phases [116]–[118]. Specifically for combustion systems in rotary kilns, Mullinger and Jenkins [54] agree that in principle, the constant velocity criterion is the most adequate criterion to maintain consistent heat transfer patterns through a cement kiln. More recent, Weber and Mancini [119] discussed the difficulties in scaling industrial burners to lab and semi-industrial scales, and vice versa. They concluded that the main reason for the impairment is related to the physical mechanisms that dominate at each scale. While for lab-scale experiments there is a strong interaction between turbulence and chemistry, in industrial furnaces convective mixing is the dominant mechanism. They finally acknowledge that more efforts are needed to further develop combustion scaling models.

4.4 Scaled burner description

In the design phase, both the constant velocity and constant residence time scaling criteria were considered. The maximum thermal input to the test rig for the tests was set to 500 kW. The based burner design refers to a BAT cement plant producing 3000 tpd clinker with a thermal heat consumption of 3026 kJ/$kg_{clinker}$ and a share of 45% of the thermal energy required in the sintering zone [120]. Based on this information the sintering zone burner would be designed for a thermal capacity of 47 MW under operating conditions, i.e. a scaling factor of approximately 100 with respect to the test rig capacity. Using the above-mentioned information the based burner design would have a base burner diameter D_{base}, depicted in Figure 4.1, of 0.62 m and the down-scaled burner a calculated diameter of 0.064 m and 0.136 m following the constant velocity and constant residence time criteria, respectively.

Downscaling of industrial size machinery requires a trade-off between prototype scaling factor, process requirements/constraints and desired machinery size on the one hand and technical constraints like manufacturability of single machinery parts, reuse, and adaptability of existing test rig/trial facility on the other hand.

In the present work the constant velocity criterion was selected. However, due to constraints according to the minimum possible manufacturable nozzle exit diameter, some adjustments in the design were required.

Table 4.1 presents the dimensions of the scaled burner compared to the base burner design and the calculated dimensions following the constant velocity and constant residence time criteria. The design constraints and facility limitations resulted in an adjustment of the burner diameter and the number of nozzles (8x). These adjustments increased by a factor of 2.2 the total nozzle cross-sectional area compared to the design of constant velocity as observed in Table 4.1. This condition impacted outlet gas velocity and specific flame momentum as discussed in the following chapters.

Figure 4.1 displays a detailed frontal view of the burner tip and Table 4.2 compares the relation between the burner and kiln dimensions. As observed, the ratio of the furnace to burner diameter in the pilot testing is slightly larger compared to the industrial-size burner. This difference, though minor, is expected to affect secondary gas velocity and therefore its entrainment to the primary gas-fuel jet flow.

Table 4.1: Comparison of burner dimensions

	Based	Present work	Constant velocity	Constant residence time
Burner diameter [m]	0.62	0.075	0.064	0.136
Primary air nozzle diameter [m]	0.029	0.005	0.003	0.006
Number of primary air nozzles	10	8	10	10
Total nozzle cross-sectional area [m^2]	-	1.6E-04	7.0E-05	3.2E-04
Carrier of fuel dust channel [m]	0.20	0.0022	0.0021	0.0044

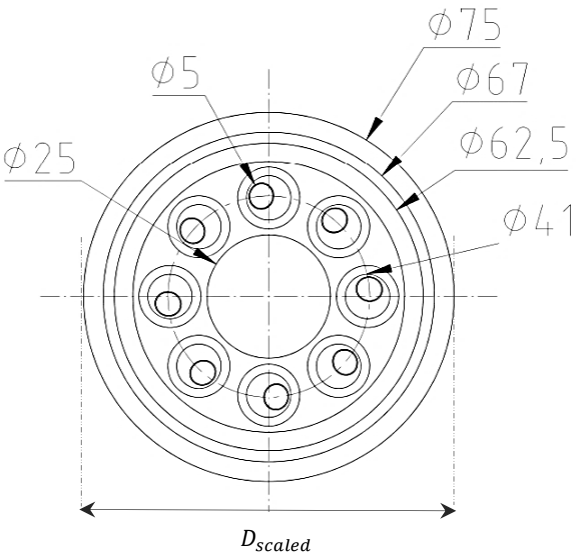

Figure 4.3: Detailed view of the burner tip (down-scaled burner). Dimensions in mm.

Table 4.2: Size ratio comparison of burner and kiln diameter

	Based	Scaled
Thermal load [MW]	47	0.5
Ratio kiln/burner diameter [-]	8.3	10.6

Figure 4.4 shows the main components of the scaled burner assembly. The burner has a diameter of 75 mm and a total length of 1114 mm. Inlets for coal and carrier gas, as well as primary gas, are indicated. The primary gas is supplied from an air compressor in the air mode and from pressurized tanks in oxyfuel mode, this gas exits through the nozzles at the burner tip. A clamp collar is used to adjust the axial position of the burner 500 mm inside the combustion chamber.

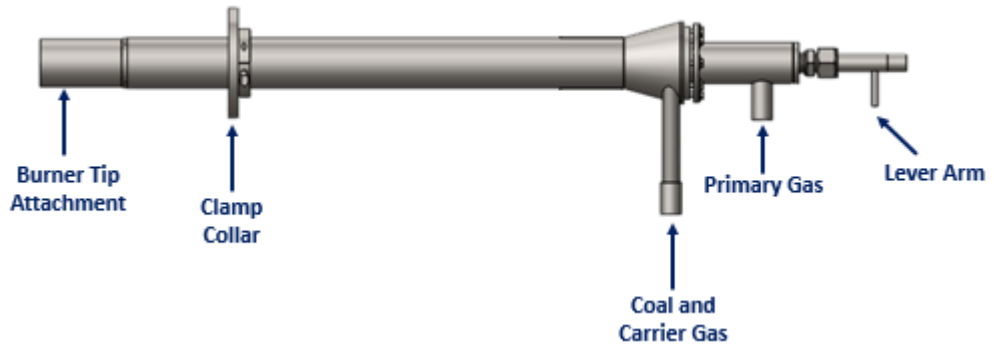

Figure 4.4: Burner assembly.

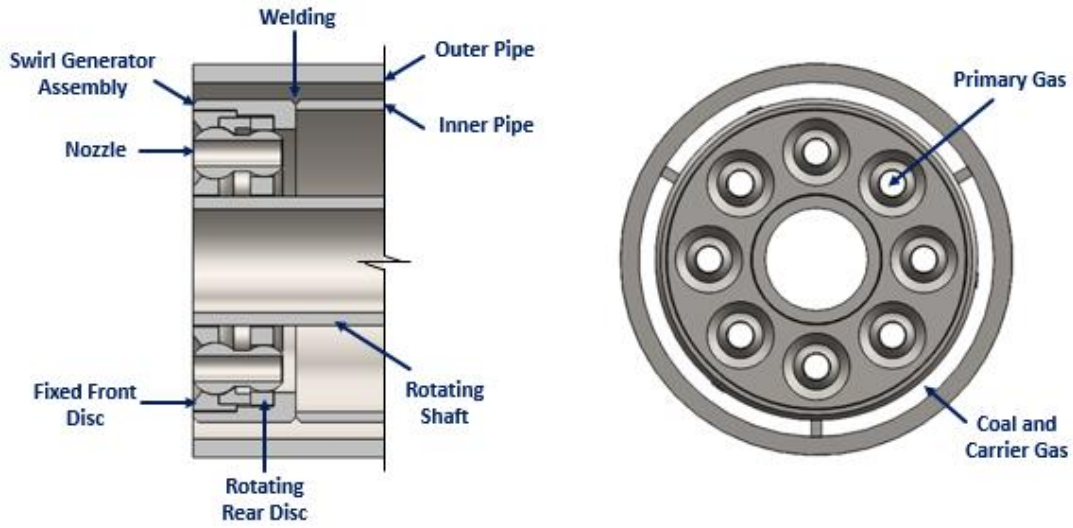

Figure 4.5: View of burner tip attachment. Left: detail of primary gas nozzle mechanism. Right: front view.

Figure 4.5 shows the tip of the downscaled burner including details of the nozzle mechanism. Between the nozzle casing and the outer pipe a 2.2 mm annular gap is formed that serves for solid fuel and carrier gas injection. This fuel carrier stream has no

rotation mechanism and is therefore not swirled. The inner pipe is used only during the startup to introduce natural gas during heat-up of the facility.

The primary gas exits with high momentum via 8 nozzles of inner diameter 5 mm evenly distributed in a circular arrangement at 20.5 mm from burner center. The inclination of the nozzles relative to the nozzle axis is adjustable from 0° to 25° by a rotating shaft and disc mechanism, which is manually actuated using a lever arm (cf. Figure 4.4 and Figure 4.5).

To characterize the relative strength of the rotation flow imparted to the primary gas, the nondimensional swirl number S is used, which is defined as the ratio of axial flux of tangential momentum over axial flux of axial momentum [121].

$$S = \frac{I_t}{I_x R} = \frac{\int_0^R 2\pi\rho u w r^2 dr}{R \int_0^R 2\pi\rho u^2 r dr} \quad \text{(Eq.18)}$$

Where I_t is the axial flux of tangential momentum and I_x the axial flux of axial momentum. R is the exit radius of the nozzle and u and w represent the axial and tangential velocity components at radius r, respectively. Assuming the axial velocity distribution is uniform over the nozzle cross-section, the axial flux of axial momentum can be simplified to:

$$I_x = \pi\rho {U_0}^2 R^2 \quad \text{(Eq.19)}$$

and:

$$I_t = 2\pi\rho {U_0}^2 tan\theta \frac{R^3}{3} \quad \text{(Eq.20)}$$

Where θ is the injection angle, i.e. the nozzle inclination angle in relation to the burner axis. Therefore, the swirl number can be simplified to the following mathematical expression [122], [123]:

$$S = \frac{2}{3} tan\theta \quad \text{(Eq.21)}$$

Using Eq. 21, the theoretical geometrical swirl number for the nozzle inclination angle of 12.5° and 25°, correspond to S values of 0.14 and 0.31, respectively.

5 Results from combustion tests

5.1 Introduction

This section presents the results of burner tests in both air firing and O_2/CO_2 conditions. As mentioned in section 3.3.5, two reference fuels are selected: Rheinland's pre-dried lignite and petroleum coke (further referred to as petcoke). These fuels cover a good spectrum of fossil fuels in the European market and its selection aims to show the differences in firing low volatile as well as high volatile pulverized fuels. Complementary, results of burner tests firing a mixture of SRF (Solid Recovered Fuel) in co-combustion with lignite, broaden the evaluation of the burner with a fuel that has been increasingly used in the last decade [103].

After assessing selected oxyfuel scenarios through in-flame measurements, an optimized burner configuration is targeted. The investigation of an optimized setting includes variations in oxygen enrichment and variation in gas distribution in burner outlets as well as an investigation on the effect of primary gas nozzles' inclination angle in shaping flame length, gas temperature and concentration.

Operating conditions in Table 5.1, Table 5.2, and Table 5.3 summarize the operation conditions during test cases classified by fuel used. The nomenclature OF*XX* is an indication of the volume percentage of oxygen in the sum of primary, secondary and carrier gas. This value is calculated to be inversely proportional to the recycle ratio in an oxyfuel system with flue gas recirculation as shown in Figure 5.1.

The fundamental approach of the experiments is to maintain a similar oxygen-to-fuel ratio between the air-blown combustion and oxyfuel tests. This condition was achieved by allowing the same stoichiometric ratio (n) between the baseline air experiments and the oxyfuel experiments. It is noted that to adjust the oxygen volumetric fraction in OF27, OF29, OF30 and OF32, the overall oxygen volume flow was kept constant while the volume flow of CO_2 in secondary gas was reduced. Further, similar volumetric flow of primary gas through the burner was kept constant for each fuel case. This method not only ensures a similar residence time of particles in the gas flow, but also a similar primary gas momentum.

Oxygen concentration in the primary gas was intentionally increased in relation to the other oxidizing streams. This decision was made based on the thesis that oxygen-enriched conditions in the flame core improve the ignition of fuel particles, overcoming the effects of the CO_2 gasification reaction (Eq. 5). This condition has been seen to obtain positive results in previous simulation results by other authors [42]. Additional parameters that were kept constant through all the experimental cases in this study

are the secondary gas temperature (750 °C) and the burner swirl angle, which is set to 12.5°. This last parameter was later varied to assess its impact on flame formation.

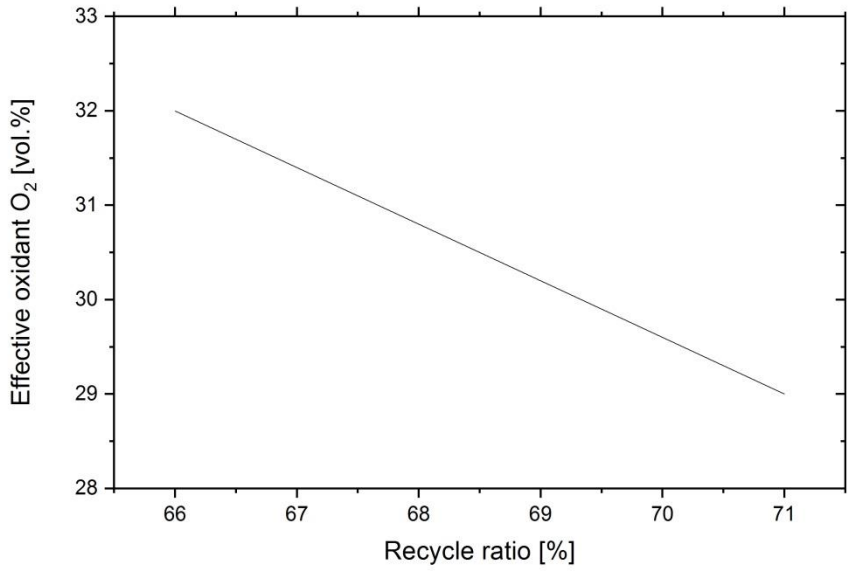

Figure 5.1: Relationship between recycle ratio and effective O_2 concentration in combustion gases (dry) based on mathematical calculation. Pre-dried lignite, 3% O_2 in flue gas fixed for all scenarios.

Table 5.1: Inflow conditions in demonstration tests with pre-dried lignite

		Air	**OF29**	**OF32**
Thermal Input	kW	400	400	400
Primary gas composition	Vol.-%, wet	Air	60% O_2 40% CO_2	60% O_2 40% CO_2
Secondary gas composition	Vol.-%, wet	Air	19.5% O_2 80.5% CO_2	23.4% O_2 76.6% CO_2
Fuel carrier gas composition	Vol.-%, wet	Air	100% CO_2	100% CO_2
Primary/secondary/carrier gas flow	m^3/h (STP)	90/300/25	90/172/25	90/141/25
n (stoichiometric ratio)	-	1.10	1.10	1.10

Note: Additional 10 m^3/h were used in the flame detector (air or CO_2 according to the case).

Table 5.2: Inflow conditions in demonstration tests with petcoke

		Air	OF27	OF32
Thermal Input	kW	482	478	482
Primary gas composition	Vol.-%, wet	Air	53% O_2 47% CO_2	70% O_2 30% CO_2
Secondary gas composition	Vol.-%, wet	Air	21% O_2 79% CO_2	25% O_2 75% CO_2
Fuel carrier gas composition	Vol.-%, wet	Air	100% CO_2	100% CO_2
Primary/secondary/carrier gas flow	m^3/h (STP)	67/328/36	85/255/29	67/175/36
n (stoichiometric ratio)	-	1.09	1.13	1.09

Note: Additional 12 m^3/h were used in the flame detector (air or CO_2 according to the case).

Table 5.3: Inflow conditions in demonstration co-combustion tests lignite+ 20 wt.% SRF.

		Air	OF30-a	OF30-b
Thermal Input	kW	405	405	405
Primary gas composition	Vol.-%, wet	Air	50% O_2 50% CO_2	20% O_2 80% CO_2
Secondary gas composition	Vol.-%, wet	Air	33% O_2 67% CO_2	43% O_2 57% CO_2
Fuel carrier gas composition	Vol.-%, wet	Air	100% CO_2	100% CO_2
Primary/ secondary/ carrier gas flow	m^3/h (STP)	80/325/48	60/180/45	60/180/45
n (stoichiometric ratio)	-	1.10	1.10	1.10

Note: Additional 10 m^3/h were used in the flame detector (air or CO_2 according to the case).

5.2 Combustion behavior

5.2.1 Gas temperature

Figure 5.2 shows the axial flame temperature during the combustion of lignite in air-blown and two oxyfuel scenarios (OF29 and OF32). The flame temperature profile was observed to be influenced by the combustion atmosphere. From the two oxyfuel cases, OF29 shows a more similar temperature profile to combustion in air. The highest temperature in air and OF29 scenarios is measured at a distance of 0.78 m (1285 °C) and 0.95 m (1348 °C), respectively. The temperature rises slightly faster in OF29 than in the air-blown case and remains higher at all measured distances up to 2.5 m away from the burner.

A clear faster ignition is achieved when increasing the oxygen enrichment to 32 vol.% (OF32). The temperature increases above 600 °C right near the outlet of the burner and reaches its highest peak of 1368 °C at 0.42 m distance from the burner. This earlier energy release is an indicator of a faster devolatilization, favored by abundant oxidizer in the near burner zone and less CO_2 in the combustion atmosphere compared to the OF29 case. Beyond the burner region, the temperature distribution between the two oxyfuel cases becomes similar.

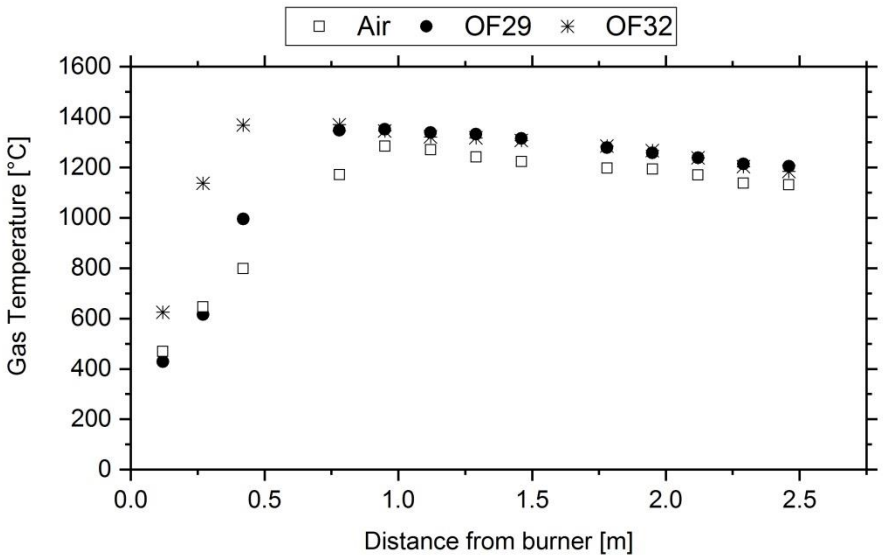

Figure 5.2: Gas temperature along the furnace centerline for lignite combustion.

Temperature measurements at the furnace wall[1] (400 mm distance from the furnace axis) are shown in Figure 5.3. Here the differences between the three cases are clearer. Fuel ignition is marked by a sudden increase in temperature at a distance near 0.7 m from the burner axis. The differences in temperature between the air case and OF29 range from 50°C to 100°C on average. The oxyfuel cases OF29 and OF32 also present important differences in temperature in the near-burner region up to 1.5 m distance from the burner, further downstream the values become comparable.

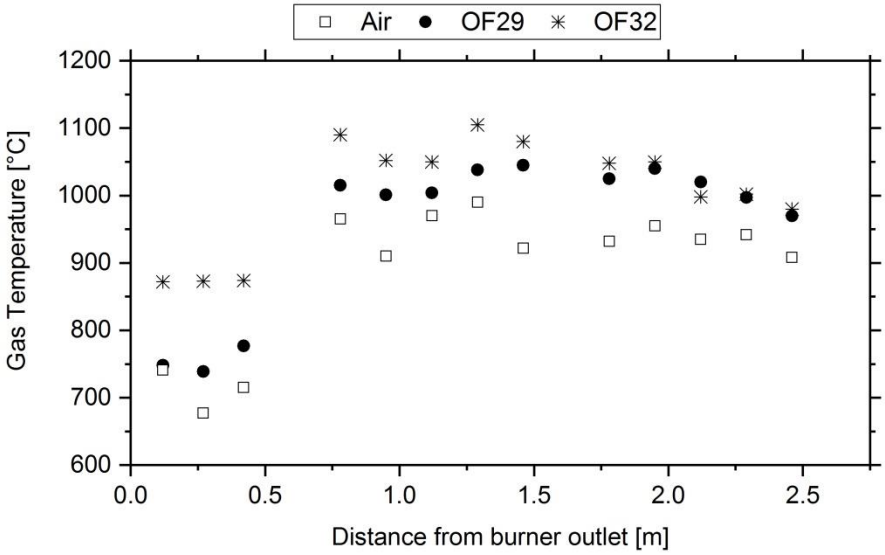

Figure 5.3: Gas temperature at the furnace wall (400 mm from furnace axis). Fuel: lignite.

A detailed assessment of the air fired and OF29 cases is possible when comparing a 2-D plane of the furnace created by interpolation of 70 radial and axial measurements of gas temperature (see Figure 5.4). A similar distribution of temperature is observed between the two cases. The extent of the gas injected into the furnace prior to ignition is observed in blue color. As particles heat up and eventually ignite temperature color is turned to green and yellow. In Figure 5.4, shorter ignition length is observed in OF29.

[1] No additional measurements were conducted to confirm flame symmetry and, and therefore symmetric temperature distribution.

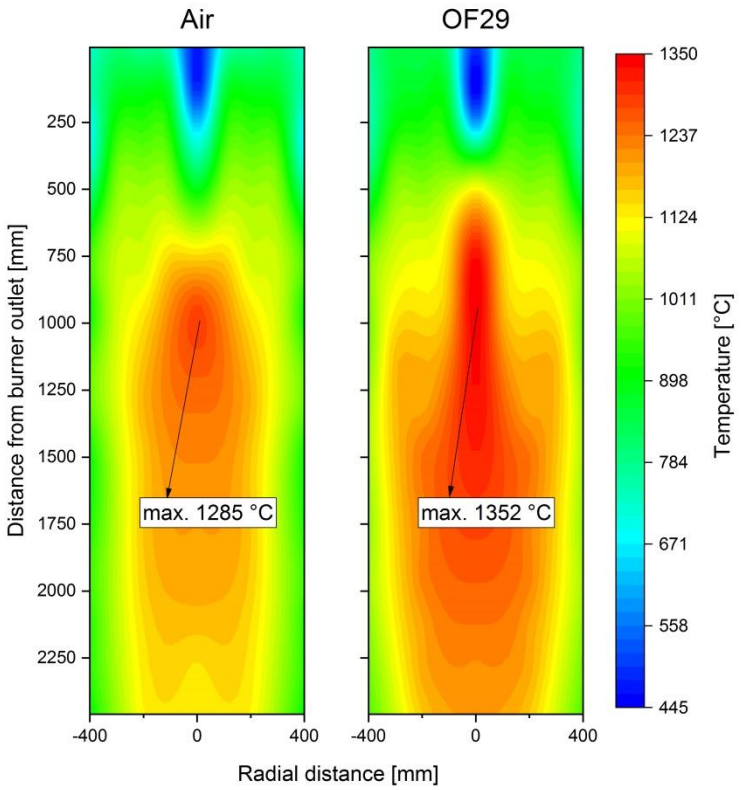

Figure 5.4: Gas temperature distribution in air (left) and OF29 (right) cases during lignite combustion.

Figure 5.5 shows the temperature measurements at furnace centerline in air-blown and both oxyfuel cases during combustion of low-volatile petcoke. As expected, the most evident difference to the lignite cases is the ignition delay. Due to its low-volatile content, longer distance is needed to achieve ignition. Both air-blown and OF27 display a similar temperature profile, although the profile for the OF27 case is marginally shifted downstream. Similar to the observations during combustion of lignite, the oxy-fuel case OF32 has a shorter ignition distance. The highest temperature peak is similar in the three cases, near 1300 °C at 0.9 m; 1.41 m, and 2.28 m for the OF32, air-blown and OF27 cases, respectively. The slightly slower ignition in OF27 case could be associated with the presence of CO_2 in the combustion atmosphere, reported to delay devolatization and char burnout [124], [125]. This effect is compensated with increased oxygen enrichment in the OF32 oxyfuel case.

A similar behavior is observed for the gas temperature measured close to the furnace wall. As observed in Figure 5.6, the ignition of petcoke particles in OF32 mode is clearly

faster than the other two cases. There are differences in wall temperature in the first two meters, while afterwards the temperature is similar in the three cases.

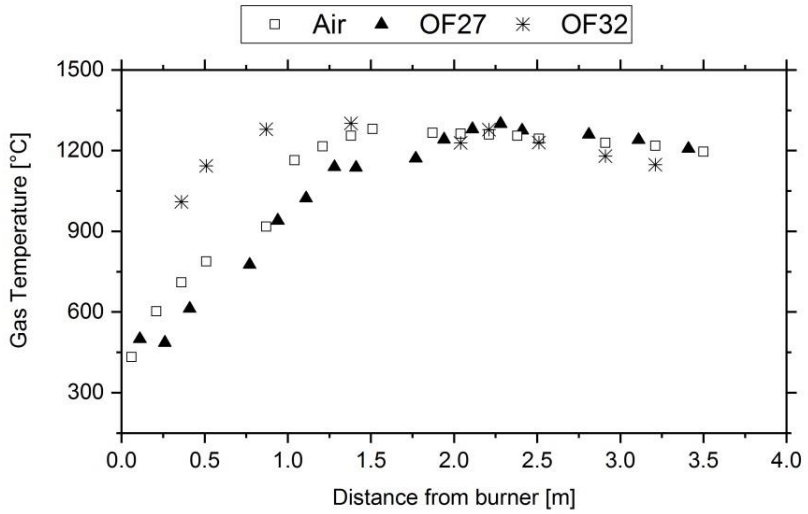

Figure 5.5: Gas temperature along the furnace centerline. Fuel: petcoke.

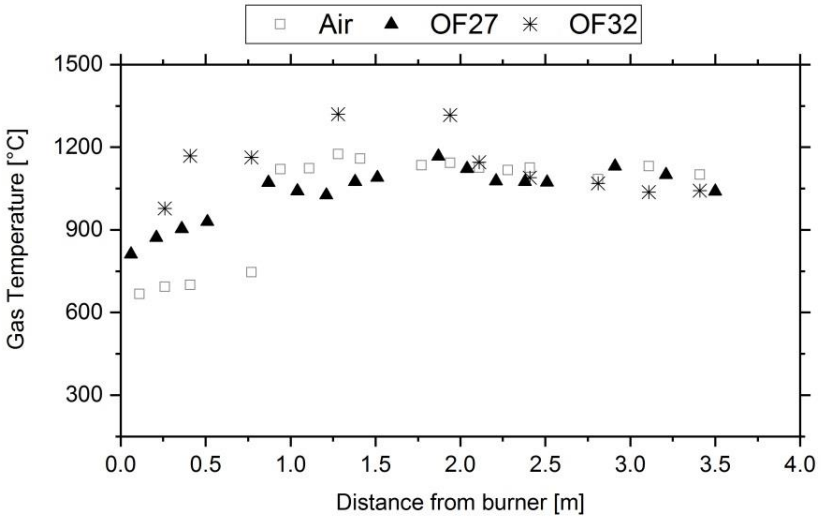

Figure 5.6: Gas temperature at the furnace wall (400 mm from furnace axis). Fuel: petcoke.

5.2.2 Gaseous species

The axial gaseous concentration profiles during lignite combustion in air-blown, OF29 and OF32 combustion are depicted in Figure 5.7.

As observed in Figure 5.7.A, the starting concentration of oxygen in both oxyfuel cases is much larger than in the air-blown case. This condition was established in Table 5.1 and has the aim of improving fuel ignition. In line with the temperature profile, the oxyfuel case OF32 shows the fastest oxygen consumption pace. The oxygen concentration reaches the value of 3.6% at a distance of 0.42 m. The air-blown case reaches a comparable value of 3.8% at a distance of 1.12 m, while the OF29 case only reaches a value of 3.7% at a distance of 1.78 m. The oxygen concentration at furnace outlet[2] is 2.4%, 3.8% and 3.2% for the air-blown, OF29 and OF32 cases, respectively.

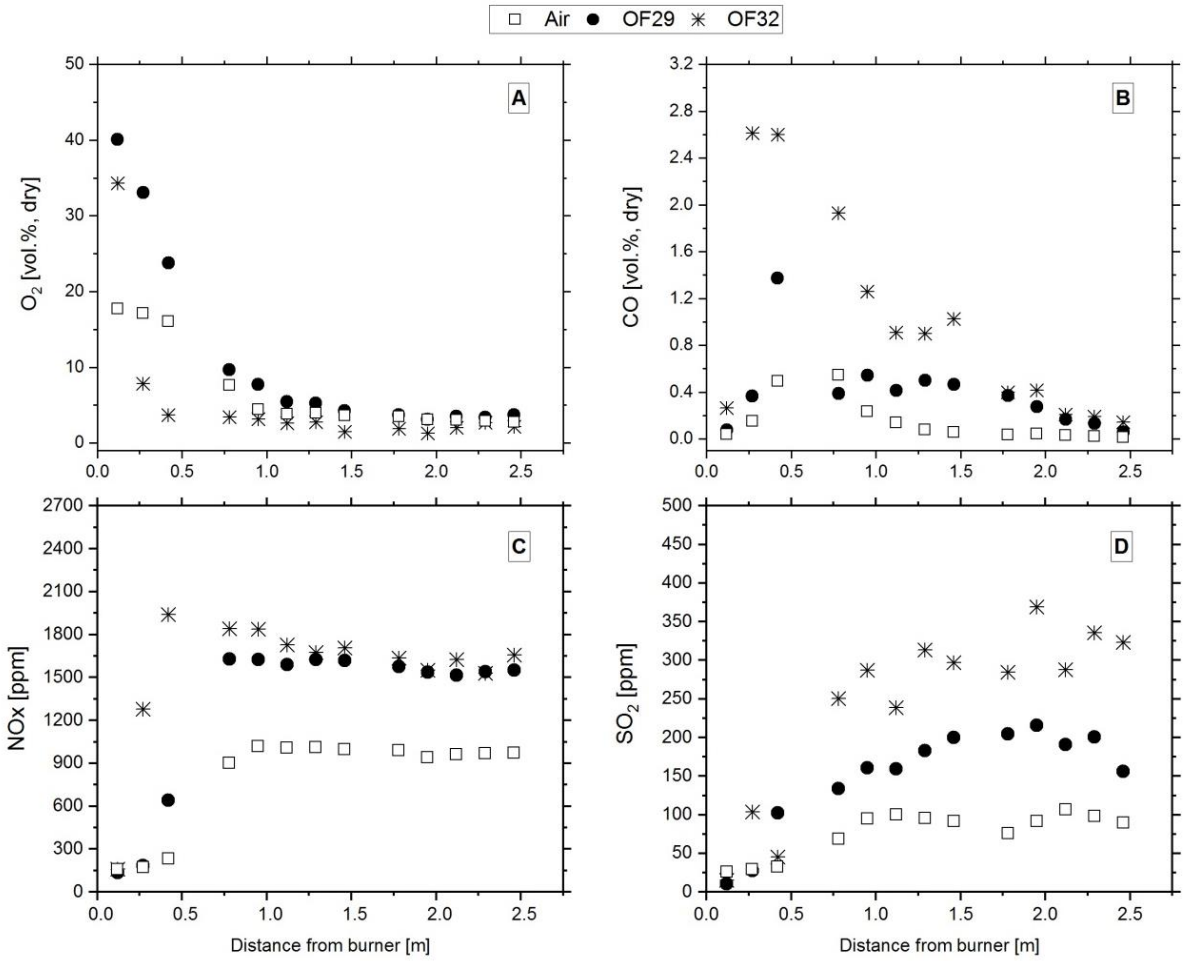

Figure 5.7: Axial (A) O_2, (B) CO, (C) NOx, and (D) SO_2 concentration profiles during air-blown, OF29, and OF32 combustion along the furnace centerline. Fuel: Lignite.

The axial measurements of carbon monoxide generation are plotted in Figure 5.7.B. The peak CO concentrations for the three cases to be compared are measured at a

[2] Furnace outlet is located at 6.4 m. Figure 5.7 shows the measurements in the first 2.5 m and therefore the values at furnace outlet are not displayed.

position 0.27 – 0.42 m distance from the burner. Clearly, the highest peak belongs to OF32 with 2.6% followed by OF29 and the air case with 1.37% and 0.54%, respectively. It is possible that the peak concentration in air-blown combustion is found between 0.5 – 0.7 m, nevertheless there are no measurement ports in this area. The concentration of CO is reduced significantly in air-blown combustion after 1.5 m. However, in the oxyfuel scenarios, the concentration remains significantly higher than combustion in air until a distance of 2.5 m from the burner.

The difference between the CO concentration in oxyfuel compared to air combustion is in agreement with the observations of other authors in other oxyfuel demonstration tests as shown in Table 5.4.

Table 5.4 Measured maximum CO concentration in oxy-fuel flames of lignite.

Group	**Referece**	**Test unit [MW_{th}]/type**	**Feed gas O_2 conc. [vol.%]**	**n**	**Max. CO [vol.% dry]**	
					Oxyfuel	**Air**
Stuttgart	This study	0.5/PC Rheinisch	29	1.1	1.4	0.6
			32	1.1	2.6	0.6
Vattenfall	Ramström et al. (2011) [126]	30/PC Lausitz	25 (wet)	1.18	6.5	3.0
			30.4 (wet)	1.18	8.0	3.0
Chalmers	Hjärtstam et al. (2009) [127]	0.1/PC Lausitz	25	1.18	1.1	1.2
			27	1.18	7.0	1.2
			29	1.18	9.0	1.2
Stuttgart	Dhungel (2009) [128]	0.02/PC Klein Kopje	21	1.15	1.2	0.7
			27	1.15	2.2	0.7
		0.02/PC Lausitz	21	1.15	4.0	2.0
			27	1.15	6.4	2.0
		0.02/PC Rheinisch	27	1.15	3.1	-
		0.02/PC Endorf	27	1.15	2.9	-

The significant large concentration of CO in the flame during oxyfuel combustion is explained by several mechanisms. During volatile release, the CO_2 present will compete with O_2 for atomic hydrogen and lead to formation of CO through the following homogeneous reaction [129]:

$$CO_2 + H \rightleftharpoons CO + OH \quad \text{(Eq.22)}$$

Reactions of CO_2 with hydrocarbon radicals may also contribute to CO formation, but are less important [129], [130]. Also important for lignite combustion is the gasification of char in the abundance of CO_2 (Eq. 5) as discussed extensively in [130]. This reaction produces two moles of CO per mol of reacting carbon in char. Further, the fraction of char converted via the gasification route has been seen to increase with temperature [128], [130]. As a consequence, higher CO concentration is observed in the OF32 case compared to OF29.

Despite air, the main source of nitrogen, is restricted during oxyfuel conditions, significant amounts of nitrogen may still be injected into the furnace through fuel-bounded nitrogen and small air leakages, and produce NO_x. This situation is exemplified in Figure 5.7.C. The concentration of nitrogen oxides is presented along the centreline of the furnace during combustion of lignite. The concentration of NO_x measured under air conditions is considerably lower than the values measured for both oxyfuel cases. Several factors may be responsible for this observation:

1. Air leakage into the combustion chamber
2. Fuel-bounded nitrogen
3. Thermal related formation of NO_x
4. The concentration of this pollutant is increased by the effect of a reduced flue gas volume

Although NO_x measurements are clearly higher in oxy-firing condition, it should be reminded that the flue gas volume from oxy-firing systems is reduced significantly depending on the recirculating ratio applied. The present experiments were conducted without a real recirculation circuit (secondary gas was injected from storage tanks). However, Figure 5.8 compares the calculated NO_x emissions considering the equivalent recirculation ratio of tested oxyfuel cases (OF29 ≈ 71%, OF32 ≈ 66%). The recirculated NO_x has no additional influence since it has been demonstrated that 50-80% of NO_x produced in oxyfuel systems can be reduced to N_2 when recycled back to the furnace [76], [128], [131]. The values in Figure 5.8 are expressed in mass per energy input to account for volume flow differences. In general terms, the emission of NO_x per unit of fuel energy supplied is reduced to about 40% of the values measured in air-fired conditions, which is in line with the result of other researchers in this area [128], [132], [133].

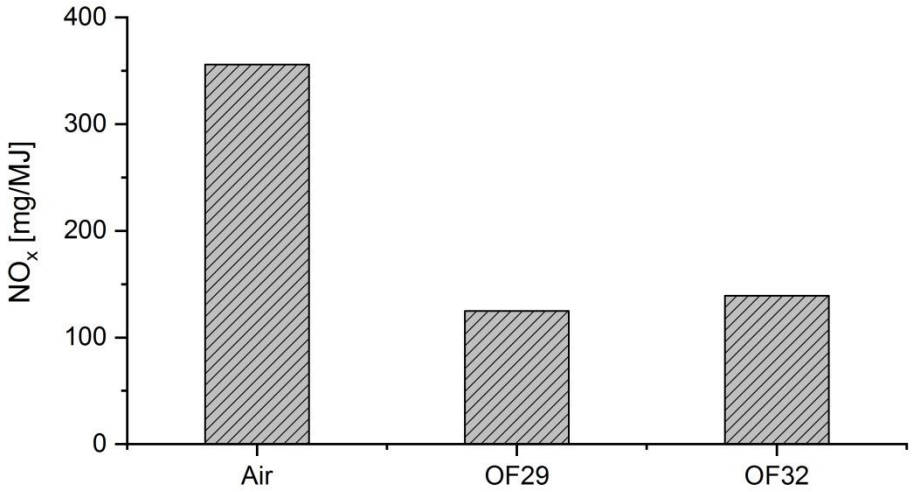

Figure 5.8: NO_x emissions expressed in mass per energy input during combustion of lignite.

Higher concentrations of SO_2 were also observed during oxyfuel firing compared to combustion in air conditions as pictured in Figure 5.7D. The concentration of SO_2 during OF32 resulted three to four times higher than the concentration measured in air-blown combustion, while the values measured during OF29 resulted close to two times higher. As evinced, the oxidation of sulfur benefits from higher oxygen availability in oxyfuel mode.

Different to recirculated NO_x which can be reduced when re-burned in the flame, sulfur in the system could experience an “accumulation effect” if this component is not removed in the flue gas path previous to recirculation. Further, when considering a real clinker production scenario, SO_2 originated from combustion of fossil fuels reacts with alkalis present in the material feedstock to form sulfates, leaving the kiln with the produced clinker [17]. This second mechanism has an important effect in the sulfur mass balance in the system.

The axial profiles of oxygen and carbon monoxide during combustion of petcoke in air and OF27 conditions are displayed in Figure 5.9. The pace of oxygen consumption is similar between the two investigated cases. As already mentioned, the ignition of low-volatile petcoke demands a longer distance compared to lignite producing a much longer flame. Total fuel combustion, marked by a stable value of residual oxygen is achieved after a distance of 3 m, which is two times the distance observed in lignite combustion.

CO emissions registered during petcoke combustion are significantly lower compared to the values measured during demonstration tests with lignite as observed in Figure 5.9.B. It has been observed by other authors that CO-peaks in oxyfuel combustion increase with volatile content in the fuels [130]. Dhungel [128] carried out several combustion tests in oxyfuel conditions with gas and different coals. During oxyfuel combustion with 27 vol.% oxygen he reported a maximum CO concentration of around 8.5 vol.% with natural gas as fuel, 6.5 and 3.1 vol.% with lignite (Lausitz; and Rheinisch, respectively) and 2.9 and 2.2 vol.% with bituminous coal (Klein Kopje and Ensdorf, respectively). The difference is explained by a lower production of CO via the homogeneous reaction route (see Eq.22). The lower CO concentration in OF27 mode compared to the air case in Figure 5.9 can be explained by the differences in gas temperature. Char gasification is strongly influenced by temperature as reported in [134]. As observed in Figure 5.5, lower peak-temperature was measured during oxyfuel in this case.

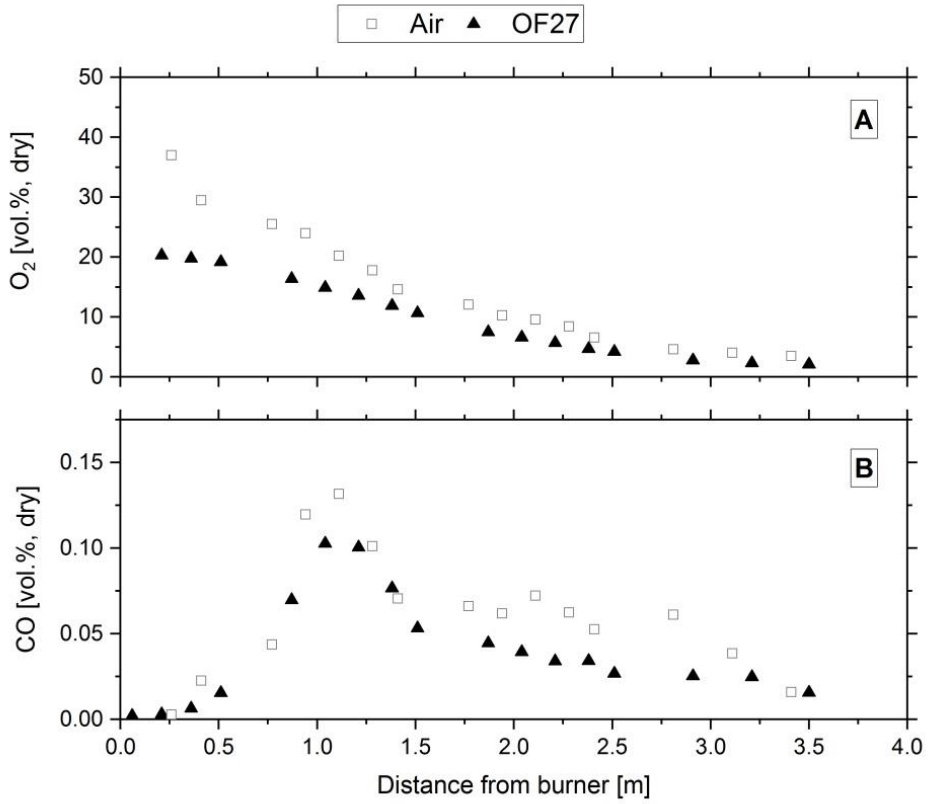

Figure 5.9: Distribution of O_2 (A) and CO (B) concentration in air-blown and OF29 cases during petcoke combustion (measurements at furnace centerline).

Figure 5.10 displays the values of NO_x and SO_2 measured at furnace outlet during combustion of low-volatile petcoke. Similar as during combustion of lignite, the oxyfuel cases display higher concentration of NO_x and SO_2 due to a higher availability of oxygen in the gas mix. The concentration of SO_2 in all cases, however, is significantly higher during the combustion of petcoke in comparison to lignite. The difference is originated in the sulfur content in each respective fuel. While lignite has a sulfur content of 0.36%, the content in petcoke rises to 3.23%.

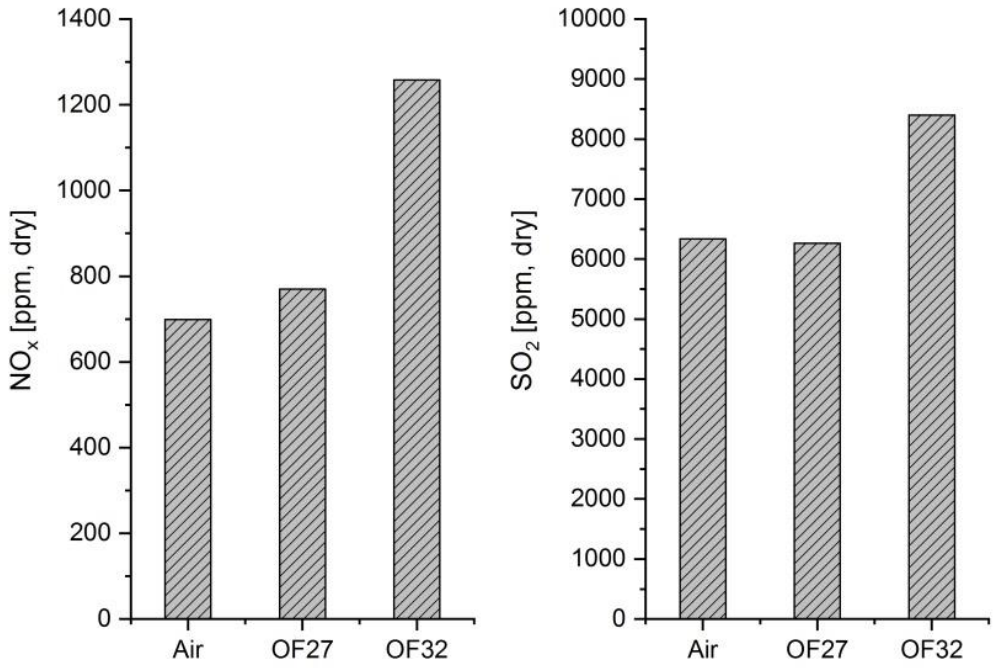

Figure 5.10: NO_x (left) and SO_2 (right) concentrations measured at furnace outlet during combustion of petcoke.

Figure 5.11 shows the values of NO_x expressed in mass per input energy during combustion of petcoke. The presented values are again a result of a calculation considering a theoretical scenario where recirculation is imposed as explained before. The results are similar to the ones observed in combustion with lignite. The oxyfuel cases have a lower NO_x emission of nearly 25-45% the values observed in combustion with air.

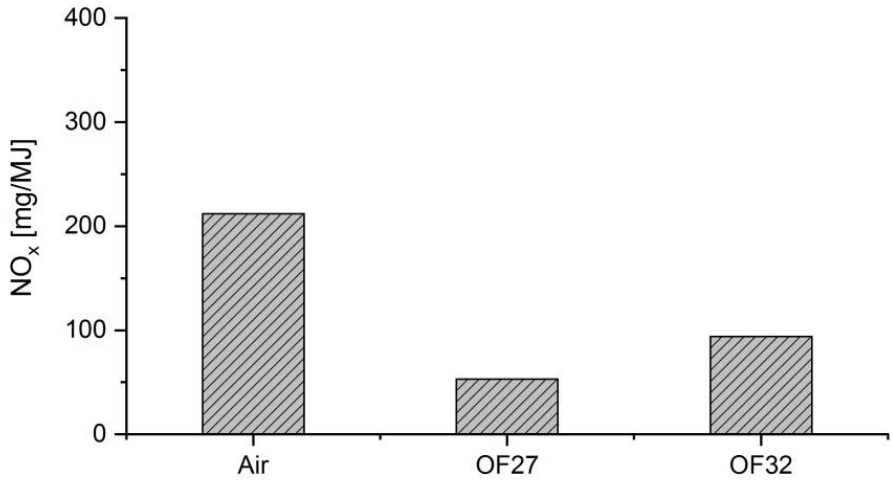

Figure 5.11: NO_x emissions expressed in mass per energy input during combustion of petcoke.

5.2.3 Heat flux

Radiation is the main mechanism of heat transfer to the material bed in cement kilns. Other mechanisms involved are conduction and convection. Differences in radiative heat transfer between oxyfuel and air combustion are expected due to the radiant nature of the main components of oxyfuel flue gases, carbon dioxide and water vapor. Additionally, as oxygen concentration increases, so does the flame temperature and the radiation intensity; the latter due to the strong non-linear relation of radiation intensity with temperature as described by the Stefan-Boltzmann equation (see (Eq.23).

$$\dot{Q}'' = \sigma \varepsilon T^4 \qquad \text{(Eq.23)}$$

Radiative heat flux measurements were conducted at the wall (400 mm from the centerline) from burner height to a distance of 2.5 m and 3.5 m during lignite and petcoke combustion, respectively. The profiles of radiative heat transfer for each combustion case are plotted in Figure 5.12.

During lignite combustion, the values of radiative heat flux show a steep increase until fuel ignition before developing a near-horizontal profile. The oxyfuel case OF29 and OF32 present similar behavior with heat flux values on average 20% higher than the values measured in air-blown combustion.

In the cases where petcoke was employed as fuel, the values observed in the air-blown combustion case are lower than in combustion with lignite. One explanation could be

the poor ignition behavior of petcoke particles. The fuel particles ignited at a larger distance and the formation of a defined flame structure was weak compared to the combustion of high-volatile lignite particles. Regarding the oxyfuel cases, the OF27 case shows heat flux values approximately 25% higher than the air case. The case with 32% oxygen, OF32, outstands with peak values of 350 kW/m^2, nearly three times the values measured in air combustion at the same distance from the burner.

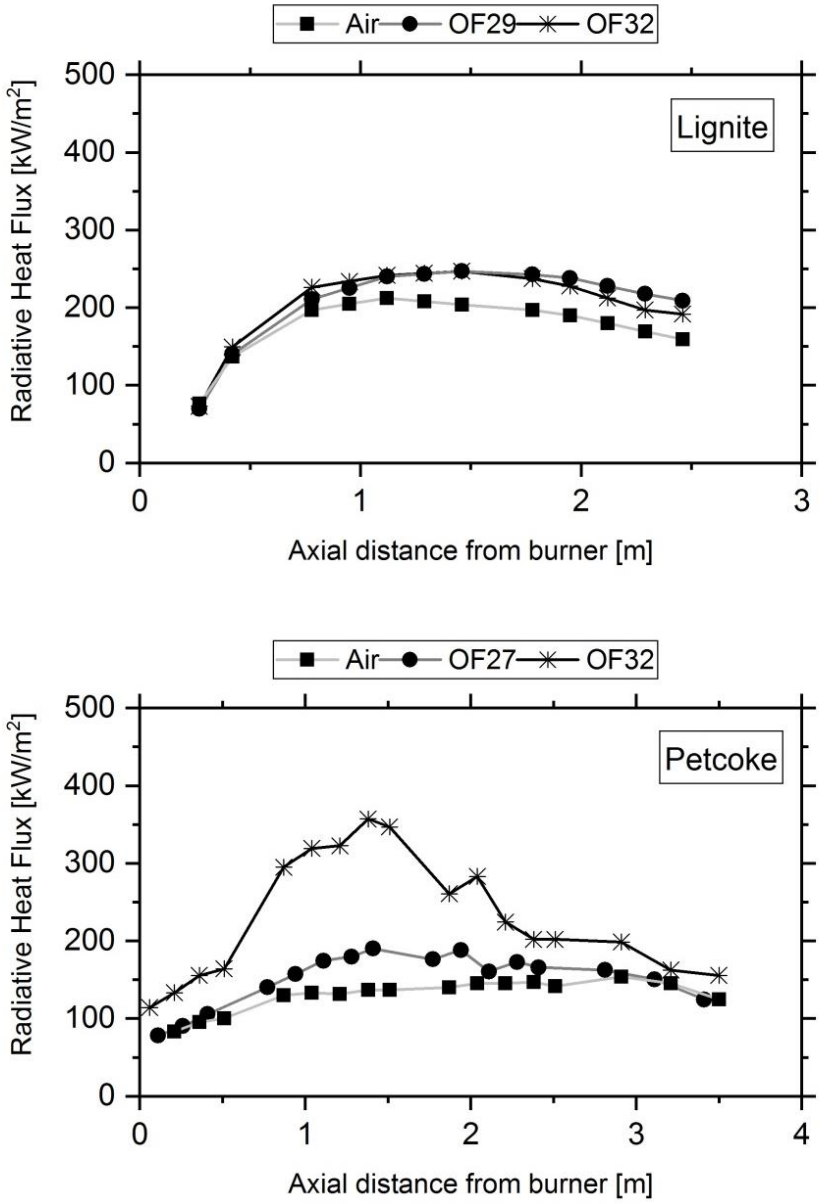

Figure 5.12: Radiative heat flux measured with the ellipsoidal radiometer during combustion of lignite (above) and petcoke (below). Measurement error ±5%.

Figure 5.13 displays the maximum peak of radiative heat flux measured during the combustion of lignite and petcoke. These values are compared against the results of Smart et al. [98], who used a similar set up with a Russian and a South African coal. The measured values are normalized by the peak values obtained in combustion with air for each respective fuel. All cases presented higher peak values of radiative heat flux in oxyfuel mode compared to their respective air cases. The values measured in this study with lignite combustion are in agreement with the values reported by Smart et al. [98]. In general, the values range from 1.07 to 1.35, which evinces that higher radiation intensity is expected when changing the combustion atmosphere from air to oxyfuel.

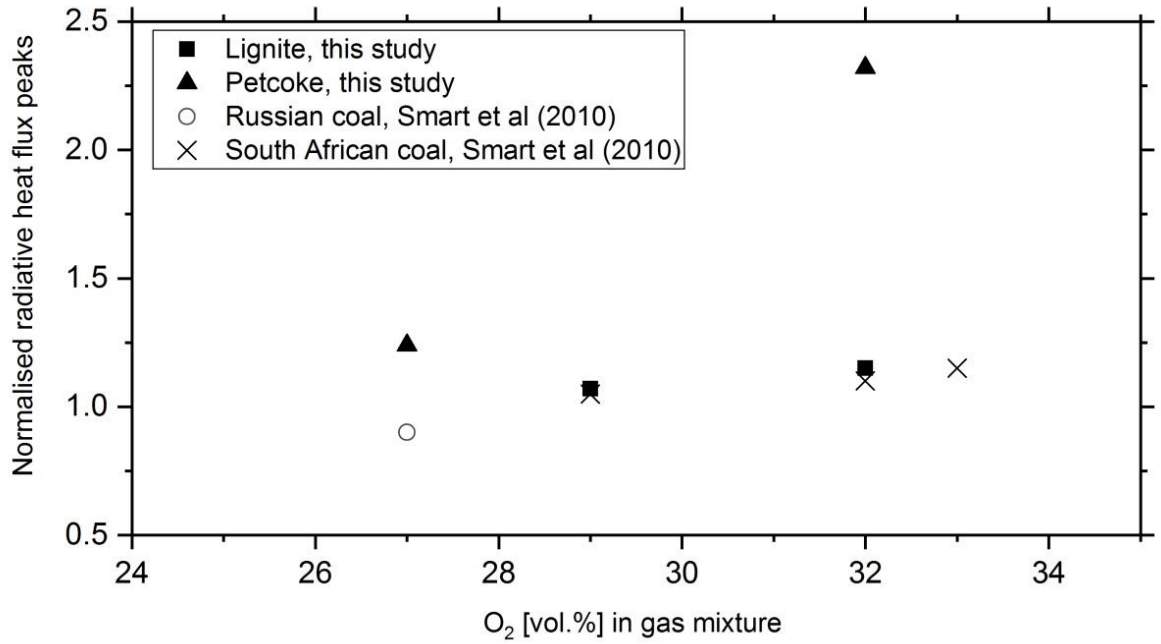

Figure 5.13: Peaks of total heat flux and radiative heat flux normalized by their respective values in air firing.

As observed in Figure 5.13, the oxyfuel cases OF27, OF29 and OF32 (lignite combustion) show only a modest increase in the radiative heat flux peaks in the range of 10 - 25% higher than the reference air case. It can be inferred that this slight increase is related to the high concentration of CO_2 and H_2O in the combustion gases. Also, particle concentration increases in the oxyfuel cases as the total volume of combustion gas decreases. As reported by several authors [64]–[66], the impact of gas radiation can be reduced by the overlapping of particle-gas radiation. Particle radiation has a more dominant presence than gas radiation as it absorbs and emits radiation in the entire electromagnetic spectrum, while gas radiation emits only at certain wavelengths.

Gas radiation continues to be important in regions of less particle-radiation dominance, e.g. the furnace outlet area.

A higher radiative heat flux peak observed during combustion of petcoke in the OF32 case cannot be explained and is probably related to the gas temperature differences between the oxyfuel and air-firing case.

5.2.4 Combustion efficiency

The efficiency of combustion can be assessed using the parameters burnout (η) and unburned carbon (φ) presented in section 3.3.4. Table 5.5 shows the values of burnout and unburned carbon for both fuels in air and oxyfuel mode. Similar values were calculated for the air and oxyfuel cases, i.e. no significant differences in combustion efficiency are shown. The values calculated for petcoke are higher compared to lignite, as expected and influenced by the initial carbon content in the fuel and its low reactivity.

Figure 5.14 presents the values of unburned carbon plotted against the exit oxygen concentration in the furnace. The results obtained during this study for the combustion of lignite are compared with the results of Smart et al. [98] burning a high-volatile bituminous Russian coal in air and oxyfuel operation. The values obtained in the present study are in a similar range to the ones they are compared with. Furthermore, the differences between the air and oxyfuel cases are minor. The results obtained with petcoke are not presented since the fuel characteristics are significantly different, which makes the results not comparable.

Table 5.5 Calculated combustion efficiency from fly ash.

	Lignite			**Petcoke**		
	Air	**OF29**	**OF32**	**Air**	**OF27**	**OF32**
Burnout (η)	99.8%	99.8%	99.8%	98.2%	98.3%	97.4%
Unburned carbon (φ)	0.09%	0.11%	0.08%	1.72%	1.36%	2.29%

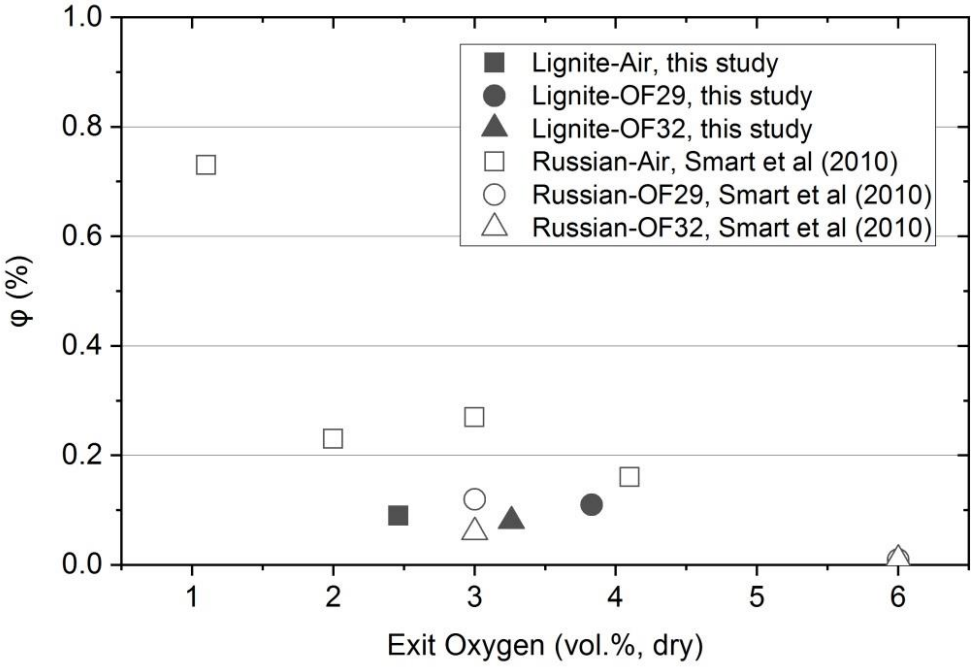

Figure 5.14: Unburned carbon (φ) results obtained during combustion of lignite (this study) and a Russian high volatile bituminous coal, oxyfuel and air operation.

5.3 Impact of burner configuration

5.3.1 Oxygen distribution

The influence of oxygen distribution in burner outlets is assessed comparing the combustion performance of three oxyfuel cases with 29 vol.% oxygen featuring a different distribution of oxygen in primary and secondary gas. Table 5.6 presents the composition of the main inlet streams in the investigated cases.

Table 5.6: Test conditions for the experimental investigations on oxygen distribution.

	Case 1 **20 vol.% O_2**	**Case 2** **40 vol.% O_2**	**Case 3** **60 vol.% O_2**
Fuel mass rate (kg/h)	65	65	65
Composition of primary stream	20% O_2 80% CO_2	40% O_2 60% CO_2	60% O_2 40% CO_2
Composition of secondary stream	40.5% O_2 59.5% CO_2	30% O_2 70% CO_2	19.4% O_2 80.6% CO_2
Composition of carrier gas	100% CO_2	100% CO_2	100% CO_2
Volume flow ratio of secondary to primary stream	3.78	3.78	3.78
n (stoichiometric ratio)	1.10	1.10	1.10

To compare these cases, the concentration of oxygen, carbon monoxide, nitric oxide and gas temperature measured over centerline are presented in Figure 5.15. The figures evince a similar gaseous and temperature profile for the cases with 20% and 40% oxygen in primary gas. Shifting more oxygen from secondary gas to primary gas does not produce significant differences in ignition as shown in the gas temperature profile of Figure 5.15.

The main factor of distinction among the cases is the CO concentration profile in the near burner field. CO concentration peaks 7 vol.% when the oxygen concentration in primary gas is only 20%. CO concentration decreases as the oxygen content in primary gas is increased. This behavior indicates a strong activity of heterogeneous char gasification reactions (Eq. 5) owing to a high CO_2 partial pressure in the center of the furnace. The differences are important in the flame region, while they become negligible towards the furnace outlet.

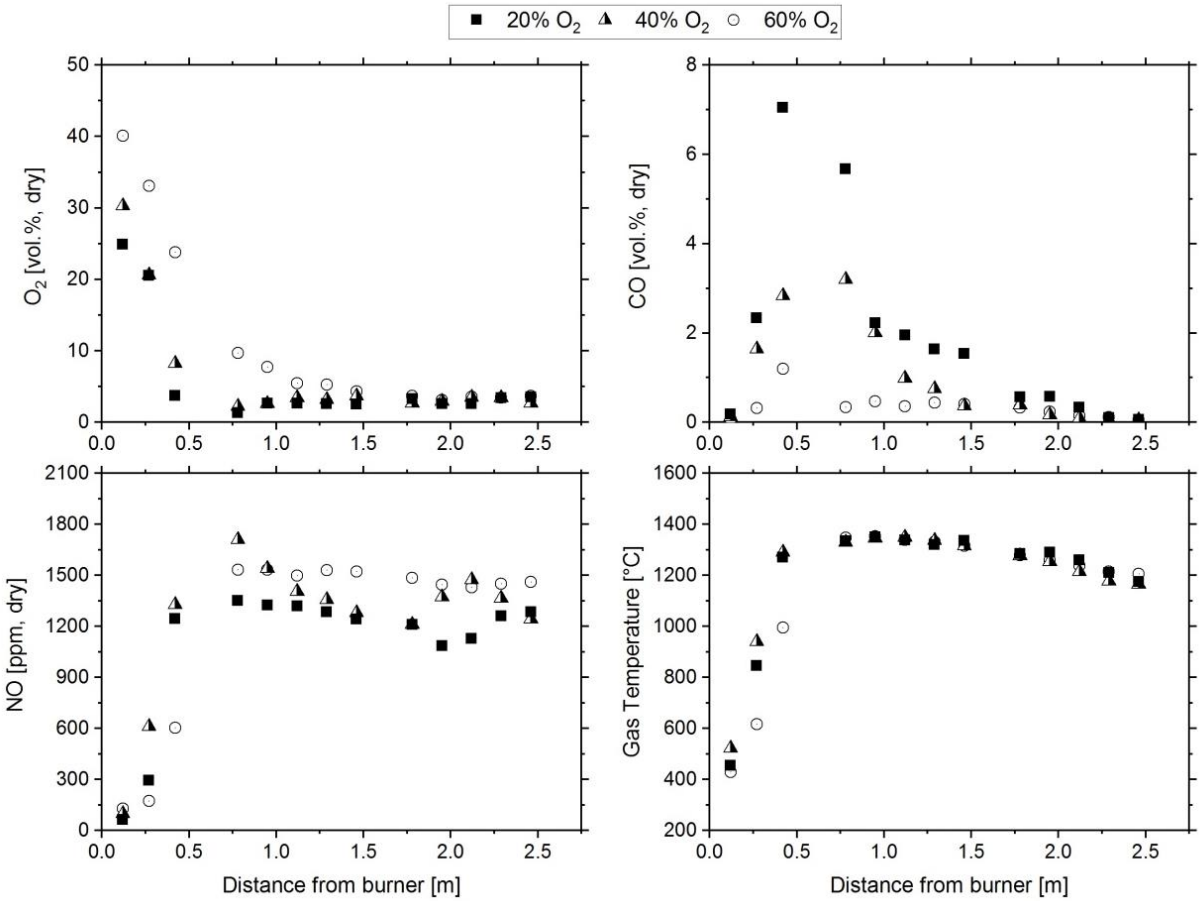

Figure 5.15: Measurements of O_2, CO, NO and gas temperature over centerline by increasing oxygen volume fraction in primary gas (20%, 40% and 60%). OF29 during lignite combustion.

Similar results were obtained during co-combustion tests of lignite and SRF (20 wt% SRF). Two oxyfuel cases both with 30 vol.% oxygen in total gas for combustion (OF30) are compared to a reference air case. The difference between the two OF30 cases lies in the concentration of oxygen in the primary gas. One of the cases was provided with 50% oxygen in primary gas (PG), while the other was set to 20% oxygen. In both cases, the concentration of oxygen in the secondary gas was compensated to obtain in total 30% oxygen (OF30) in the sum of primary, secondary and carrier gas. Figure 5.16 presents the profile of gaseous components and gas temperature in the axial direction. Here again, the differences in the ignition are not significant. Judging by the oxygen consumption rate, a slightly faster ignition is observed by the case with 50% oxygen in primary gas.

Regarding CO formation, the air-blown case and the OF30 case with 50% oxygen in primary gas present similar profiles. CO concentration increases in the oxyfuel case

with 20% oxygen in primary, particularly in the region near the burner similar to the observations in Figure 5.15, due to the intense action of the gasification reactions.

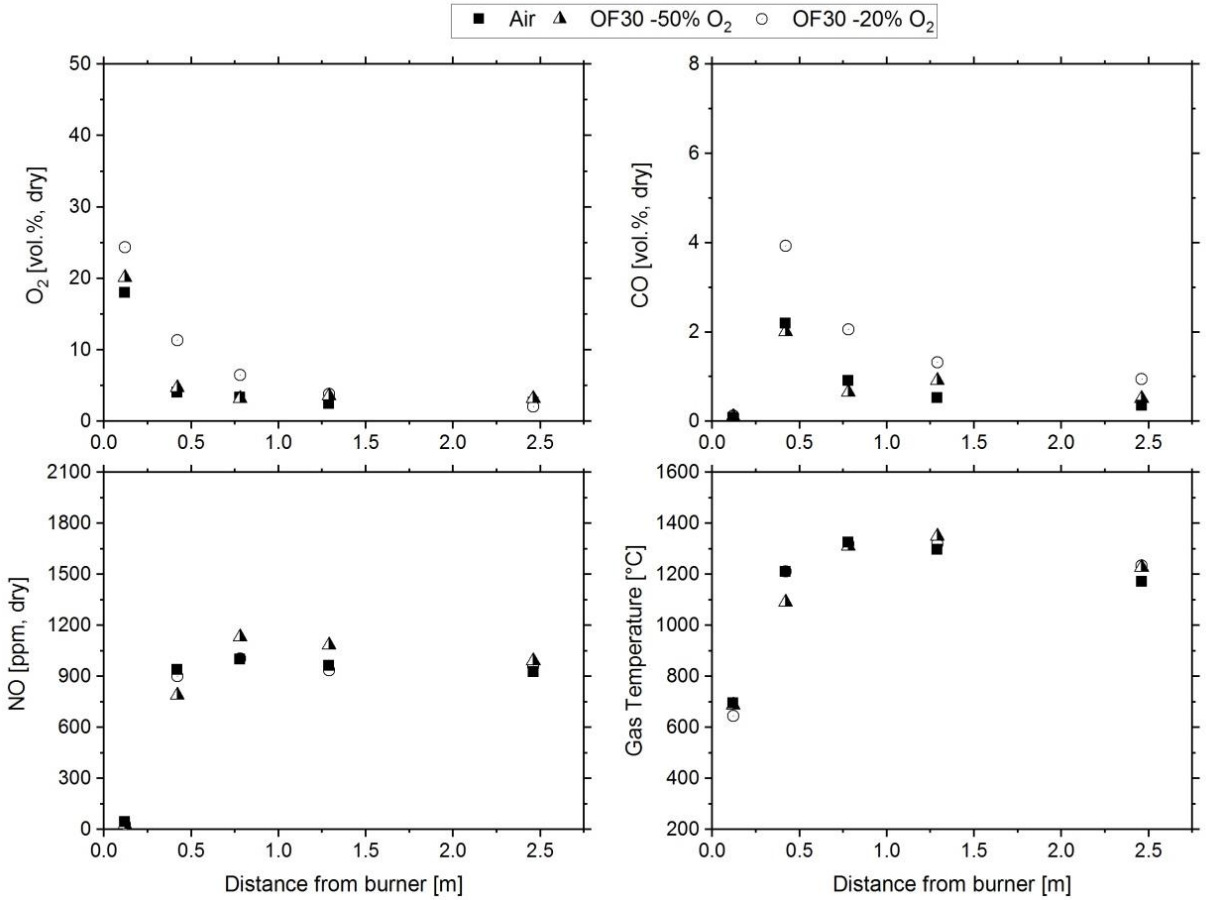

Figure 5.16: Measurements of O_2, CO, NO and gas temperature over centerline during co-combustion of lignite and SRF. Three cases compared: air-blown, OF30 (20% oxygen in PG) and OF30 (50% oxygen in PG).

.

5.3.2 Swirl flow

A classic tool to adjust flame shape is the use of swirling flows. By increasing the angle of injection of primary gas in the tangential direction a stronger mixing between fuel particles and oxidizer can be achieved, and in turn a shorter and more intense flame. This parameter is widely used by burner manufacturers to shape the flame and increase the burnout of difficult or alternative fuels in rotary kilns [135], [136].

Figure 5.17 presents measurements of gas concentration and temperature when variating the angle of injection of the primary gas nozzles in the tangential direction using 0°, 12.5° and 25°, which represent a swirl number 0, 0.14 and 0.31 respectively. The investigation was done in the oxyfuel case OF29 with 60% oxygen in primary gas. As

expected, the temperature profile increases at a shorter distance when increasing the angle of injection to 25°, which evinces a change in flame length.

When adjusting the angle of injection to 0° (straight flow), higher CO values are registered in a quite extended region. This behavior is the result of a weaker mixing between fuel and oxidizer, and therefore, incomplete combustion of fuel particles. By increasing the swirl number, the CO values reduce and temperature increases towards the burner.

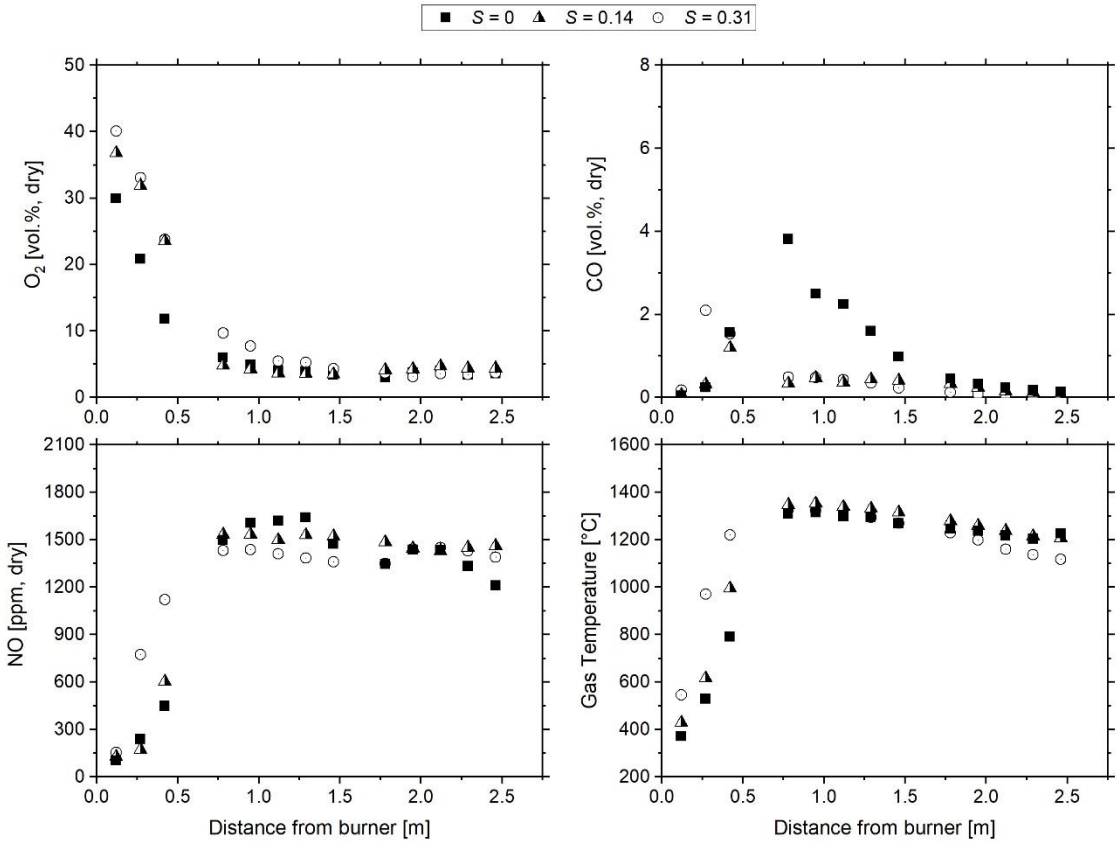

Figure 5.17: Measurements of O_2, CO, NO and gas temperature at furnace centerline when varying the swirl number implemented in primary gas during combustion of lignite in the OF29 case.

5.4 Flame length

There are several means of dimensioning the flame length. It can be done visually by observing the flame intensity or by measuring a species or temperature profile along the centreline. For the combustion tests with lignite, the flame length is defined at the point in the streamwise direction where the concentration of carbon monoxide is lower than 0.1 vol.% (dry basis). According to Figure 5.7B, flame length was dependent on the oxygen enrichment in oxyfuel mode. The flame length was seen to shorten as the oxygen concentration was increased to 32%. The flame was also observed to shift towards the burner or ignite faster as the oxygen enrichment was increased. The flame screenshots presented in Figure 5.18 display this effect. Further, Figure 5.15 and Figure 5.17 showed that flame shortens also when increasing oxygen concentration in the primary stream and increasing the swirl angle.

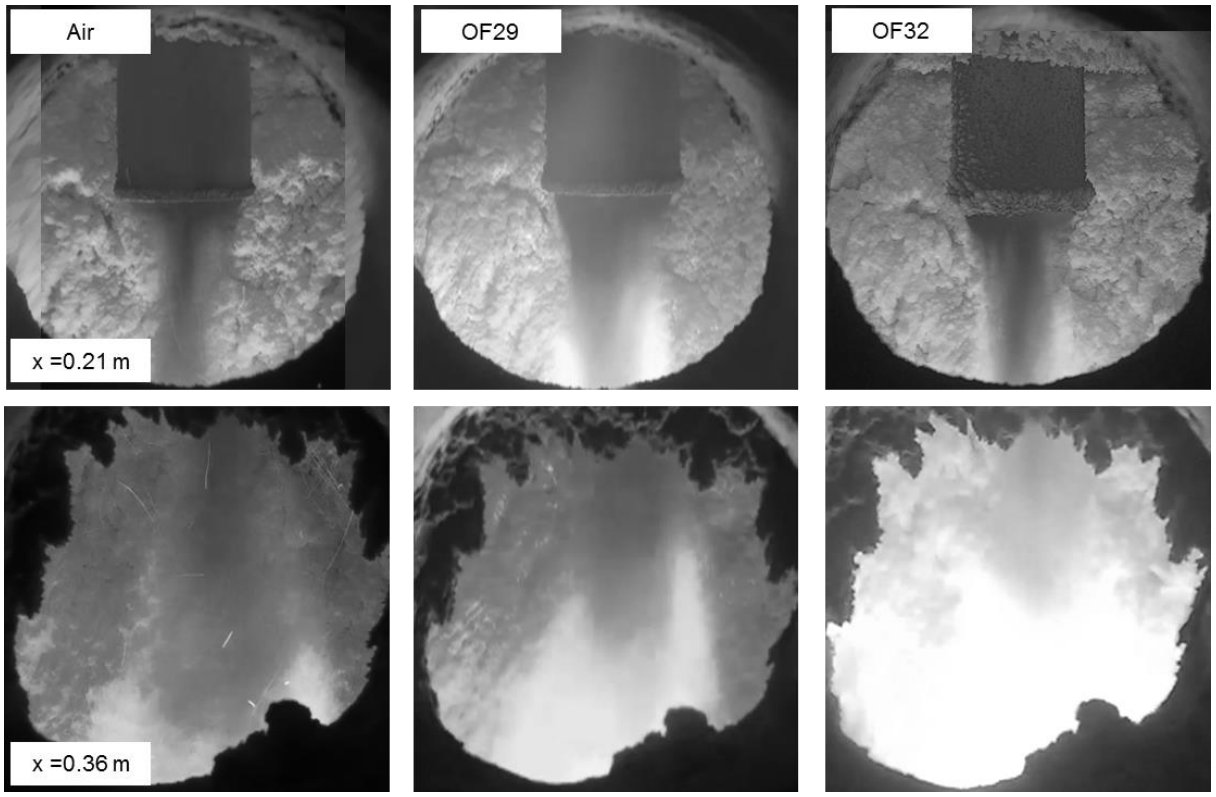

Figure 5.18: Flame snapshots taken at three different x distances in axial direction during combustion of lignite. Left column: air; middle column: OF29 and right column: OF32.

The flame length during petcoke combustion was not evaluated according to the concentration of CO since very low values were observed in comparison with lignite (see Figure 5.9). However, a similar trend is observed if the peak temperature is taken as reference in Figure 5.5. The distance to the peak temperature decreased when the oxygen content in the gas mixture increased. The oxyfuel case with 27% oxygen in

combustion gas showed a similar flame length compared to their respective reference air case.

In general, the flame lengths observed during the trials were relatively long compared to typical flame research conducted in the past at the test facility. Long flames are typical in rotary kilns in the cement industry. Further, typical dry-process cement kilns are constructed with a L/D not lower than 11 [137] while the pilot furnace has a length to diameter ratio (L/D) of 8.75. Very long flames summed with high water content in the flue gases especially during oxyfuel combustion caused clogging of the heat exchanger at furnace outlet limiting the duration of the trials.

5.5 Secondary air entrainment

Even though the based burner is designed to operate at primary gas velocities in the range of 200-250 m/s, the scaled burner was limited in this regard due to larger nozzle as dictated by the constant velocity scaling criterion. In order to compensate this condition, higher mass flow was injected through the primary gas nozzles. Table 5.7 shows the calculated gas velocity and the share of primary gas (including carrier gas) during the combustion tests of lignite and petcoke. The share of primary gas reported in the experiments is in the range of 22-41%, which is significantly higher than the industrial scenario (6-13%). The relative low temperature peaks observed during the trials may be explained by the high proportion of “cold gas” related to the sum of primary and hot secondary gas.

In general terms, high specific flame momentum G_0, discussed in section 2.4.1, is used to efficiently entrain hot secondary gas into the flame. A moderate recirculation of flue gas products back to the flame root is an indication that fuel and gases are mixed, while an absence of recirculation is an indication that not all secondary gas has been entrained into the primary jet [54].

A mathematical formulation to calculate if primary gas momentum is sufficient to entrain secondary gas is given by Craya-Curtet parameter m (see Eq. 2).

The last two columns in Table 5.7 include the values of primary gas momentum and the Craya-Curtet parameter calculated for the tested cases. As observed, all cases except the air case with petcoke have values of m larger than 1.5. Further, the values calculated for the oxyfuel cases are larger compared to their respective air reference scenarios. The explanation for this result is higher density of CO_2 compared to nitrogen and reduced volume flows of secondary gas.

Table 5.7: Velocity, share of primary gas and specific flame momentum of primary gas.

	Primary gas velocity [m/s]	Share of primary gas + carrier gas [%]	G_0 [N/MW]	Craya-Curtet parameter m
Lignite				
Air	177	26.1	5.1	1.8
OF29	177	36.3	6.5	5.0
OF32	177	41.2	6.5	7.4
Petcoke				
Air	132	22.7	2.9	0.9
OF27	167	28.2	6.0	2.2
OF32	132	34.5	3.5	2.9

5.6 Conclusions from experimental work

The constructed burner was employed to investigate the combustion behavior of selected fuels in air and oxyfuel combustion modes under cement production conditions. The results presented here showed that the oxygen concentration in the mixture of gas for combustion is a key parameter to obtain similar results as in air-blown firing. For the tested conditions an oxygen volume fraction of 27-29% resulted in a similar temperature profile as in air-blown combustion.

Both, gas temperature profile and radiation heat fluxes to the furnace walls are dependent on the combustion atmosphere. Due to the difference in emissivity of CO_2 compared to N_2, higher heat fluxes to the walls were observed for oxyfuel cases with 27, 29 and 32 vol. % oxygen in oxyfuel mode compared to air firing. As the oxygen concentration raises the peak temperature moves closer to the burner and heat transferred to furnace walls increases accordingly. For an oxyfuel case with a similar temperature profile as air-firing, an increase of 10-20% in radiative heat fluxes is expected.

CO emissions measured at furnace outlet are similar for air-blown and oxyfuel cases, which reinforces the thesis that CO emissions are not a problem when moving from

combustion in air to oxyfuel combustion. Elevated CO concentration was observed in the burner vicinity during oxyfuel combustion of lignite and in the co-combustion of lignite and SRF. Homogeneous reaction with CO_2 during fuel devolatilization (Eq.22) and the heterogeneous char gasification reaction (Eq. 5), favoured under high CO_2 partial pressures and high temperature, are assumed to be responsible for this behavior.

Even though N_2 from the air was excluded as much as possible, some fuel-N and air leakage were responsible for some NO_x formation. These emissions were observed to be 55-75% lower in oxyfuel mode compared to air firing when expressed in units of mass per energy of input. The observations are in line with previous investigations. Despite these demonstration tests were conducted in a once-through furnace without flue gas recirculation, no important differences are expected when recirculating flue gases due to the re-burning of NO_x in the flame.

No significant differences between air-firing and oxyfuel cases were observed in combustion efficiency as observed in the results of fuel burnout and unburned carbon. These results support the conclusion that combustion efficiency is not altered with an operational change to a high CO_2 atmosphere.

The operation in oxyfuel mode opens the possibility to redistribute the oxygen mass flow in the primary and secondary gas stream of a cement kiln. According to the tests conducted in this section, if the oxygen concentration is increased in primary gas (with a corresponding decrease in secondary gas) the generation of CO in the near burner field decreases significantly. Comparable result was observed when increasing the angle of injection of primary gas. With larger swirl number CO reduces in the burner vicinity and ignition is moved closer to the burner.

The flame length remains similar when changing the combustion atmosphere from air to oxyfuel condition if a total oxyfuel concentration in combustion gas of 27-29% is sustained. Higher oxygen concentration apparently reduces flame length.

The prototype burner was suitable to investigate both air and oxyfuel combustion. However, due to larger nozzles as required by the constant velocity criterion, the share of “cold” primary gas had to be increased to compensate primary gas velocity and momentum. The calculation of the Craya-Curtet parameter revealed sufficient primary gas momentum to entrain all secondary gas into the jet flame.

6 Numerical Simulation

6.1 Introduction

This chapter presents the numerical simulation of the investigated burner with the help of Computational Fluid Dynamics (CFD). The purpose of the simulations is to investigate additional scenarios not tested experimentally. Firstly, a computational model of the pilot furnace and the small scale burner is presented to conduct the simulation of two burner designs following the constant velocity and constant residence time scaling criteria. Secondly, a full-scale burner is simulated in air and oxyfuel mode focusing on the optimized operating conditions determined from the pilot experiments. The results are compared to numerical simulations conducted by other authors. The results from CFD simulations are used to adapt a process simulation tool and simulate of a full-scale cement plant operated in oxyfuel mode.

6.2 Background

In the last years dedicated mathematical sub-models have been proposed and implemented in diverse CFD packages to adequately model oxyfuel combustion [138]–[145]. CFD modeling has also been an important tool to understand the heat transfer phenomena occurring in rotary kilns for cement production [96], [146]. Although most of the numerical investigations on cement kilns have been limited to conventional air firing, recently the interest in researching the oxyfuel combustion technology for carbon capture in cement kilns has raised. Granados [48] studied the effect of flue gas recirculation from an oxyfuel cement kiln on gas temperature and a way to optimize it. A study published by ECRA included the CFD simulation of a kiln burner operated in air and oxyfuel conditions with a generic burner [16]. It was concluded that significant differences can be expected in both combustion atmospheres in terms of flame length and radiation to walls.

An existing cement process model developed by VDZ was adapted to include oxyfuel operation using the results of CFD simulation conducted by Ditaranto and Bakken [147], [148]. The heat transfer by radiation from the kiln gas to the material for the oxyfuel operation could be matched to the air-fired operation by adapting the burner settings. This was achieved by switching mainly oxygen input from secondary to primary gas. Ditaranto and Bakken based the simulation of the burner settings on the results of the experiments presented in this work.

6.3 Mathematical models

CFD modeling in the present work is carried out with the help of the software AIOLOS developed at the Institute of Combustion and Power Plant Technology (IFK) at the University of Stuttgart. The code is based on the well-known Finite Volume Method and has been successfully applied in the past to model oxyfuel combustion in pilot as well as in semi-industrial facilities [139], [144]. More information concerning the software AIOLOS can be found elsewhere [149]–[151].

For the present simulation work, an Eulerian approach is used to simulate the two-phase flow field. The coupling between pressure and velocity is modeled with the SIMPLE algorithm and the ALLSPEED method developed by Anany [152] and previously implemented in AIOLOS [153]. The standard *k-ε* model [154] is used to model mean flow turbulence, while the Eddy Dissipation Concept accounts for the turbulence-chemistry interactions. This combustion model incorporates important heterogeneous reactions like the char gasification reaction or Boudouard reaction (Eq. 5) and the heterogeneous water-gas shift reaction (Eq.24), both relevant to oxyfuel firing [139].

$$\mathrm{C} + \mathrm{H_2O} \rightarrow \mathrm{CO} + \mathrm{H_2} \qquad \text{(Eq.24)}$$

Further, the Discrete Ordinates Method is selected to solve the radiative heat transfer equation (RTE). Gas emissivity for combustion in oxyfuel mode is calculated with the Leckner model [155], which predicts total emissivity of a gas mixture depending on its composition (CO_2 and H_2O) and temperature and has shown to yield accurate results when compared with band models [139]. Particle emissivity is modelled according to the Rizvi model. Table 6.1 summarizes the mathematical models used in the present analysis.

Table 6.1: Selected models for the CFD simulations.

Parameter	**Model**
Flow field	Eulerian approach
Turbulence	k-epsilon model
Chemistry	Eddy-Dissipation Concept (for gas-phase reactions), 2-Step Pyrolysis model, 2-Step Heterogeneous combustion model, char gasification reaction, water-gas shift reaction.
Radiation	Discrete Ordinates
Absorption coefficients	Gas: Leckner model, Particles: Rizvi model
Solver	SIMPLE-ALLSPEED

6.4 Simulation of the pilot test rig

6.4.1 Computational domain

A 180° section of the structured grid used for the simulation of the pilot tests at the 500 kW combustion test rig is presented in Figure 6.1. The mesh covers the interior of the combustion chamber from the top of the furnace down to a length of 3 m. The light blue zones in Figure 6.1 indicate the definition of the inlets, while the red line indicates the division of subdomains.

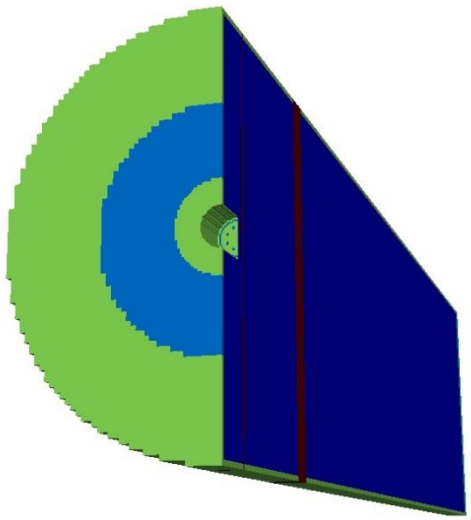

Figure 6.1: Longitudinal section of the computational domain used for the simulation of the 500 kW_{th} combustion facility.

At the outlets of primary gas injection, a 25° nozzle inclination angle is imposed to acceptably model the swirled flow (see Figure 6.2). Three different burner grid concepts were evaluated before starting with the more elaborated simulation process, detailed information on the evaluation of these mesh concepts can be found in [156].

The 360° mesh concept comprises three subdomains in Cartesian coordinates summing 1.1 x 10^6 cells for computation. The definition of the inlet vectors is defined according to the angle of inclination applied to the primary gas nozzles in order to produce the desired rotational motion as observed in Figure 6.3.

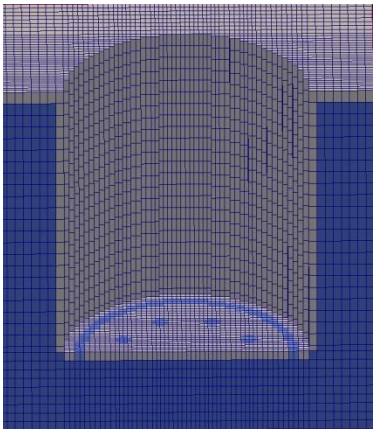

Figure 6.2: Detail of the burner outlet in generated grid.

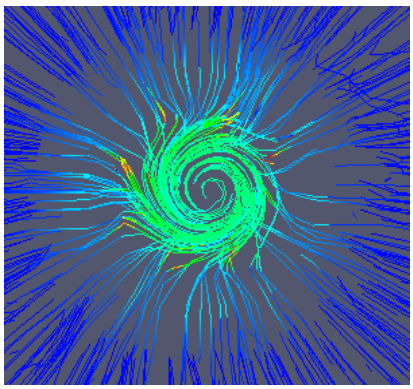

Figure 6.3: Velocity streamlines generated with defined inlet vector.

6.4.2 Validation with experimental data

A validation of the selected computational model was established by comparing the simulation results with the measurements of gas concentration and temperature obtained during the combustion of lignite in air. The boundary conditions were set according to the values presented in Table 5.1. Figure 6.4 presents the results over the furnace axis at centerline and a position 200 mm from the burner axis.

The computational model suffers of accuracy when predicting the temperature and gas concentrations at the center line. The predictions of the model are shifted downstream by approximately 0.7 m. In the other hand, the predictions at 200 mm from the burner axis provide better accuracy compared to the experimental data.

The discrepancy of the values predicted by the CFD model at the centerline can be explained by the incapacity of the turbulence model to accurately predict the swirl motion of the flow and subsequent mixing process. Further, the selection of a simplified

chemistry model implies that detailed chemical reactions ocurring in the gas and particle phase are not considered by the model. Finally, the centerline is characterized by important gradients of temperature and concentration and therefore the values tend to variate largely in space.

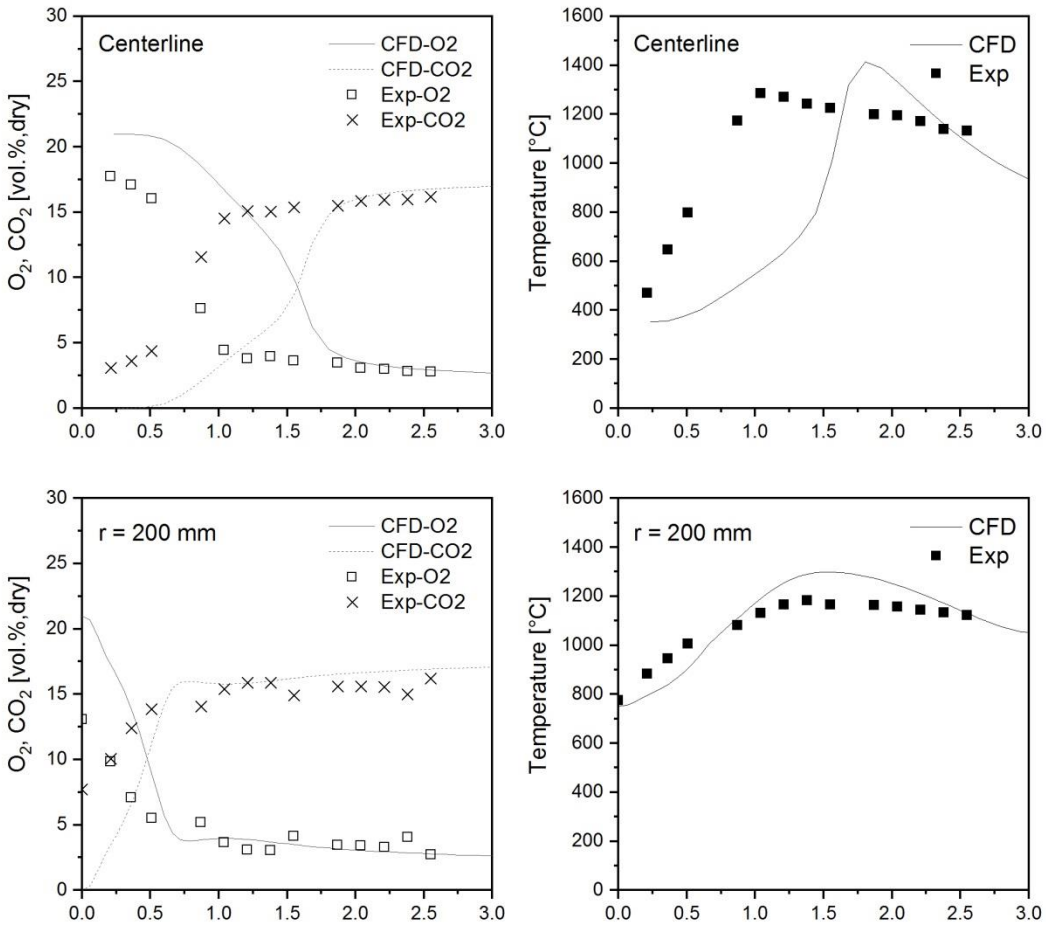

Figure 6.4: Validation of selected computational models with experimental data from the combustion of lignite in air conditions. Top: concentration of oxygen, carbon dioxide and temperature in centerline. Bottom: concentration of oxygen, carbon dioxide and temperature at r = 200 mm.

The computational model enables further investigation on different scaling concepts. As stated in Chapter 4, two different scaling criteria were initially considered for the burner design, the constant velocity and the constant residence time criteria. Even though the constant velocity criterion was selected, manufacturing constraints influenced the final dimensions of the burner.

A computational model was used to simulate the combustion of lignite with model burners following the constant velocity and the constant residence time criteria. Figure 6.5 shows a comparison of the temperature profile obtained with the manufactured burner and modelled burners. To make the results comparable, same input conditions were

imposed in all the cases. The low temperature area in the right side of the contour map is caused due to air injected though the flame detector and observation ports.

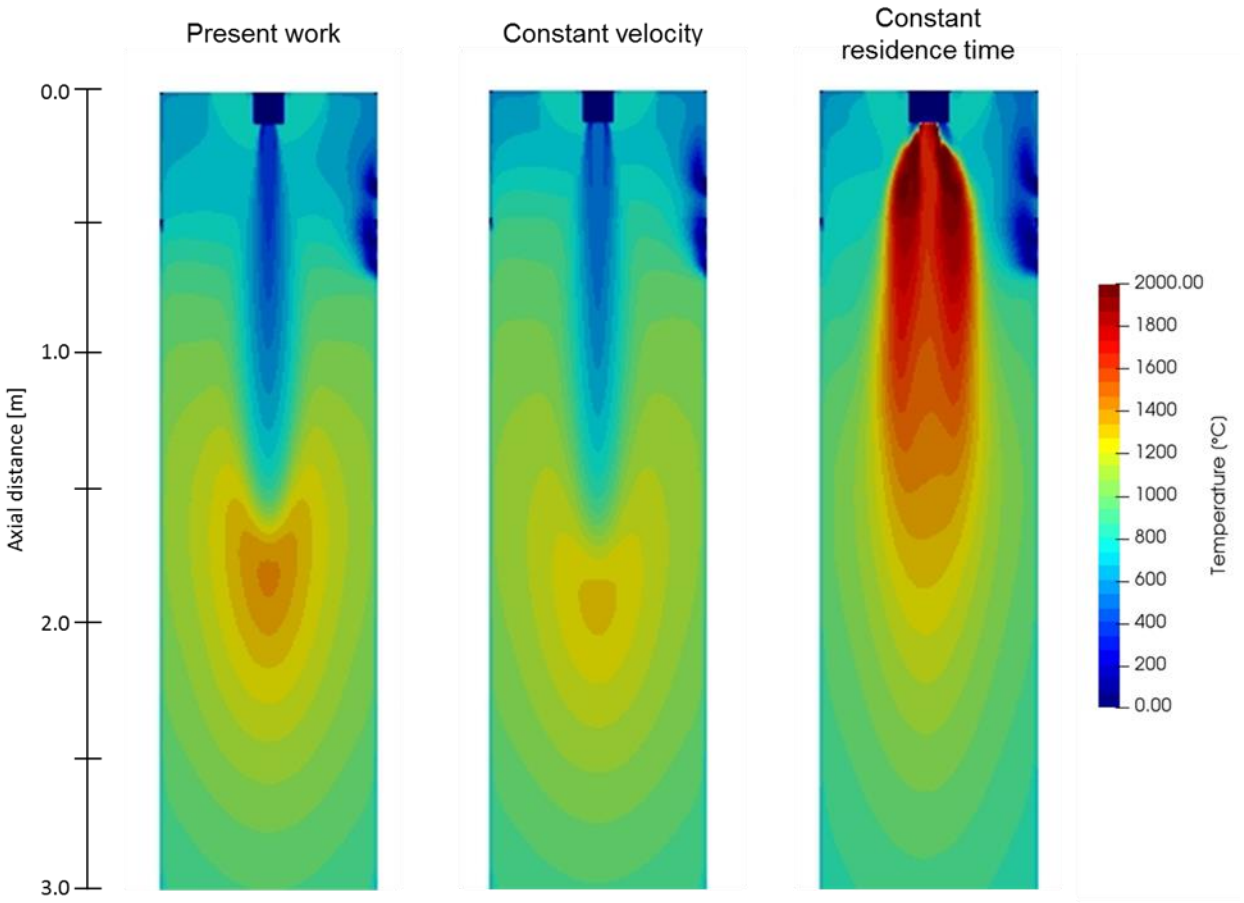

Figure 6.5: Temperature profile [°C] of the reference air case using distinct scaling criteria. Simulation of the first 3 meters of the test facility in the axial direction.

It is clearly seen in Figure 6.5 that the manufactured burner presents a similar temperature profile as the burner following a constant velocity criterion. The temperature profile of the burner following a constant residence time criterion is very distinct to the other two. The computational model predicts a much wider reaction zone and higher peak temperatures located near the coal and primary gas outlets. Additionally, the modeled burner following the constant residence time criterion shows internal recirculation zones that boost a shorter ignition point and the formation of a round flame. This temperature profile is more similar to the simulated in a full-scale rotary kiln as later observed in the next section. The shape is strongly influenced by lower velocity of the fuel particles carried by the primary gas flow providing longer time to react with the oxidizer.

6.5 Simulation of a full-scale oxyfuel kiln

6.5.1 Computational domain

The full-scale rotary kiln was modeled based on the dimensions of a cement kiln with a total length of 60 m and inner diameter of 3.76 m as described in a reference BAT cement plant [120]. The CFD domain is delimited at its back end by the secondary gas inlet area, where the burner is placed 1 m inside the combustion chamber at the kiln center as depicted in Figure 6.6. At the opposite end the exhausted flue gas exits the domain. For simplicity reasons no rotation is considered and the clinker material temperature boundary is set according to the literature [157]. Further, it is considered that clinker material is covering the refractory wall in the entire cylinder. This layer is modeled as a solid material with physical properties similar to those of clinker in order to capture the correct heat transfer properties between the flame and the material.

Similar to the mesh generated for the pilot experiments, the kiln is modeled with a 360° Cartesian grid with 1.1 x 10^6 cells. The mesh was adjusted to be more dense near the burner, this because the importance of the flame region in this study. The burner design with 10 nozzles was implemented

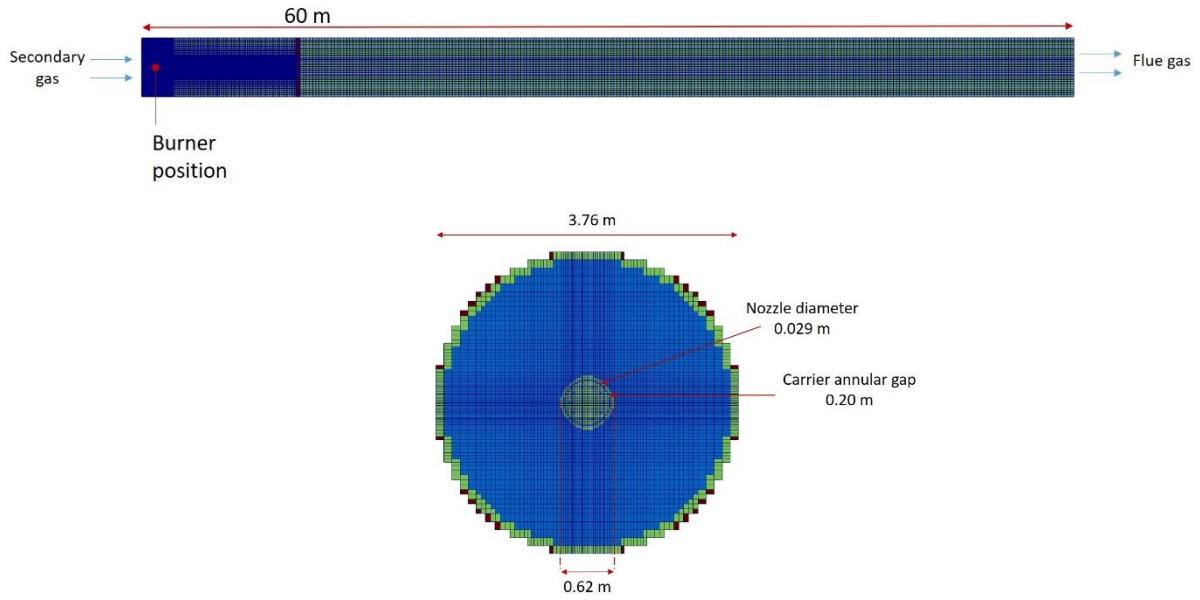

Figure 6.6: Slices of the computational domain used for the simulation of the full-scale oxyfuel kiln.

6.5.2 Process model

As mentioned previously in Section 2.3.2, the implementation of oxyfuel technology in a full-scale cement plant demands the adaptation or re-engineering of some production units, since the composition or characteristics of the exhaust gases are distinct to conventional operation. To evaluate the operation of the oxyfuel burner in an industrial-size kiln the conduction of both CFD and process simulations is appropriate.

The goal of the simulation work is to determine suitable combustion settings (gas flows and composition) that could be implemented in the rotary kiln to be capable of switching between conventional operation with air and oxyfuel operation without altering the heat transfer flux profile in the kiln.

The process simulation tool was developed by VDZ and incorporates mathematical models for each relevant unit that constitutes the clinker production process. More information on the implemented mathematical models can be found elsewhere [158], [159]. Three units require additional information to the models in order to adequately portrait the results in oxyfuel mode: rotary kiln, calciner and clinker cooler. The adaptation of the process model in the clinker cooler and calciner has been reported by Jamali [73]. These adaptations included information about the calcination temperature in O_2/CO_2 atmosphere, as well as the cooling rate in a high CO_2 atmosphere, among other.

The rotary kiln model also requires adaptation. The kiln is modelled in 1D and discretized into up to 50 segments in which mass and energy balances are calculated to create kiln profiles. The information required to complement the model is the differences in flame length and shape when operated in oxyfuel mode, as well as the heat radiation profile to the material bed in these altered conditions. CFD simulation of the rotary kiln is used to provide this information.

6.5.3 Inlet conditions

Ditaranto and Bakken [147], [157] conducted a series of CFD simulations of the oxyfuel kiln to find an optimized oxyfuel case with a radiative heat flux profile similar to the reference air case. They conducted the simulations with the commercial CFD software ANSYS Fluent 17.2 and a 36° wedge of the geometry imposing periodic boundary conditions. The CFD simulation of the full-scale kiln was conducted after validation of the model using the pilot burner experiments in the test facility presented in Chapter 5. The findings of the pilot experiments regarding the oxygen concentration needed to obtain an oxyfuel case that would reproduce similar profiles of temperature and heat transfer to walls were considered in the CFD settings. Further, the importance of high oxygen concentration in the primary gas to damper the negative effects of the

gasification reactions in the near burner region was also considered. The results of the CFD simulation were implemented into the process simulation tool to calculate if the material temperature profile was also similar as in air operation incorporating the total clinker production process. In an iterative procedure between kiln CFD simulation and process simulation it was revealed that the inlet conditions shown in Table 6.2 would satisfy this ambition.

Table 6.2: CFD inlet conditions for the reference air case and optimized oxyfuel simulation [129].

Parameter	**Units**	**Air**	**Oxyfuel**
Primary gas			
Volume flow rate	m^3/h (STP)	5100	4500
Temperature	K	323	323
O_2	%	21	60
Velocity	m/s	250	221
Nozzle inclination	angle	20º	30º
Carrier gas			
Volume flow rate	m^3/h (STP)	4040	1050
Temperature	K	323	323
O_2	%	21	18
Velocity	m/s	38.3	10.0
Coal mass flow rate	kg/s	1.469	1.469
Secondary gas			
Volume flow rate	m^3/h (STP)	29090	28126
Temperature	K	1073	1273
O_2	%	21	20.8
Velocity	m/s	3.7	4.3

The inlet conditions presented in Table 6.2 are implemented in the present simulation work and the results are compared with the work of Ditaranto and Bakken [147].

6.5.4 Simulation results

Figure 6.7 shows the temperature maps corresponding to the first 20 m of the kiln in axial direction under air (top) and oxyfuel operation (bottom). The maps evince a very similar flame shape formation in both combustion conditions. The swirl motion of the fluid created by the inclined primary gas nozzles generates a compact and axis-centered flame with internal recirculation. The highest temperature peak over centerline is located at 10.9 m and 9.3 m from the kiln back end for the air and oxyfuel combustion cases, respectively. Over centerline the peak temperature is slightly lower in the oxyfuel case (1806 °C in the air case and 1762 °C in the oxyfuel case). As observed in Figure 6.7, the highest temperature is not located over centerline but near the burner circumference. This is not an unusual result considering that the fuel channel is located near the burner periphery. In this region the oxyfuel case has a peak temperature of 2477 °C and the reference case 2258 °C. This difference may be related to the high oxygen concentration implemented in the primary gas for the oxyfuel case. The enrichment of oxygen in primary gas can also explain the differences in the penetration of the primary gas jet. Even though the exit velocity is comparable in both primary gas jet flows, the oxyfuel case is observed to penetrate less, or in other words to consume faster. The temperature at the kiln gases outlet is similar in both combustion conditions, 877 °C for the reference case and 890 °C for the oxyfuel case.

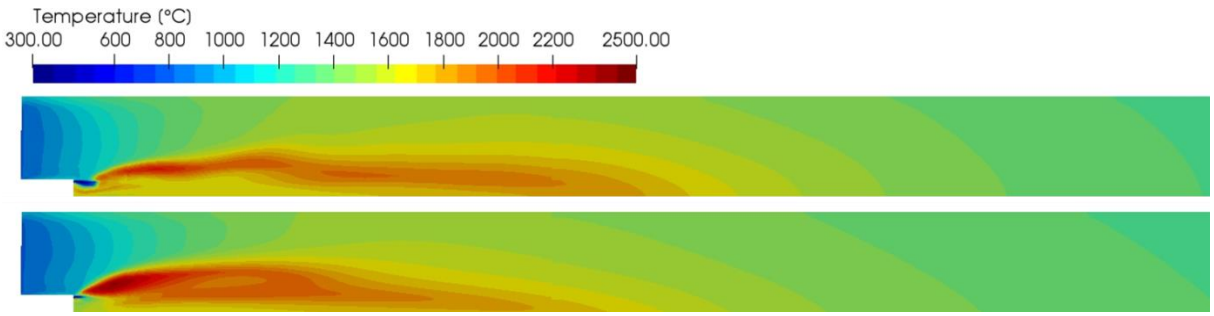

Figure 6.7: Contour maps of temperature (ºC). Air reference (top) and oxyfuel (bottom) cases. First 20 m of a total kiln length of 60 m.

The contours maps of temperature obtained by Ditaranto and Bakken shown in Figure 6.8 contrast with the results of the present work. Two important differences are the distance for ignition and the fact that the flame is not axis centered but displaced toward the kiln wall. A possible explanation is related to the computational domain employed to simulate the combustion process and especially the swirl motion created by the primary gas swirl angle. Ditaranto and Bakken modeled the burner swirled flow using only one nozzle in a 1/10th slice of the kiln. The interaction with other sections of the kiln

was modeled imposing a periodic boundary condition [147]. With this approach, the computational cost is reduced significantly, but interactions between the different nozzle exit flows may lack accuracy. The simulation of temperature shows a flame with a conic shape and impingement onto the kiln wall. Flame impingement in walls is more visible when observing the contour maps of carbon monoxide presented in Figure 6.9. This figure reveals that the reaction between fuel and oxidizer takes place not near the burner but in direction towards the kiln wall.

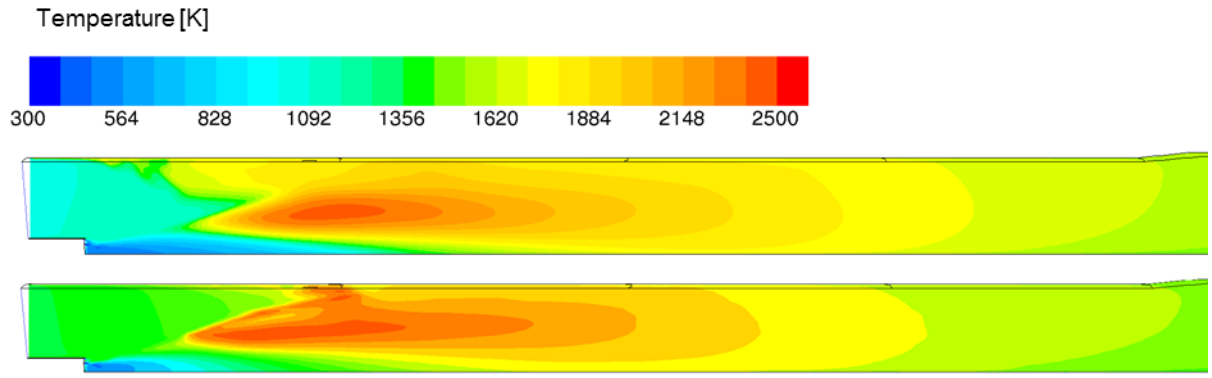

Figure 6.8: Contour maps of temperature (K) in the plane crossing the nozzle centerline. Air reference (top) and oxyfuel (bottom) cases with respectively 2360 K and 2239 K peak values. Results from Ditaranto and Bakken [147]

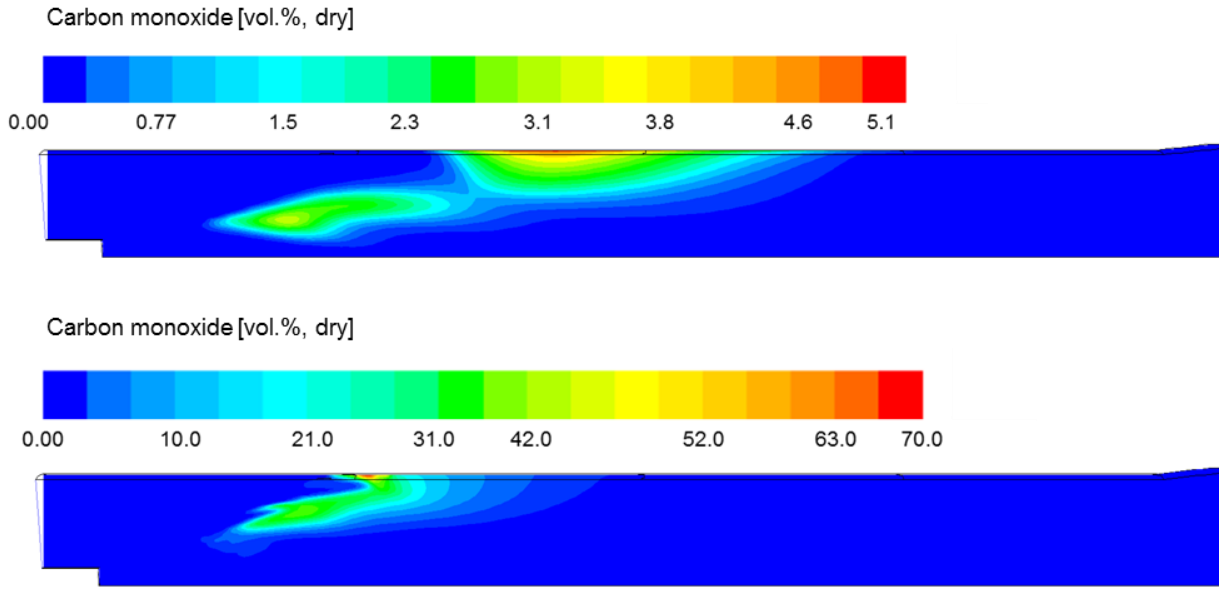

Figure 6.9: Contour maps of CO volume fraction in the plane crossing the nozzle centerline by Ditaranto and Bakken [147]. Air reference (top) and oxyfuel (bottom) cases.

In the present work the kiln was modeled with a 360° computational domain that included all nozzles with vector definition in the axial and tangential direction. The result is a flow that interlaces or weaves the individual nozzle exit flows to produce an efficient mixing of fuel and oxidizer evinced by a shorter ignition point and a flame centered in the axial direction.

Flame length is defined in this case as the point in the streamwise direction where the decreasing mean temperature profile crosses 1400 °C. This is also the definition that was used in the ECRA CCs project [42], and corresponds to the inflexion point in the temperature decay. Results for the reference and the oxyfuel cases are given in Table 6.3. In the present work slightly longer flame lengths were calculated and explained by differences in the flame shape. The differences between the reference and oxyfuel cases are not significant.

Table 6.3: Flame length results from the CFD simulations.

Case	Flame length
Ref. Air (present work)	18.4 m
Oxyfuel (present work)	18.0 m
Ref. Air (Ditaranto et al.)	17.0 m
Oxyfuel (Ditaranto et al.)	16.8 m

The corresponding CO contour maps of the present work are displayed in Figure 6.10. The differences between Figure 6.9 and Figure 6.10 are explained by the computational domain as described before. Figure 6.10 shows that the mixing between primary gas and fuel is intense in the center of the furnace and consequently CO is formed in the burner vicinity. With the implemented swirl angle the high CO concentration is only observed in the center of the kiln and therefore, doesn't represent a risk for the material since the formation of reducing conditions near the material bed can strongly affect clinker color and quality [17].

As expected and confirmed by the pilot scale burner tests, the concentration of CO is significantly higher in the oxyfuel case. The peak concentration for the oxyfuel case is 32.1 vol.%, while for the reference it is 6.8 vol.%. Also in the contour maps of Figure 6.9, high concentration of CO is observed during the simulation of oxyfuel combustion. Clearly the difference between the air and oxyfuel cases is very significant, and larger than the observed at lower scale in the pilot tests. The simulation results evince an important activity of homogeneous and heterogeneous reactions with CO_2. The main reactions responsible for higher CO generation have been described in section 2.4.2.1.

At the kiln outlet, however, the concentration of CO is reduced below 1 ppm in both combustion conditions.

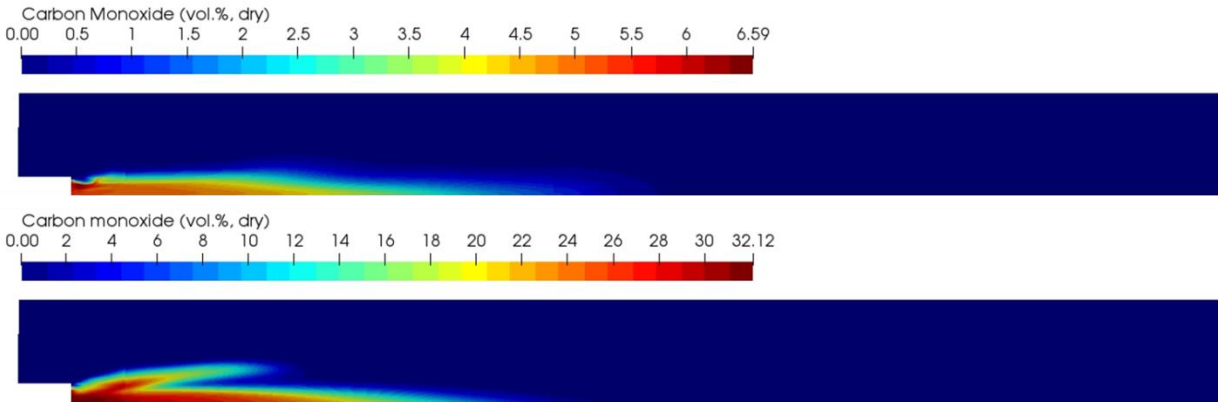

Figure 6.10: Contour maps of carbon monoxide. Air reference (top) and oxyfuel (bottom) cases. First 20 m from a total kiln length of 60 m.

The evolution of oxygen is shown in Figure 6.11 for both combustion conditions. Very similar concentration profiles are observed in both cases. As previously mentioned, the primary gas stream has a high oxygen concentration in oxyfuel mode while the secondary gas has an oxygen concentration similar to the air. The simulation shows that the oxygen content in the primary gas stream is consumed very rapidly as it exits the burner. The secondary gas entrainment into the main jet stream is similar in both combustion cases. Towards the kiln gas outlet, the concentration of oxygen is reduced to 4 vol.% and 4.4 vol.% in the air and oxyfuel cases, respectively.

The corresponding oxygen concentration profile of Ditaranto et al. is presented in Figure 6.12. The differences between Figure 6.11 and Figure 6.12 are also a consequence of the modeling of the primary gas nozzles, which confirms that the burner configuration has a significant role on flame shape and ignition.

Finally, the simulation results of incident wall heat flux in both combustion conditions are displayed in Figure 6.13. A good correspondence between the air and oxyfuel case is critical since product quality strongly depends on the satisfactory heat flux transfer to material/walls. The oxyfuel case reassembles a very similar behavior as the air case with a difference of only 2% in the highest peak found at the distance of 8.4 m from kiln back end. When integrated over the clinker burning zone (assumption 5 – 20 m from kiln back end) the difference between the cases is 2.4% higher in the oxyfuel case. Ditaranto and Bakken [147] also simulated a similar incident wall heat flux profile. However, their results of heat flux in the first 20 m produce a narrower curve with higher

peak in the air case (see Figure 6.14). A possible explanation is the delayed ignition related to the implemented swirl modeling. The difference in incident heat radiation to the walls in the same zone is 2.1% higher in the air case.

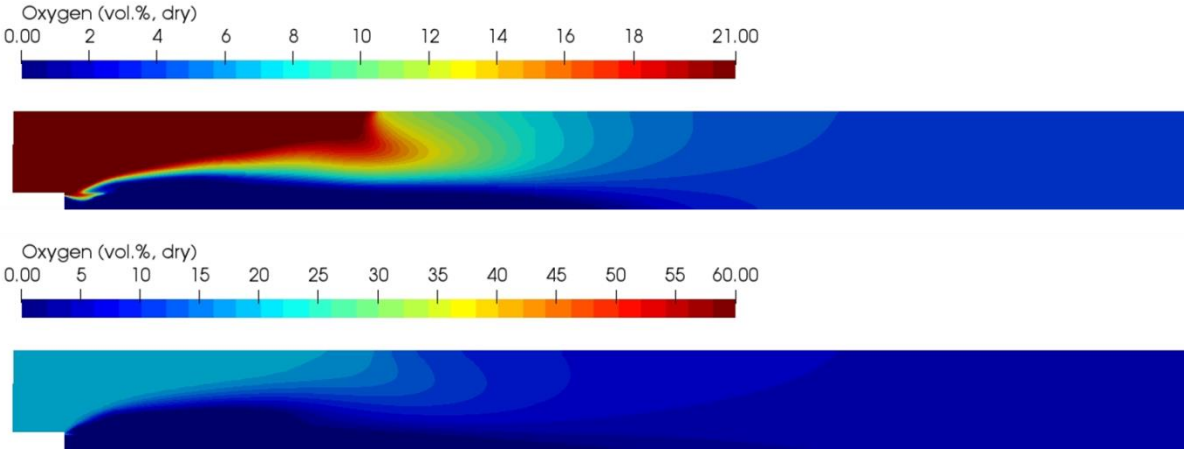

Figure 6.11: Contour maps of oxygen. Air reference (top) and oxyfuel (bottom) cases. First 20 m from a total kiln length of 60 m.

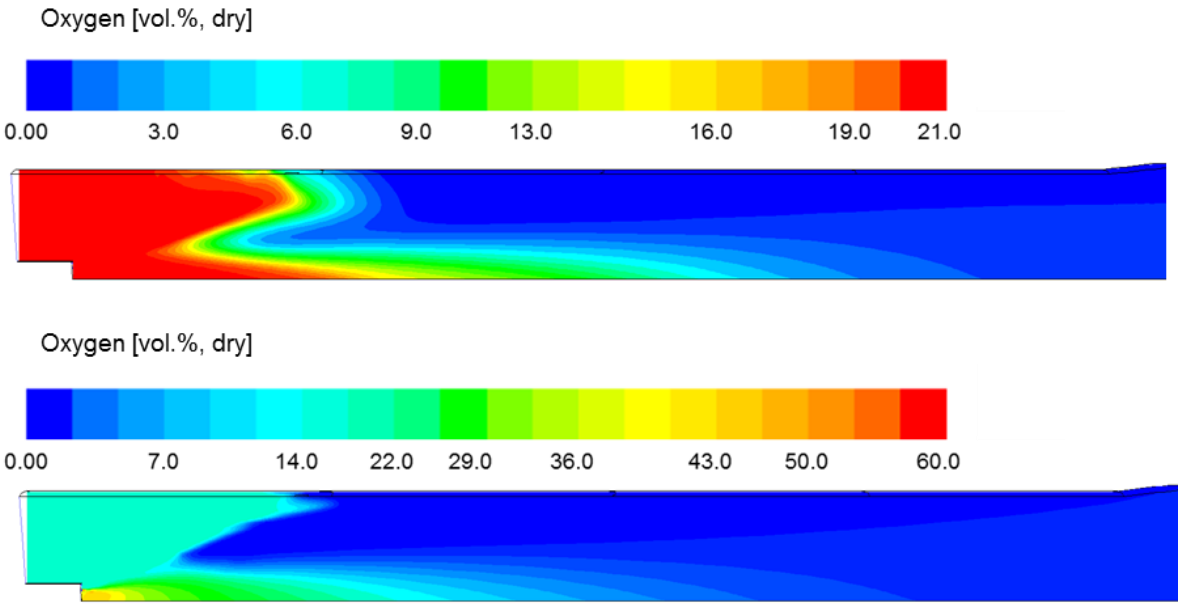

Figure 6.12: Contour maps of O_2 volume fraction in the plane crossing the nozzle centerline by Ditaranto and Bakken [147]. Air reference (top) and oxyfuel (bottom) cases.

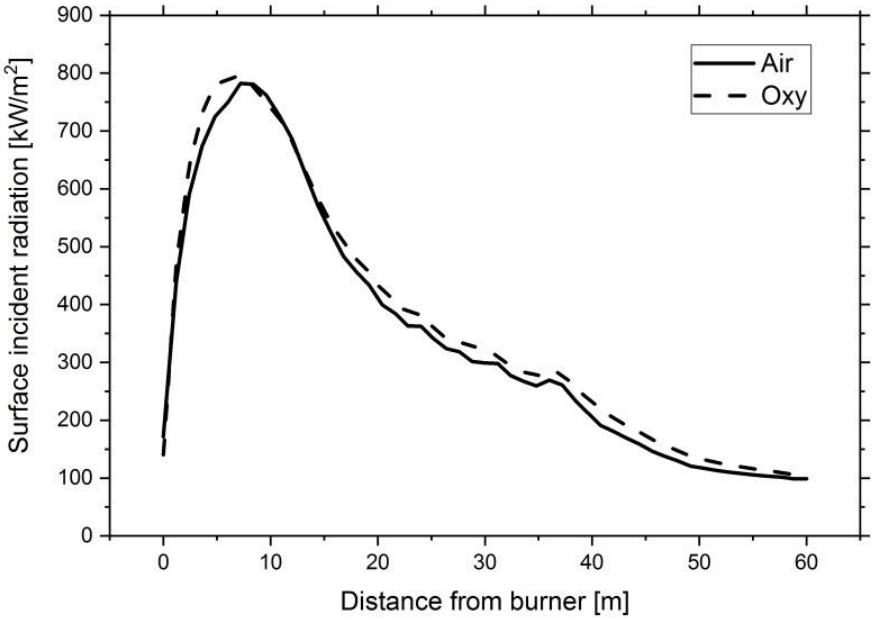

Figure 6.13: CFD simulation result of the wall heat flux profile.

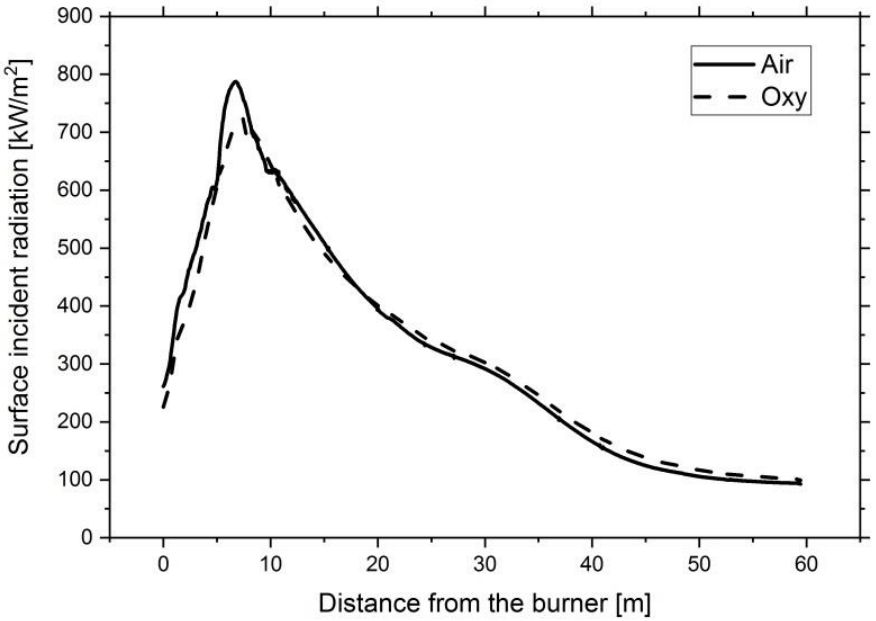

Figure 6.14: CFD simulation of the wall heat flux profile by Ditaranto et al. [147].

Figure 6.15 shows the kiln radiation profile obtained from the process simulation [73]. For orientation, the kiln outlet/burner is located in the right side of the figure. Three profiles are shown. The blue line called BAT3000 is the reference profile of combustion with air. The red line presents the results of an oxyfuel scenario with theoretical assumptions of a previous study [42]. The green line represents the optimized or refined oxyfuel solution using the burner configuration (gas flows, compositions and distribution) used in CFD simulations presented in this section. The optimized oxyfuel solution is very similar to the air reference scenario, especially at its maximum peak. This result is necessary to provide the same heat transfer from gas to the material. Furthermore, under this scenario no especial coating of the kiln is needed in oxyfuel operation.

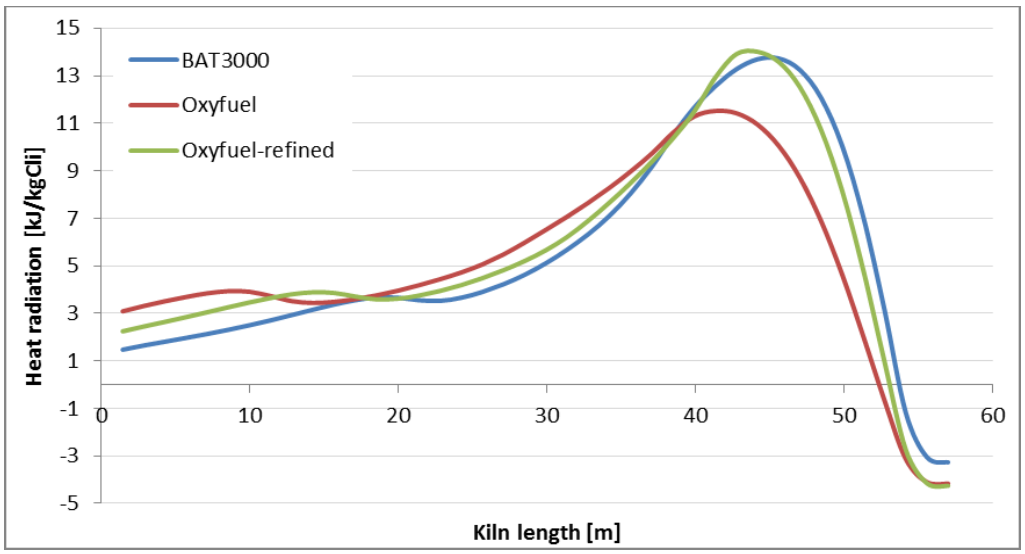

Figure 6.15: Kiln heat radiation profile from process model [73]

6.6 Conclusions from simulation work

CFD simulation and a process model tool were used to determine a set of optimized inlet conditions for the operation of a full size oxyfuel cement kiln. The oxygen enrichment and distribution in the burner were key parameters to obtain a temperature wall heat flux profile similar as in conventional operation with air. It can be expected that the coating behavior of the material in the kiln and the thermal load of the rotary kiln is similar for these both cases and therefore fulfill the optimum operational mode.The flame length and shape were also observed to remain similar between the optimized oxyfuel and reference case and to be strongly influenced by the swirl angle implemented in the burner. The results are in agreement with the work of other authors on similar simulation conditions.

7 Summary, conclusions, and outlook

The main objective of this study was to experimentally and numerically investigate the combustion and emission behavior of reference fuels using O_2/CO_2 as combustion atmosphere and in relevant operation conditions to cement production. The focus of the present work was on oxyfuel burner technology, and therefore, a modern kiln burner was scaled down and used as a prototype oxyfuel burner in the 500 kW combustion test rig. The scaling of the burner was conducted aiming to maintain similar burner outlet velocities as industrial kilns. Two mixtures of O_2 and CO_2 supplied from tanks were used as primary and secondary gas, while fuel was transported with CO_2. A highly flexible pre-heater system was designed and installed to increase the temperature of the secondary gas stream to 800 °C to mimic the condition when secondary gas is heated in the clinker cooler in real scale plants. Conducted investigations included cases in air-blown combustion in order to serve as reference when comparing the combustion and emission behavior with the O_2/CO_2 mixture. Three fuels ranging from low-volatile petcoke to pre-dried lignite and high-volatile SRF served as reference fuels. The results of pilot tests were used to validate CFD simulations and then to simulate a full-scale cement kiln burner operated in oxyfuel conditions. Major results and conclusions drawn from this study can be summarised as:

1. Oxygen concentration in oxyfuel mode plays an important role in achieving a temperature profile similar as in reference combustion with air. Due to the higher heat capacity of CO_2, higher oxygen concentration as in air is required. From the investigated conditions in the pilot tests an oxygen volume fraction of 29% resulted in a similar temperature profile as in air-blown combustion. In the simulation work including CFD and process simulation a 26% oxygen concentration resulted in an optimum value.
2. Flame length is also influenced by oxygen concentration in an inverse relationship. As the oxygen concentration increases, flame shortens, the concentration of CO rises and its peak is shifted towards the burner due to the influence of the CO_2 gasification reactions. Flame length is also influenced by the swirl angle imposed in the burner.
3. The radiative wall heat fluxes to the furnace walls can be influenced by the combustion atmosphere. In the pilot tests, 10-20% higher heat fluxes to the walls were observed when switching from air to oxygen mode. In a full scale simulation of a cement kiln in oxyfuel mode with optimized inlet values, a similar heat radiation profile was observed in the clinker sintering zone.

4. By keeping a similar air and radiative heat profile in the kiln it can be expected that the coating behavior of the material and the thermal load of the rotary kiln can remain similar for both air and oxyfuel operation mode.
5. It is expected that CO emissions at furnace outlet are similar for air-blown and oxyfuel cases. During oxyfuel combustion elevated CO concentration is observed only in the burner vicinity and therefore, does not present a risk for the material regarding change of colour or quality detriment due to reducing conditions.
6. Even though N_2 from the air is excluded in the combustion gas, NO_x concentration can be observed in oxyfuel firing due to air in-leakage and/or fuel-N. In the pilot combustion tests, O_2/CO_2 gas mixture was calculated to produce less NO_x emissions expressed in the unit of mass per energy of input, an average reduction of 50-60% is observed in comparison to air-blown firing.
7. The burner swirl has an important role on ignition, flame shape and length. In the experimental work swirl was seen to also impact CO formation in the burner vicinity.
8. No significant differences between air-firing and oxyfuel cases are expected regarding the combustion efficiency as observed in the calculation of fuel burnout and unburned carbon in the experimental tests.
9. The operation in oxyfuel mode opens the possibility to freely redistribute the oxygen mass flow between the primary and secondary gas streams. According to the experimental tests and simulations conducted in this work, if the concentration of oxygen is increased in primary gas (with a corresponding decrease in secondary gas to keep the overall targeted oxygen enrichment) the generation of CO in the near burner field decreases significantly.
10. Burner scaling was done based on a constant velocity scaling criterion, but adjusted according to manufacturing constraints. A larger mass flow of primary gas stream was needed to compensate primary gas velocity and momentum. According to the calculated Craya-Curtet parameter, primary gas momentum was sufficient to entrain all secondary gas into the jet flame.

In general terms, the results of the present work confirm that the findings from research conducted by other authors on oxyfuel combustion for the power industry are also applicable to the cement production.

7.1 Outlook

While the focus of this work was on burner technology, no comparison of different burners with different scaling methodologies was conducted due to time and resources

limitation. An interesting approach to complement this work would be to study a second burner with scaling based on the constant residence time criterion. By following the constant residence time criterion, the resultant burner diameter is larger and the gas velocities are reduced. CFD simulation presented in this work has shown very different flame performance when using the residence time criterion. A comparison of experimental results would be beneficial to better understand adequate criteria to scale burners of the cement industry.

In a cement kiln operated under oxyfuel conditions special attention should be put to minor gas species in the recirculated stream. The recirculation of combustion gases back to the combustion chamber was not on the scope of the present work and is therefore as task for further investigations. It is relevant to investigate the effect on some pollutants known to have a cycling behavior in the kiln (e.g. S, Hg and HCl) as they return to the kiln with the recirculation stream. This task should involve preferably tests in a pilot rotary kiln with clinker production to include the reactions with raw meal.

Bibliography

[1] J. Hawksworth and D. Chan, ‘The World in 2050: How will the global economic order change?’, PwC, 2015. Accessed: Apr. 29, 2019. [Online]. Available: www.pwc.com/gx/en/issues/the-economy/assets/world-in-2050-february-2015.pdf

[2] Reuters, ‘EU’s climate chief calls for bloc to go for net-zero emissions by 2050’, Nov. 27, 2018. https://www.reuters.com/article/climate-change-eu-idUSL8N1Y25AZ (accessed Apr. 29, 2019).

[3] European Climate Foundation, ‘Net-zero 2050’. https://europeanclimate.org/net-zero-2050/ (accessed Apr. 29, 2019).

[4] IPCC, ‘Summary for Policymakers. In: Global warming of 1.5°C above pre-industrial levels and related global greenhouse emissions pathways, in the context of strengthening the global response to the threat of climate change, sustainable development, and efforts to eradicate poverty.’, World Meteorological Organization, Geneva, Switzerland, 2018.

[5] International Energy Agency, ‘World Energy Outlook 2018’, IEA, Paris, 2018. [Online]. Available: https://www.oecd-ilibrary.org/content/publication/weo-2018-en

[6] CEMBUREAU, ‘The Role of Cement in the 2050 Low Carbon Economy’, The European Cement Association, Jan. 2013. [Online]. Available: https://cembureau.eu/media/1500/cembureau_2050roadmap_lowcarboneconomy_2013-09-01.pdf

[7] Global Cement and Concrete Association, ‘GNR Project: Reporting CO2’. Accessed: Feb. 03, 2020. [Online]. Available: www.gccassociation.org/gnr/

[8] IEA-CSI, ‘Technology Roadmap - Low-Carbon Transition in the Cement Industry’, p. 66, Mar. 2018.

[9] M. Voldsund *et al.*, ‘Comparison of Technologies for CO2 Capture from Cement Production—Part 1: Technical Evaluation’, *Energies*, vol. 12, no. 3, p. 559, Jan. 2019, doi: 10.3390/en12030559.

[10] M. Schneider, ‘ECRA´s cement carbon capture project’, presented at the ECRA/CEMCAP/CLEANKER Workshop, Brussels, Belgium, Oct. 17, 2018. Accessed: Dec. 07, 2019. [Online]. Available: https://ecra-online.org/fileadmin/ecra/media/ECRA-CEMCAP-CLEANKER_2018/Presentations/2_ECRAs_cement_carbon_capture%20_project_M_Schneider.pdf

[11] F. Carrasco-Maldonado, R. Spörl, K. Fleiger, V. Hoenig, J. Maier, and G. Scheffknecht, ‘Oxy-fuel combustion technology for cement production – State of the art research and technology development’, *International Journal of Greenhouse Gas Control*, vol. 45, pp. 189–199, Feb. 2016, doi: 10.1016/j.ijggc.2015.12.014.

[12] F. Carrasco, S. Grathwohl, J. Maier, J. Ruppert, and G. Scheffknecht, ‘Experimental investigations of oxyfuel burner for cement production application’, *Fuel*, vol. 236, pp. 608–614, Jan. 2019, doi: 10.1016/j.fuel.2018.08.135.

[13] F. Carrasco-Maldonado *et al.*, ‘Oxy-fuel burner investigations for CO2 capture in cement plants’, *Energy Procedia*, vol. 120, pp. 120–125, Aug. 2017, doi: 10.1016/j.egypro.2017.07.160.

[14] F. Carrasco, J. Maier, E. Willms, and J. Ruppert, ‘D 7.2: Oxyfuel burner prototype performance tests.’, Deliverable of the CEMCAP H2020 Project, 2018. Accessed: Oct. 03, 2020. [Online]. Available: https://zenodo.org/record/2597125#.XoSjVd9fhwF

[15] F. Schorcht, I. Kourti, B. M. Scalet, S. Roudier, L. Delgado Sancho, and Institute for Prospective Technological Studies, *Best available techniques (BAT) reference document for the production of cement, lime and magnesium oxide: Industrial Emissions Directive 2010/75/EU (integrated pollution prevention and control).* Luxembourg: Publications Office, 2013. Accessed: May 03, 2019. [Online]. Available: http://dx.publications.europa.eu/10.2788/12850

[16] ECRA, ‘Technical Report. TR-0123/2013/E. Deployment of CCS in the Cement Industry’, European Cement Research Academy, Düsseldorf, Germany, 2013.

[17] F. W. Locher, *Zement: Grundlagen der Herstellung und Verwendung*. Düsseldorf, Germany: Verlag Bau+Technik GmbH, 2000.

[18] H.-M. Sylla, ‘Einfluß der Klinkerzusammensetzung und Klinkerkühlung auf di Zementeingenschaften. Verfahrenstechnik der Zementherstellung’, in *Proceedings of the VDZ Kongress 1993*, Düsseldorf, Germany, 1993, pp. 135–145.

[19] J. N. Knudsen, O. M. Bade, I. Askestad, O. Gorset, and T. Mejdell, ‘Pilot Plant Demonstration of CO2 Capture from Cement Plant with Advanced Amine Technology’, *Energy Procedia*, vol. 63, pp. 6464–6475, Jan. 2014, doi: 10.1016/j.egypro.2014.11.682.

[20] K. Guenioui, ‘Skyonic launches Capitol SkyMine® at cement plant in Texas’, *World Cement*, Oct. 20, 2014. https://www.worldcement.com/the-americas/20102014/Skyonic-opens-commercial-scale-CCU-facility-at-Texan-cement-plant-697/ (accessed May 02, 2019).

[21] T. O. Nelson, A. Kataria, P. Mobley, M. Soukri, and J. Tanthana, ‘RTI’s Solid Sorbent-Based CO2 Capture Process: Technical and Economic Lessons Learned for Application in Coal-fired, NGCC, and Cement Plants’, *Energy Procedia*, vol. 114, pp. 2506–2524, Jul. 2017, doi: 10.1016/j.egypro.2017.03.1409.

[22] M. Naranjo, D. T. Brownlow, and A. Garza, ‘CO2 capture and sequestration in the cement industry’, *Energy Procedia*, vol. 4, pp. 2716–2723, Jan. 2011, doi: 10.1016/j.egypro.2011.02.173.

[23] M. C. Balfe, O. Augustsson, R. Tahoces-soto, and L.-M. H. Bjerge, ‘Alstom’s Regenerative Calcium Cycle - Norcem Derisking Study: Risk Mitigation in the Development of a 2nd Generation CCS Technology.’, *Energy Procedia*, vol. 63, pp. 6440–6454, Jan. 2014, doi: 10.1016/j.egypro.2014.11.679.

[24] World Cement, ‘CO2 captured by HECLOT can be injected underground for enhanced oil and gas recovery’, *World Cement*, Oct. 22, 2014. https://www.worldcement.com/asia-pacific-rim/22102014/HECLOT-can-achieve-90-percent-capture-rate-says-ITRI-712/ (accessed May 02, 2019).

[25] Charles. Dean, Thomas. Hills, Nick. Florin, Denis. Dugwell, and P. S. Fennell, ‘Integrating Calcium Looping CO2 Capture with the Manufacture of Cement’, *Energy Procedia*, vol. 37, pp. 7078–7090, Jan. 2013, doi: 10.1016/j.egypro.2013.06.644.

[26] CLEANKER, ‘Clean Clinker by Calcium Looping for low-CO2 cement’. http://www.cleanker.eu/index.php/home-page-it (accessed May 02, 2019).

[27] L.-M. Bjerge and P. Brevik, ‘CO2 Capture in the Cement Industry, Norcem CO2 Capture Project (Norway)’, *Energy Procedia*, vol. 63, pp. 6455–6463, Jan. 2014, doi: 10.1016/j.egypro.2014.11.680.
[28] M. Church, ‘St Marys Cement emissions used to grow microalgae’, *Canadian Biomass*. https://www.canadianbiomassmagazine.ca/biofuel/emissions-from-st-marys-cement-plant-used-to-grow-microalgae-6200 (accessed May 02, 2019).
[29] J. Theulen, ‘From CO2 to fish feed’, *HeidelbergCement Group Blog*, Oct. 23, 2019. https://blog.heidelbergcement.com/en/from-co2-to-fish-feed (accessed Oct. 06, 2020).
[30] NORCEM, ‘Carbon capture – a part of our zero vision’. https://www.norcem.no/en/carbon_capture (accessed May 08, 2019).
[31] L.-A. Tokheim, N. Eldrup, and A. Mathisen, ‘Benchmark Study - Commercial Scale Perspective. Preliminary results from WP7 Benchmark Study’, Langesund, Norway, 21.05 2015.
[32] P. Brevik, ‘Norcem Brevik CO2-capture project; assessment of post-combustion technologies for cement plants’, Oct. 17, 2018. Accessed: Oct. 03, 2020. [Online]. Available: https://www.sintef.no/globalassets/project/cemcap/presentasjoner/17-oct-2018/10_norcem_brevik_co2-capture_project_assessment_post-combustion_technologies_p.brevik.pdf
[33] C. A. Hendriks *et al.*, ‘Emission reduction of greenhouse gases from the cement industry’, in *Greenhouse Gas Control Technologies 4*, Elsevier, 1999, pp. 939–944. doi: 10.1016/B978-008043018-8/50150-8.
[34] M. B. Toftegaard, J. Brix, P. A. Jensen, P. Glarborg, and A. D. Jensen, ‘Oxy-fuel combustion of solid fuels’, *Progress in Energy and Combustion Science*, vol. 36, no. 5, pp. 581–625, Oct. 2010, doi: 10.1016/j.pecs.2010.02.001.
[35] T. Wall *et al.*, ‘An overview on oxyfuel coal combustion—State of the art research and technology development’, *Chemical Engineering Research and Design*, vol. 87, no. 8, pp. 1003–1016, Aug. 2009, doi: 10.1016/j.cherd.2009.02.005.
[36] G. Scheffknecht, L. Al-Makhadmeh, U. Schnell, and J. Maier, ‘Oxy-fuel coal combustion—A review of the current state-of-the-art’, *International Journal of Greenhouse Gas Control*, vol. 5, pp. S16–S35, Jul. 2011, doi: 10.1016/j.ijggc.2011.05.020.
[37] R. Stanger *et al.*, ‘Oxyfuel combustion for CO2 capture in power plants’, *International Journal of Greenhouse Gas Control*, vol. 40, pp. 55–125, Sep. 2015, doi: 10.1016/j.ijggc.2015.06.010.
[38] B. J. P. Buhre, L. K. Elliott, C. D. Sheng, R. P. Gupta, and T. F. Wall, ‘Oxy-fuel combustion technology for coal-fired power generation’, *Progress in Energy and Combustion Science*, vol. 31, no. 4, pp. 283–307, Jan. 2005, doi: 10.1016/j.pecs.2005.07.001.
[39] L. Chen, S. Z. Yong, and A. F. Ghoniem, ‘Oxy-fuel combustion of pulverized coal: Characterization, fundamentals, stabilization and CFD modeling’, *Progress in Energy and Combustion Science*, vol. 38, no. 2, pp. 156–214, Apr. 2012, doi: 10.1016/j.pecs.2011.09.003.
[40] M. Gimenez *et al.*, ‘The oxycombustion option’, *International Cement Review*, pp. 37–43, May 2014.
[41] F. Zeman, ‘Oxygen combustion in cement production’, *Energy Procedia*, vol. 1, no. 1, pp. 187–194, Feb. 2009, doi: 10.1016/j.egypro.2009.01.027.

[42] ECRA, ‘Report on Phase III. ECRA CCS Project’, European Cement Research Academy, Düsseldorf, Germany, Technical Report TR-119/2012, 2012. Accessed: May 04, 2018. [Online]. Available: http://www.ecra-online.org/fileadmin/redaktion/files/pdf/ECRA_Technical_Report_CCS_Phase_III.pdf
[43] IEAGHG, ‘Deployment of CCS in the Cement Industry. Report 2013/19’. IEA, 2013. Accessed: Feb. 03, 2020. [Online]. Available: www.ieaghg.org/docs/General_Docs/Reports/2013-19.pdf
[44] P. Higginbotham, V. White, K. Fogash, and G. Guvelioglu, ‘Oxygen supply for oxyfuel CO2 capture’, *International Journal of Greenhouse Gas Control*, vol. 5, pp. S194–S203, Jul. 2011, doi: 10.1016/j.ijggc.2011.03.007.
[45] Q. Fu, Y. Kansha, C. Song, Y. Liu, M. Ishizuka, and A. Tsutsumi, ‘A cryogenic air separation process based on self-heat recuperation for oxy-combustion plants’, *Applied Energy*, vol. 162, pp. 1114–1121, Jan. 2016, doi: 10.1016/j.apenergy.2015.03.039.
[46] S. Santos, ‘Challenges in the Development of Oxy-Coal Combustion Power Plant with CO2 Capture’, presented at the Asia Pacific Programme (APP). Oxyfuel Working Group Capacity Building Course, Daejeon, South Korea, Feb. 05, 2009.
[47] T. Lockwood, ‘Developments in oxyfuel combustion of coal’, *IEA Clean Coal Centre*, no. CCC/240, p. 122, Aug. 2014.
[48] D. A. Granados, F. Chejne, J. M. Mejía, C. A. Gómez, A. Berrío, and W. J. Jurado, ‘Effect of flue gas recirculation during oxy-fuel combustion in a rotary cement kiln’, *Energy*, vol. 64, pp. 615–625, Jan. 2014, doi: 10.1016/j.energy.2013.09.045.
[49] V. Hoenig and J. Ruppert, ‘Perspective on oxyfuel capture technology application in a cement plant’, presented at the ECRA-CEMCAP- CLEANKER Workshop, Brussels, Belgium, Oct. 17, 2018. Accessed: Sep. 05, 2019. [Online]. Available: https://ecra-online.org/fileadmin/ecra/media/ECRA-CEMCAP-CLEANKER_2018/Presentations/8_Perspective_on_oxyfuel_capture_technology_application_in_a_cement_plant_V_Hoenig_J_Ruppert.pdf
[50] M. Lindemann Lino, M. Böhm, V. Hoenig, J. Ruppert, S. Becker, and R. Mathai, ‘D9.2 - revision 1. Analysis of oxyfuel clinker cooler operational performance.’, VDZ gGmbH, Deliverable 9.2, Aug. 2018.
[51] K. Burgers, S. Laux, and M. Shah, ‘CO2 processing unit for oxyfuel fired rotary cement kiln’, presented at the 3rd Oxyfuel Combustion Conference, Ponferrada, Spain, Sep. 2013.
[52] A. K. Chatterjee, ‘Chemistry and engineering of the clinkerization process — Incremental advances and lack of breakthroughs’, *Cement and Concrete Research*, vol. 41, no. 7, pp. 624–641, Jul. 2011, doi: 10.1016/j.cemconres.2011.03.020.
[53] Verein Deutsche Zementwerke e.V., *Zement-Taschenbuch 51. Ausgabe*, vol. 51. Ausgabe. Düsseldorf, Germany: Verlag Bau+Technik GmbH, 2008.
[54] P. Mullinger and B. G. Jenkins, *Industrial and Process Furnaces. Principles, Design and Operation.* Oxford, UK: Butterworth-Heinemann, 2008.
[55] A. Boateng, *Rotary Kilns, Transport Phenomena and Transport Processes*, First edition. USA: Butterworth-Heinemann, 2008.
[56] T. Abbas, M. Akritopoulos, and T. Lowes, ‘Burners for Kilns and Calciners. Part I - Kiln Burners’, *World Cement*, vol. 40, no. 12, Dec. 2009.

[57] X. D´hubert, ‘There´s no such thing as a “perfect” burner...’, *Global Cement*, Jan. 30, 2017. Accessed: May 13, 2019. [Online]. Available: http://www.globalcement.com/magazine/articles/1014-theres-no-such-thing-as-a-perfect-burner

[58] P. Mullinger and B. G. Jenkins, ‘NOx reduction techniques for rotary kilns’, *Joint AFRC/JFRC Confererence*, Hawaii, 1994.

[59] B. G. Jenkins, ‘Oxygen Enrichment in the Cement Industry’, presented at the Topic Oriented Technical Meeting (TOTeM) 17: The Use of Oxygen for Industrial Combustion, Paris, Sep. 25, 2000.

[58] M. Vaccaro and Pillard P. E.G.C.I, ‘Low NOx Rotary Kiln Burner Technology: Design Principles & Case Study’, presented at the IEEE-IAS/PCA 44th Cement Industry Technical Conference, Jacksonville, Florida, May 2002.

[61] ADEME, ‘The French Cement Industry Guide to NOx Emissions Reductions Measures’. ADEME & the Cement Industry under the aegis of MEED, Dec. 16, 2002. Accessed: May 13, 2019. [Online]. Available: https://www.ademe.fr/sites/default/files/assets/documents/33324_guide_nox_anglais.pdf

[62] G. Mayes, ‘Oxygen enrichment at the TXI Midlothian cement plant’, in *IEEE-IAS/PCA 2001 Cement Industry Technical Conference. Conference Record (Cat. No.01CH37150)*, Apr. 2001, pp. 289–292. doi: 10.1109/CITCON.2001.934118.

[63] Unitherm, ‘M.A.S. Kiln Burner’. Accessed: Dec. 07, 2019. [Online]. Available: https://www.unitherm.at/en/products/mas-kiln-burner

[64] K. Andersson, R. Johansson, S. Hjärtstam, F. Johnsson, and B. Leckner, ‘Radiation intensity of lignite-fired oxy-fuel flames’, *Experimental Thermal and Fluid Science*, vol. 33, no. 1, pp. 67–76, Oct. 2008, doi: 10.1016/j.expthermflusci.2008.07.010.

[65] R. Johansson, B. Leckner, K. Andersson, and F. Johnsson, ‘Influence of particle and gas radiation in oxy-fuel combustion’, *International Journal of Heat and Mass Transfer*, vol. 65, pp. 143–152, Oct. 2013, doi: 10.1016/j.ijheatmasstransfer.2013.05.073.

[66] D. Bäckström, R. Johansson, K. Andersson, H. Wiinikka, and C. Fredriksson, ‘On the use of alternative fuels in rotary kiln burners — An experimental and modelling study of the effect on the radiative heat transfer conditions’, *Fuel Processing Technology*, vol. 138, pp. 210–220, Oct. 2015, doi: 10.1016/j.fuproc.2015.05.021.

[67] B. J. MacBride, M. J. Zehe, and S. Gordon, ‘NASA Glenn Coefficients for Calculating Thermodynamics Properties of Individual Species’. 2002.

[67] K. Koring, ‘CO2-Emissionsminderungspotential und technologische Auswirkungen der Oxyfuel-Technologie im Zementklinkerbrennprozess.’, Doctoral Dissertation, Technische Universität Clausthal, Düsseldorf, Germany, 2013.

[69] M. Paneru, A. Mack, J. Ruppert, G. Cinti, and J. Maier, ‘Calciner Technology for Oxyfuel Process’, presented at the ECRA/CEMCAP/CLEANKER Workshop, Brussels, Belgium, Oct. 17, 2018. [Online]. Available: https://ecra-online.org/fileadmin/ecra/media/ECRA-CEMCAP-CLEANKER_2018/Posters/CEMCAP_WP8_Calciner_technology_for_oxyfuel_process.pdf

[69] S. Oberhauser and A. Kather, ‘CO2-Capture from Cement Plants Applying Oxyfuel Concepts’, 2nd International Conference on Energy Process Engineering - Efficient Carbon Capture for Coal Power Plants, June 20-22, 2011 Frankfurt am Main, Germany

[71] N. Meunier, S. Laribi, L. Dubois, D. Thomas, and G. De Weireld, ‘CO2 Capture in Cement Production and Re-use: First Step for the Optimization of the Overall Process’, *Energy Procedia*, vol. 63, pp. 6492–6503, Jan. 2014, doi: 10.1016/j.egypro.2014.11.685.
[72] C. Farrell, ‘Experimental Verification of Sealing Potential for Oxyfuel Combustion Process. ECRA CCS Project Phase IV.A.’, Master Thesis, Düsseldorf, Germany, 2013.
[73] A. Jamali, K. Fleiger, J. Ruppert, V. Hoenig, and R. Anantharaman, ‘Optimised operation of an oxyfuel cement plant. D 6.1’. CEMCAP Project, Apr. 11, 2018. Accessed: May 15, 2019. [Online]. Available: www.sintef.no/globalassets/project/cemcap/d-6.1-optimised-oxyfuel-operation.pdf.pdf
[73] P. B. Nielsen and O. L. Jepsen, ‘An overview of the formation of SOx and NOx in various pyroprocessing systems’, in *IEEE Technical Conference on cement Industry*, May 1990, pp. 255–276. doi: 10.1109/CITCON.1990.111066.
[74] A. Scheuer, ‘Minderung der NOx-Emission beim Brennen von Zementklinker.’, *Zem. Kalk Gips Int.*, vol. 41 (1988), pp 37–42.
[76] C. Ndibe, R. Spörl, J. Maier, and G. Scheffknecht, ‘Experimental study of NO and NO2 formation in a PF oxy-fuel firing system’, *Fuel*, vol. 107, pp. 749–756, May 2013, doi: 10.1016/j.fuel.2013.01.055.
[77] T. Seidler and V. Hoenig, ‘Investigations into the formation and reduction of raw-material-derived SO2 emissions in the cement industry.’, *Cem. Int. 202*, vol. 1, pp. 66–84, 2002.
[78] S. Sprung, *Technological Problems in Pyroprocessing Cement Clinker: Cause and Solution.* Düsseldorf, Germany: Beton-Verlag, 1985.
[79] D. Liu, T. Wall, and R. Stanger, ‘CO2 quality control in Oxy-fuel technology for CCS: SO2 removal by the caustic scrubber in Callide Oxy-fuel Project’, *International Journal of Greenhouse Gas Control*, vol. 51, pp. 207–217, Aug. 2016, doi: 10.1016/j.ijggc.2016.05.026.
[80] R. J. Schreiber, S. Hasan, C. Yonley, and C. D. Kellett, ‘Mercury Emissions Control for the Cement Manufacturing Industry’, in *Mercury Control: for Coal-Derived Gas Streams*, Wiley-VCH Verlag GmbH & Co. KGaA, 2015.
[81] R. L. Axelbaum and P. Biswas, ‘Multi-Pollutant Control Through Novel Approaches to Oxygen Enhanced Combustion’, Washington University in Saint Louis, Saint Louis, Final Report DE-FG26-05NT42531, Dec. 2009.
[82] A. Fry, B. Van Otten, and B. Adams, ‘Mercury Speciation and Emission from Pilot-Scale PC Furnaces under Air- and Oxy-fired Conditions’, presented at the IEAGHG Workshop on SO2/SO3/Hg/Corrosion, London, UK, Jan. 2011.
[83] R. Spörl *et al.*, ‘Mercury Emissions and Removal by Ash in Coal-Fired Oxy-fuel Combustion’, *Energy Fuels*, vol. 28, no. 1, pp. 123–135, Jan. 2014, doi: 10.1021/ef4014604.
[83] B. Van Otten, A. Fry, and L. Bool, ‘Mercury speciation and emissions from pilot-scale PC furnaces under air- and oxy-fired conditions.’, presented at the Air Quality III Conference, Crystal City, California, Oct. 2011.
[85] Y. Zhuang and J. H. Pavlish, ‘Fate of hazardous air pollutants in oxygen-fired coal combustion with different flue gas recycling’, *Environ. Sci. Technol.*, vol. 46, pp. 4657–4665, doi: 10.1021/es300143q.

[86] A. Bäck, J. Grubbström, H. Ecke, M. Strand, and J. Pettersson, ‘Operation of an Electrostatic Precipitator at a 30 MWth Oxyfuel Plant’, *International Journal of Plasma Environmental Science and Technology*, p. 5, 2011.

[87] C. Spero, C. Energy, T. Yamada, and P. Nelson, ‘Callide Oxyfuel Project: Combustion and Environmental Performance’, Oxy-Fuel Combustion Conference, IEGHG, Ponferrada, Spain, Sep. 10, 2013. Accessed: May 15, 2019. [Online]. Available: https://ieaghg.org/docs/General_Docs/OCC3/Secured%20presentations/1a_2_OCC3%20-%20COP%20Comb%20&%20Env%20Performance%20CSpero.pdf

[88] V. White, A. Wright, S. Tappe, and J. Yan, ‘The Air Products Vattenfall Oxyfuel CO2 Compression and Purification Pilot Plant at Schwarze Pumpe’, *Energy Procedia*, vol. 37, pp. 1490–1499, Jan. 2013, doi: 10.1016/j.egypro.2013.06.024.

[89] R. Ritter, T. Stoffregen, N. Schödel, and F. Winkler, ‘NOx processing experiences for removal in the CO2 plant for the Oxyfuel combustion process’, presented at the 3rd Oxy-Fuel Combustion Conference, IEAGHG, Ponferrada, Spain, Sep. 12, 2013. Accessed: May 15, 2019. [Online]. Available: https://ieaghg.org/docs/General_Docs/OCC3/Secured%20presentations/S5B-03%20-%20Ritter%20(Linde).pdf

[90] R. Stanger, T. Ting, and T. Wall, ‘High pressure conversion of NOx and Hg and their capture as aqueous condensates in a laboratory piston-compressor simulating oxy-fuel CO2 compression’, *International Journal of Greenhouse Gas Control*, vol. 29, pp. 209–220, Oct. 2014, doi: 10.1016/j.ijggc.2014.08.006.

[91] S. Syrigos and A. Kather, ‘Experimentelle Untersuchung der Schadstoffrückhaltung bei der Rauchgaskühlung und -verdichtung’, presented at the Public Final Project Meeting of the German Research Project ‘ADECOS-Komponenten’, Cottbus, Germany, Jul. 05, 2014.

[92] D. Copin, ‘The Storage Dimension of the Oxycombustion Based Integrated CCS Project of LACQ and ROUSSE’, presented at the 3rd IEAGHG Oxy-Fuel Combustion Conference, Ponferrada, Spain, Sep. 09, 2013. Accessed: May 15, 2019. [Online]. Available: https://ieaghg.org/docs/General_Docs/OCC3/Secured%20presentations/DC_Presentation%20OCCC3%20september%202013.pdf

[93] ECRA, ‘Report on Phase II. ECRA CCS Project’, European Cement Research Academy, Düsseldorf, Germany, Technical Report TR-106/2009, 2009. Accessed: May 04, 2018. [Online]. Available: http://www.ecra-online.org

[94] S. O. Gardarsdottir *et al.*, ‘Comparison of Technologies for CO2 Capture from Cement Production—Part 2: Cost Analysis’, *Energies*, vol. 12, no. 3, p. 542, Jan. 2019, doi: 10.3390/en12030542.

[95] J. Rowland, ‘ECRA launches industrial-scale carbon capture project’, *World Cement*, Feb. 2018, Accessed: May 16, 2019. [Online]. Available: https://www.worldcement.com/europe-cis/05022018/ecra-launches-industrial-scale-carbon-capture-project/

[96] E. Mastorakos, A. Massias, C. D. Tsakiroglou, D. A. Goussis, V. N. Burganos, and A. C. Payatakes, ‘CFD predictions for cement kilns including flame modelling, heat transfer and clinker chemistry’, *Applied Mathematical Modelling*, vol. 23, no. 1, pp. 55–76, Jan. 1999, doi: 10.1016/S0307-904X(98)10053-7.

[97] IFRF, ‘Doc. No. C76/y/1/6-Measurement Equipment-Heat Flux Meter’. Mar. 1994.

[98] J. P. Smart, R. Patel, and G. S. Riley, ‘Oxy-fuel combustion of coal and biomass, the effect on radiative and convective heat transfer and burnout’, *Combustion and Flame*, vol. 157, no. 12, pp. 2230–2240, Dec. 2010, doi: 10.1016/j.combustflame.2010.07.013.
[99] M. Kutz, *Mechanical Engineer´s Handbook*, vol. Volume 4: Energy and Power. New Jersey, USA: WILEY, 2014.
[100] S. Su, J. H. Pohl, D. Holcombe, and J. A. Hart, ‘Techniques to determine ignition, flame stability and burnout of blended coals in p.f. power station boilers’, *Progress in Energy and Combustion Science*, vol. 27, no. 1, pp. 75–98, Jan. 2001, doi: 10.1016/S0360-1285(00)00006-X.
[101] S. Badzioch and P. G. W. Hawksley, ‘Kinetics of Thermal Decomposition of Pulverized Coal Particles’, *Ind. Eng. Chem. Process Des. Dev.*, vol. 9, no. 4, pp. 521–530, Oct. 1970, doi: https://doi.org/10.1021/i260036a005.
[102] H. Kobayashi, J. B. Howard, and A. F. Sarofim, ‘Coal devolatilization at high temperatures’, *Symposium on Combustion and Flame, and Explosion Phenomena*, vol. 16, no. 1, pp. 411–425, 1977, doi: https://doi.org/10.1016/S0082-0784(77)80341-X.
[103] Verein Deutsche Zementwerke e.V., *Zahlen und Daten. Zementindustrie in Deutschland 2018*. Erkrath, Germany: Verlag Bau+Technik GmbH, 2018.
[104] A. Andrews and R. K. Lattanzio, ‘Petroleum Coke: Industry and Environmental Issues’, Congressional Research Service, 7–5700, Oct. 2013.
[105] S. Bell, *A beginner´s guide to uncertainty of measurement*. Teddington, Middlesex, United Kingdom: National Physical Laboratory, 1999.
[106] International organization for Standardization (ISO), *Guide to the expression of uncertainty in measurement*, First Edition. Switzerland, 1995.
[107] ‘DIN 1319-1 Grundlagen der Meßtechnik - Teil 1: Grundbegriffe’. Jan. 1995.
[108] TKIS, ‘POLFLAME clinkering zone burner for clinker production’. https://www.thyssenkrupp-industrial-solutions.com/en/products-and-services/cement-plants/clinker-production/burning/polflame-clinkering-zone-burner (accessed Jul. 01, 2019).
[108] D. B. Spalding, ‘The art of partial modelling’, *Ninth Symposium on Combustion,* Academic Press, New York, 1963, pp. 833–843.
[109] J. M. Beér, ‘Phenomenological models for flames in furnaces’, presented at the DOE Workshop on modelling of combustion in practical systems, Los Angeles, USA, Jan. 1978.
[111] G. Salvi and R. Payne, ‘Combustion System Scaling. Report D07/a/69’. International Flame Research Foundation, 1978.
[112] J. P. Smart and D. J. Morgan, ‘Exploring the Effects of Employing Different Scaling Criteria on Swirl Stabilised Pulverised Coal Burner Performance’, *Combustion Science and Technology*, vol. 100:1–6, pp. 331–343, 1994, doi: 10.1080/00102209408935459.
[112] J. P. Smart, D. J. Morgan, and P. A. Roberts, ‘The effect of scale on the performance of swirl stabilised pulverised coal burners’, *Twenty-Fourth Symposium on Combustion,* Volume 24, Issue 1, 1992, p. 1365-1372
[114] J. P. Smart, ‘On the effect of burner scale and coal quality on low NOx burner performance’, Doctoral Dissertation, University of London, London, UK, 1992.
[115] R. Weber and F. Breussin, ‘Scaling Properties of Swirling Pulverized Coal Flames: From 180kW to 50MW Thermal Input’, in *Twenty-Seventh Symposium (International) on Combustion*, 1998, pp. 2957–2964.

[116] S. Orsino and R. Weber, ‘Scaling of Low NOx Flames of Natural Gas’, *IFRF Combustion Journal*, no. Article Number 200005, Jun. 2000.
[117] J. P. Smart and W. L. van de Kamp, ‘The Impact of Scaling Criteria on the Characteristics of Pulverised Coal Flames’, *Dev. Chem. Eng. Mineral Process*, vol. 7, no. 3/4, pp. 301–331, 1999.
[117] R. Weber, ‘Scaling characteristics of aerodynamics, heat transfer, and pollutant emissions in industrial flames’, *Twenty-Sixth Symposium on Combustion*, 1996, Pittsburgh, USA, vol. 26–2, pp. 3343–3354. doi: https://doi.org/10.1016/S0082-0784(96)80182-2.
[119] R. Weber and M. Mancini, ‘On scaling and mathematical modelling of large scale industrial flames’, *Journal of the Energy Institute*, vol. 93 (2020), pp. 43–51.
[120] R. Anantharaman *et al.*, ‘D 3.1 CEMCAP preliminary framework for comparative techno-economic analysis of CO2 capture from cement plants’. CEMCAP Project, Aug. 31, 2015.
[121] A. K. Gupta, D. G. Lilley, and N. Syred, *Swirl Flows*. Kent, England: Abakus Press, 1984.
[122] F. El-Mahallawy and S. E.-D. Habik, *Fundamentals and Technology of Combustion*, First Edition. Kidlington, UK: Elsevier Science Ltd, 2002.
[123] J. M. Beér and N. A. Chigier, *Combustion Aerodynamics*. London, England: Applid Science Publishers, 1972.
[124] C. R. Shaddix and A. Molina, ‘Coal particle ignition and devolatilization during oxy-coal combustion’, in *Proceedings of the 31st international technical conference on coal utilization & fuel systems*, Clearwater, USA, May 2006, vol. Vol I, pp. 169–180.
[125] C. R. Shaddix and A. Molina, ‘Particle imaging of ignition and devolatilization of pulverized coal during oxy-fuel combustion’, *Proceedings of the Combustion Institute*, vol. 32, no. 2, pp. 2091–2098, 2009, doi: 10.1016/j.proci.2008.06.157.
[126] E. Ramström, I. Mann, M. Anheden, and O. Jidingern, ‘First results from detailed furnace measurements performed in the 30MWth Vattenfall Oxyfuel Pilot Plant’, presented at the 35th International technical conference on coal utilization & fuel systems, Clearwater, USA, 2010.
[127] S. Hjärtstam, K. Andersson, F. Johnsson, and B. Leckner, ‘Combustion characteristics of lignite-fired oxy-fuel flames’, *Fuel*, vol. 88, no. 11, pp. 2216–2224, Nov. 2009, doi: 10.1016/j.fuel.2009.05.011.
[128] B. Dhungel, ‘Experimental Investigations on Combustion and Emission Behaviour during Oxy-Coal Combustion’, Doctoral Dissertation, IFK, University of Stuttgart, Stuttgart, Germany, 2009.
[129] P. Glarborg and L. B. Bentzen, ‘Chemical Effects of a High CO2 Concentration in Oxy-Fuel Combustion of Methane’, *Energy & Fuels*, vol. 22, no. 1, pp. 291–296, 2008.
[130] D. Kühnemuth, F. Normann, K. Andersson, and F. Johnsson, ‘On the carbon monoxide formation in oxy-fuel combustion—Contribution by homogenous and heterogeneous reactions’, *International Journal of Greenhouse Gas Control*, vol. 25, pp. 33–41, Jun. 2014, doi: 10.1016/j.ijggc.2014.02.014.
[131] L. D. Smoot, S. C. Hill, and H. Xu, ‘NOx control through reburning’, *Progress in Energy and Combustion Science*, vol. 24, no. 5, pp. 385–408, Oct. 1998, doi: 10.1016/S0360-1285(97)00022-1.

[132] P. Mönckert, D. Reber, J. Maier, and G. Scheffknecht, 'Operation of a Retrofitted 0.5 MWth PF Combustion Facility under Oxyfuel Conditions', presented at the 32nd International technical conference on coal utilization & fuel systems, Clearwater, USA, 2007.
[133] F. Normann, K. Andersson, F. Johnsson, and B. Leckner, 'Emission control of nitrogen oxides in the oxy-fuel process.', *Progress in Energy and Combustion Science*, vol. 35 (5), pp. 385–397, Oct. 2009.
[134] D. G. Roberts, E. M. Hodge, D. J. Harris, and J. F. Stubington, 'Kinetics of Char Gasification with CO2 under Regime II Conditions: Effects of Temperature, Reactant, and Total Pressure', *Energy Fuels*, vol. 24, no. 10, pp. 5300–5308, Oct. 2010, doi: 10.1021/ef100980h.
[131] H. Baier, 'Erstzbrennstoffe für den Einsatz in Mitverbrennungsanlagen (Alternative fuels for co-combustion)', *Zement-Kalk-Gips International*, vol. 59, no. No. 3-2006, pp. 78–85, 2006.
[136] H. Baier, 'Disruptive substances and the burning behaviour of solid alternative fuels', *Zement-Kalk-Gips International*, vol. 63, no. No. 6-2010, pp. 58–67, 2010.
[137] P. A. Alsop, *The Cement Plant Operations Handbook for Dry-Process Plants*, Sixth Edition. Tradeship Publications Ltd, 2007.
[138] P. Edge *et al.*, 'Combustion modelling opportunities and challenges for oxy-coal carbon capture technology', *Chemical Engineering Research and Design*, vol. 89, no. 9, pp. 1470–1493, Sep. 2011, doi: 10.1016/j.cherd.2010.11.010.
[139] S. Leiser, 'Numerical simulation of oxy-fuel combustion', Doctoral Dissertation, Universität Stuttgart, Stuttgart, 2010.
[140] D. Toporov *et al.*, 'Detailed investigation of a pulverized fuel swirl flame in CO2/O2 atmosphere', *Combustion and Flame*, vol. 155, no. 4, pp. 605–618, Dec. 2008, doi: 10.1016/j.combustflame.2008.05.008.
[141] S. P. Khare, T. F. Wall, A. Z. Farida, Y. Liu, B. Moghtaderi, and R. P. Gupta, 'Factors influencing the ignition of flames from air-fired swirl pf burners retrofitted to oxy-fuel', *Fuel*, vol. 87, no. 7, pp. 1042–1049, Jun. 2008, doi: 10.1016/j.fuel.2007.06.026.
[142] C. Yin, L. A. Rosendahl, and S. K. Kær, 'Chemistry and radiation in oxy-fuel combustion: A computational fluid dynamics modeling study', *Fuel*, vol. 90, no. 7, pp. 2519–2529, Jul. 2011, doi: 10.1016/j.fuel.2011.03.023.
[143] J. Andersen, C. L. Rasmussen, T. Giselsson, and P. Glarborg, 'Global Combustion Mechanisms for Use in CFD Modeling under Oxy-Fuel Conditions', *Energy Fuels*, vol. 23, no. 3, pp. 1379–1389, Mar. 2009, doi: 10.1021/ef8003619.
[140] M. Müller, U. Schnell, S. Grathwohl, Jörg Maier, and G. Scheffknecht, 'Evaluation of Oxy-coal Combustion Modelling at Semi-industrial Scale', *Energy Procedia*, vol. 23, pp. 197–206, Jan. 2012, doi: 10.1016/j.egypro.2012.06.054.
[145] A. H. Al-Abbas, J. Naser, and D. Dodds, 'CFD modelling of air-fired and oxy-fuel combustion of lignite in a 100KW furnace', *Fuel*, vol. 90, no. 5, pp. 1778–1795, May 2011, doi: 10.1016/j.fuel.2011.01.014.
[146] F. C. Lockwood, B. Shen, and T. Lowes, 'Numerical study of petroleum coke fired cement kiln flames', presented at the Third International Conference on Combustion Technologies for a Clean Environment, Lisbon, 1995.

[147] M. Ditaranto and J. Bakken, ‘Study of a full scale oxy-fuel cement rotary kiln’, *International Journal of Greenhouse Gas Control*, vol. 83, pp. 166–175, Apr. 2019, doi: 10.1016/j.ijggc.2019.02.008.
[148] A. Jamali, K. Fleiger, V. Hoenig, and J. Ruppert, ‘Modelling and optimization of the oxyfuel clinker burning process’, *Cement International*, vol. 16, no. 5, pp. 44–47, 2018.
[149] U. Schnell, ‘Numerical Modelling of Solid Fuel Combustion Processes using advanced CFD-based Simulation Tools’, *Progress in Computational Fluid Dynamics*, vol. 1, no. 4, pp. 208–2018, 2001.
[150] J. Ströhle, ‘Spectral modelling of Radiative Heat Transfer in Industrial Furnaces’, Doctoral Dissertation, Universität Stuttgart, Stuttgart, 2003.
[147] D. Förtsch, ‘A Kinetic Model of Pulverised Coal Combustion for Computational Fluid Dynamics’, Doctoral Dissertation, Universität Stuttgart, Stuttgart, 2003.
[152] M. N. Anany, ‘Numerical Modelling of Combustion Processes at Elevated Pressured’, Doctoral Dissertation, Universität Stuttgart, Stuttgart, 2010.
[153] M. Fürst, ‘Flow Field Investigations for the CFD-Simulation of Combustion Processes at High Velocities’, Master Thesis No. 3579, Universität Stuttgart, Stuttgart, 2014.
[154] B. E. Launder and D. B. Spalding, ‘The numerical computation of turbulent flows’, *Computer Methods in Applied Mechanics and Engineering*, vol. 3, no. 2, pp. 269–289, Mar. 1974, doi: 10.1016/0045-7825(74)90029-2.
[155] B. Leckner, ‘Spectral and total emissivity of water vapor and carbon dioxide’, *Combustion and Flame*, vol. 19, no. 1, pp. 33–48, Aug. 1972, doi: 10.1016/S0010-2180(72)80084-1.
[156] L. C. Sanchez Herrera, ‘Simulation of solid fuel combustion with a prototype kiln burner using AIOLOS’, Master Thesis No. 3525, Universität Stuttgart, Stuttgart, 2017.
[153] M. Ditaranto *et al.*, ‘D 7.3 Oxyfuel CFD burner and large kiln simulations’. Zenodo, Jan. 2018, doi: 10.5281/zenodo.2605047
[158] G. Locher, ‘Mathematische Modelle zum Prozess des Brennens von Zementklinker, Teile 1-5’, *Zement-Kalk-Gips*, vol. 55, no. 3, 2002.
[159] H. Klein and V. Hoenig, ‘Modellrechnungen zum Brennstoffenergiebedarf des Klinkerbrennprozesses’, *Cement International*, no. 3, pp. 44–63, 2006.